NCAR/TN-371+STR
NCAR TECHNICAL NOTE

April 1992

Monthly Mean Global Satellite Data Sets Available in CCM History Tape Format

James W. Hurrell
G. Garrett Campbell

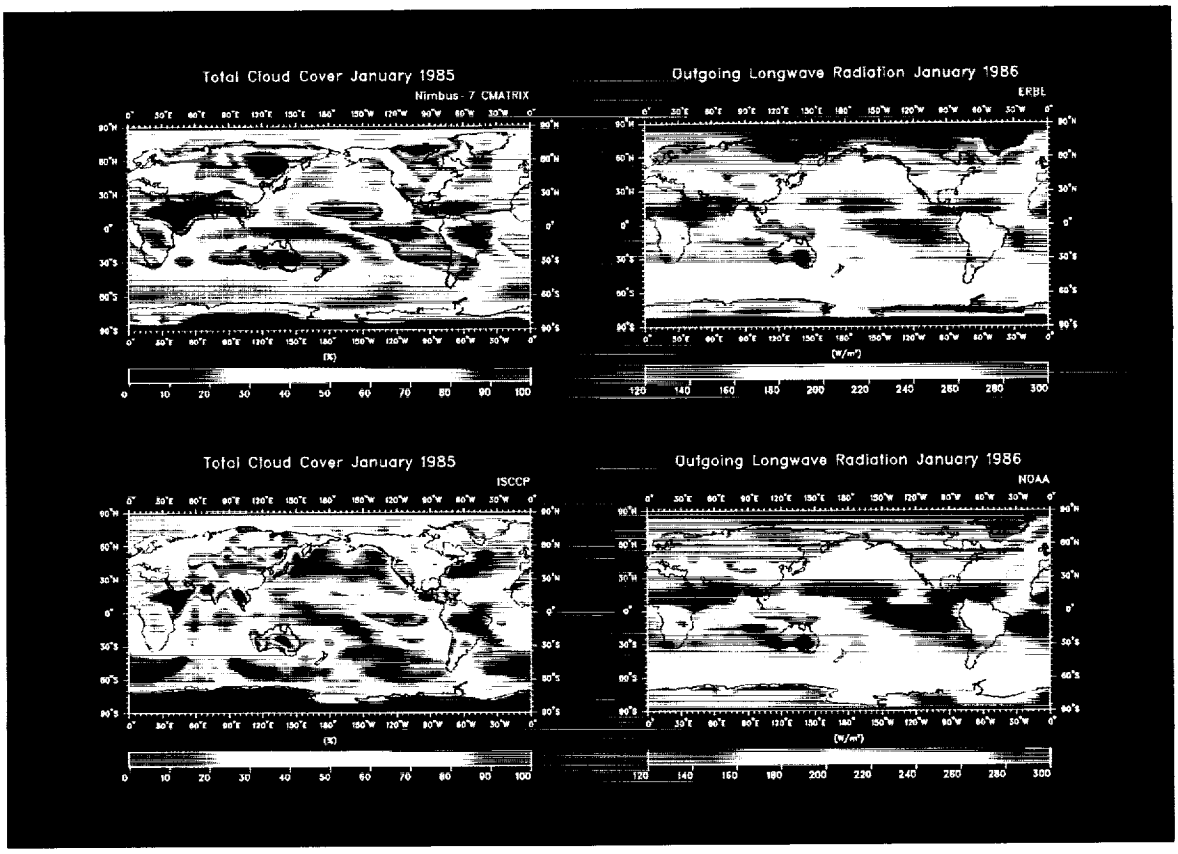

CLIMATE AND GLOBAL DYNAMICS DIVISION

NATIONAL CENTER FOR ATMOSPHERIC RESEARCH
BOULDER, COLORADO

NCAR TECHNICAL NOTES

The Technical Note series provides an outlet for a variety of NCAR manuscripts that contribute in specialized ways to the body of scientific knowledge but which are not suitable for journal, monograph, or book publication. Reports in this series are issued by the NCAR Scientific Divisions; copies may be obtained on request from the Publications Office of NCAR. Designation symbols for the series include:

EDD – *Engineering, Design, or Development Reports*

Equipment descriptions, test results, instrumentation, and operating and maintenance manuals.

IA – *Instructional Aids*

Instruction manuals, bibliographies, film supplements, and other research or instructional aids.

PPR – *Program Progress Reports*

Field program reports, interim and working reports, survey reports, and plans for experiments.

PROC – *Proceedings*

Documentation of symposia, colloquia, conferences, workshops, and lectures. (Distribution may be limited to attendees.)

STR – *Scientific and Technical Reports*

Data compilations, theoretical and numerical investigations, and experimental results

The National Center for Atmospheric Research is operated by the University Corporation for Atmospheric Research and is sponsored by the National Science Foundation. Any opinions, findings, conclusions, or recommendations expressed in this publication are those of the author(s) and do not necessarily reflect the views of the National Science Foundation.

NCAR/TN-371+STR
NCAR TECHNICAL NOTE

April 1992

Monthly Mean Global Satellite Data Sets Available in CCM History Tape Format

James W. Hurrell
G. Garrett Campbell

CLIMATE AND GLOBAL DYNAMICS DIVISION

NATIONAL CENTER FOR ATMOSPHERIC RESEARCH
BOULDER, COLORADO

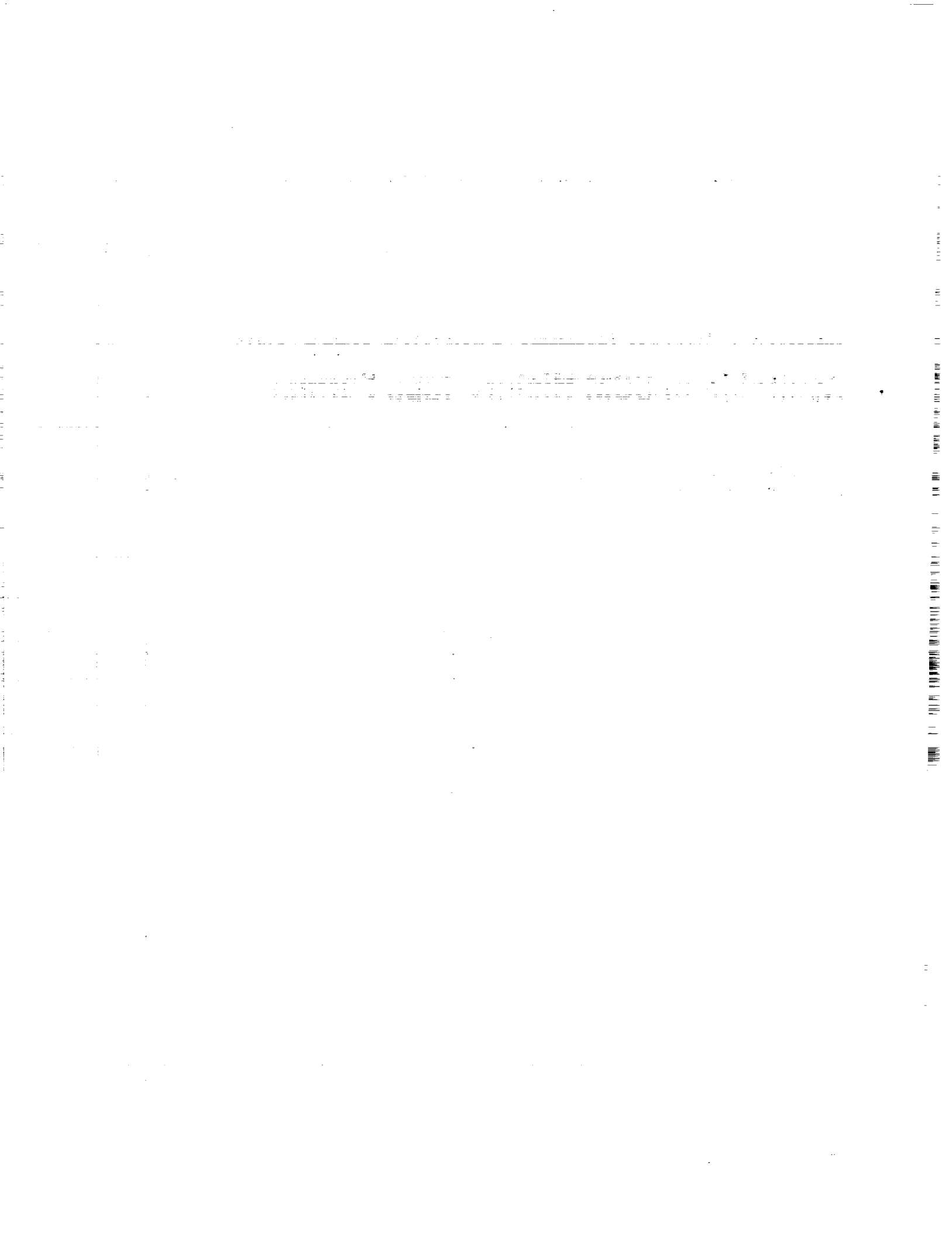

TABLE OF CONTENTS

	Page
List of Figures	v
List of Appendices	ix
Foreword	xi
Preface	xiii
Acknowledgments	xv
1. Introduction	1
2. Data Set Descriptions	2
2.1 Microwave Sounding Unit (MSU)	2
2.2 International Satellite Cloud Climatology Project (ISCCP)	7
2.3 Earth Radiation Budget Experiment (ERBE)	12
2.4 Nimbus-7	14
2.5 Outgoing Longwave Radiation (OLR) Data from NOAA	17
3. Processing Techniques	20
4. Results	22
4.1 Intercomparison of ISCCP and Nimbus-7 CMATRIX Cloud Statistics	23
4.2 Intercomparison of ERBE, Nimbus-7 ERB, and NOAA OLR Data	38
4.3 MSU Data	47
4.4 Climatologies	52
5. Summary and Future Work	58
References	61
Appendices	65

LIST OF FIGURES

		Page
Figure 1.	Normalized weighting functions for MSU channels 2 (53.74 GHz), 4 (57.95 GHz) and 2R for a 22° view angle through a U.S. Standard Atmosphere. The dashed line represents the level of the tropopause.	3
Figure 2.	Periods of operation and overlap between MSUs from 1979 through 1990 (from Christy, personal communication). Gaps indicate one or more days of less than 85% global coverage.	5
Figure 3.	Percent of global coverage provided by geostationary and polar-orbiting satellites for ISCCP from July 1983 (from Rossow, personal communication).	8
Figure 4.	Schematic defining the ten ISCCP cloud types by their cloud-top pressures and optical thicknesses (from Rossow and Schiffer 1991). Low, middle and high clouds are defined by cloud-top pressures from IR data only.	10
Figure 5.	Zonally averaged total cloud cover from ISCCP (solid) and Nimbus-7 CMATRIX (dash) expressed in percent for (a) July 1984 and (b) January 1985.	24
Figure 6.	Total cloud cover in percent for July 1984 from (a) ISCCP and (b) Nimbus-7 CMATRIX. Cloud cover less than 20% is indicated by hatching and cloud cover greater than 80% is indicated by stippling. The contour increment is 10%.	25
Figure 7.	As in Fig. 6 except for January 1985.	26
Figure 8.	Percent occurrence of high cloud for July 1984 from (a) ISCCP and (b) Nimbus-7 CMATRIX. High cloud cover greater than 40% is indicated by stippling. The contour increment is 10%. The comparison is complicated by different definitions of high cloud between ISCCP and CMATRIX.	28
Figure 9.	As in Fig. 8 except for January 1985.	29
Figure 10.	Percent occurrence of low cloud for July 1984 from (a) ISCCP and (b) Nimbus-7 CMATRIX. Low cloud cover greater than 40% is indicated by stippling. The contour increment is 10%. The comparison is complicated by different definitions of low cloud between ISCCP and CMATRIX. Missing data in the ISCCP analysis are also indicated by stippling in high surface elevation regions.	30
Figure 11.	As in Fig. 10 except for January 1985.	31

LIST OF FIGURES—Continued

		Page
Figure 12.	Time series of monthly total cloud cover averaged over the globe from ISCCP (solid) and Nimbus-7 CMATRIX (dash). The lower solid curve from ISCCP represents the "unadjusted" total cloud estimate (see text for details).	33
Figure 13.	Time series of monthly total cloud cover from ISCCP (solid) and Nimbus-7 CMATRIX (dash) averaged over (a) global land areas and (b) global ocean areas.	35
Figure 14.	Time series of monthly total cloud cover from ISCCP (solid) and Nimbus-7 CMATRIX (dash) averaged over (a) the Northern Hemisphere and (b) the Southern Hemisphere.	36
Figure 15.	Time series of monthly total cloud cover from ISCCP (solid) and Nimbus-7 CMATRIX (dash) averaged over (a) the western tropical Pacific, (b) the eastern tropical Pacific and (c) the Indian summer monsoon region. The regions are defined in the text.	37
Figure 16.	Outgoing longwave radiation in W m^{-2} for July 1985 from (a) ERBE, (b) NOAA and (c) Nimbus-7 ERB. Values less than 225 W m^{-2} are indicated by stippling, and values greater than 275 W m^{-2} are hatched. The contour increment is 25 W m^{-2}.	39
Figure 17.	As in Fig. 16 except for January 1986.	40
Figure 18.	As in Fig. 16 (July 1985) except the (a) ERBE and (b) NOAA OLR data have been truncated to T15 and placed on a 4.5° rectangular grid for a more direct comparison with the (c) Nimbus-7 ERB measurement.	41
Figure 19.	As in Fig. 18 except for January 1986.	42
Figure 20.	Scatter plot of outgoing longwave radiation for July 1985 from (a) ERBE and NOAA and (b) ERBE and Nimbus-7 ERB. Each point in (a) represents a gridpoint on the T42 grid sampled between 70°S and 70°N, while each point in (b) is sampled between 70°S and 70°N from the 4.5° resolution grid with ERBE data truncated to T15.	43
Figure 21.	As in Fig. 20 except for January 1986.	44

LIST OF FIGURES—Continued

		Page
Figure 22.	Scatter plot of outgoing longwave radiation measurements from ERBE from July 1985 and July 1986. Each point represents a gridpoint on the T42 grid sampled between 70°S and 70°N.	46
Figure 23.	Time series of monthly outgoing longwave radiation from Nimbus-7 ERB (solid), ERBE (dash) and NOAA (dash-dot) averaged from 70°S to 70°N.	48
Figure 24.	As in Fig. 23 except averaged from (a) 0° to 70°N, (b) 0° to 25°N and (c) 25°N to 70°N.	49
Figure 25.	As in Fig. 23 except averaged over (a) 0° to 70°S, (b) 0° to 25°S and (c) 25°S to 70°S.	50
Figure 26.	As in Fig. 23 except averaged over (a) the western tropical Pacific and (b) the eastern tropical Pacific. The regions are defined in the text.	51
Figure 27.	Time series of monthly global MSU brightness temperature anomalies, defined relative to the 1982–1991 annual cycle, for (a) channel 2R, (b) channel 2 and (c) channel 4.	53
Figure 28.	As in Fig. 27 except for Northern Hemisphere averages.	54
Figure 29.	As in Fig. 27 except for Southern Hemisphere averages.	55
Figure 30.	As in Fig. 27 except for tropical (20°S to 20°N) averages.	56
Figure 31.	Brightness temperature anomalies from MSU channel 2R for (a) January 1982, (b) January 1983 and (c) January 1984. The contour increment is 1 K and negative values are indicated by the dashed lines.	57
Figure 32.	Average total cloud cover in percent from ISCCP for (a) January 1984–1988 and (b) July 1983–1987. Cloud cover less than 20% is indicated by hatching and cloud cover greater than 80% is indicated by stippling. The contour increment is 10%.	59
Figure 33.	Average outgoing longwave radiation from NOAA for 1979–1991 for (a) January and (b) July. Values less than 225 W m^{-2} are indicated by stippling, and values greater than 275 W m^{-2} are hatched. The contour increment is 25 W m^{-2}.	60

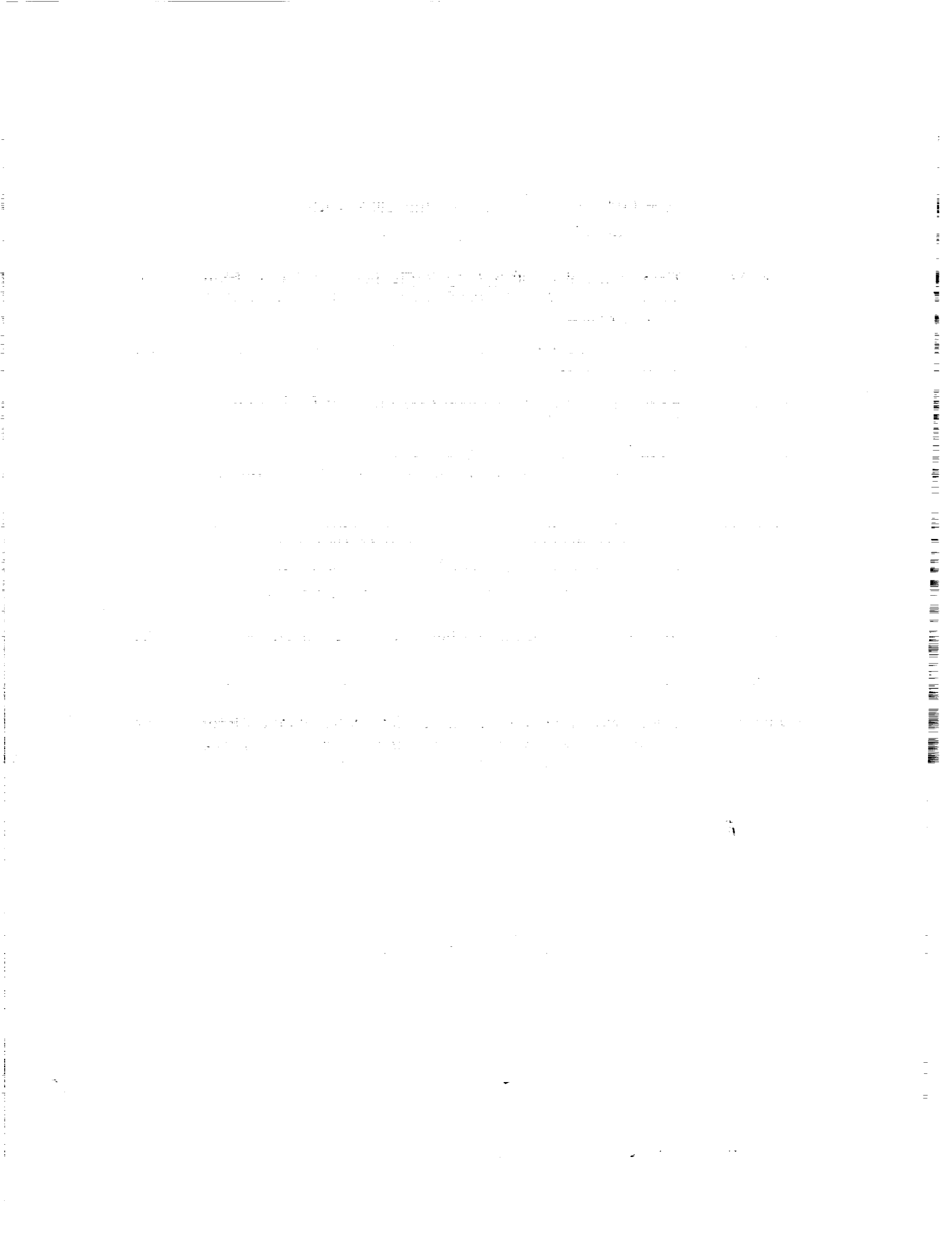

LIST OF APPENDICES

Page

Appendix 1. List of Acronyms 65

Appendix 2. Table of day number (for use in the CCM processor) 66

Appendix 3. MSU data on the Mass Store 67

Appendix 4. ISCCP data on the Mass Store 69

Appendix 5. ERBE data on the Mass Store 76

Appendix 6. Nimbus-7 ERB and CMATRIX data on the Mass Store 78

Appendix 7. NOAA OLR data on the Mass Store 85

Appendix 8. Surface flags 86

Appendix 9. Sample CCM Processor jobs 87

FOREWORD

The preparation of satellite data for the climate modeling community is an important task for the ultimate improvement of climate models. Generally, satellite data have not been used to their full potential because of the difficulty of transforming the data into a format to allow easy comparison with model output. The National Center for Atmospheric Research (NCAR) has built a Community Climate Model (CCM) processor that easily accesses and analyzes CCM data. The CCM processor has also been used by NCAR and university communities to access archived operational analysis products from the major numerical weather prediction centers. This technical note extends the data archived in this format to include several long-term satellite data sets.

Warren M. Washington
Director, Climate & Global Dynamics Division
National Center for Atmospheric Research

April 1992

PREFACE

This report describes work completed on the National Aeronautics and Space Administration (NASA) project, "Intercomparison of Satellite-Based Global Data Sets with Global Atmosphere/Ocean Model Experiments on the Greenhouse Effect" (NASA Grant W-17214, UPN 578-41-29-03). A goal of the project has been to acquire and analyze global satellite data sets that can potentially provide a standard for validating coupled atmosphere-ocean models. Such models are used to simulate the present climate and investigate possible climate change caused by increased concentrations of greenhouse gases. Global satellite data sets are also useful for many diagnostic studies of the climate system. Emphasis has been placed on acquiring satellite data with records of, at least, several years.

The intercomparison of satellite data with model data is facilitated by putting the observed data into "history tape" format for use with the NCAR Community Climate Model (CCM) processor. This format is widely used to analyze CCM output as well as global data sets from the European Centre for Medium-Range Weather Forecasts and the National Meteorological Center. The satellite data sets that have been archived in CCM history tape format include data from:

- Microwave Sounding Unit (MSU)
- International Satellite Cloud Climatology Project (ISCCP)
- Earth Radiation Budget Experiment (ERBE)
- Nimbus-7 Earth Radiation Budget (ERB)
- Nimbus-7 Cloud-Matrix (CMATRIX)
- Outgoing Longwave Radiation (OLR) Data from NOAA

It is likely that additional satellite data will be archived in the future. Access to the archived data above is described in this report, and brief summaries of each data set are given. Current and future work will include more detailed evaluations of the quality of the satellite data. Intercomparisons with model output will be reported elsewhere.

James W. Hurrell
G. Garrett Campbell

April 1992

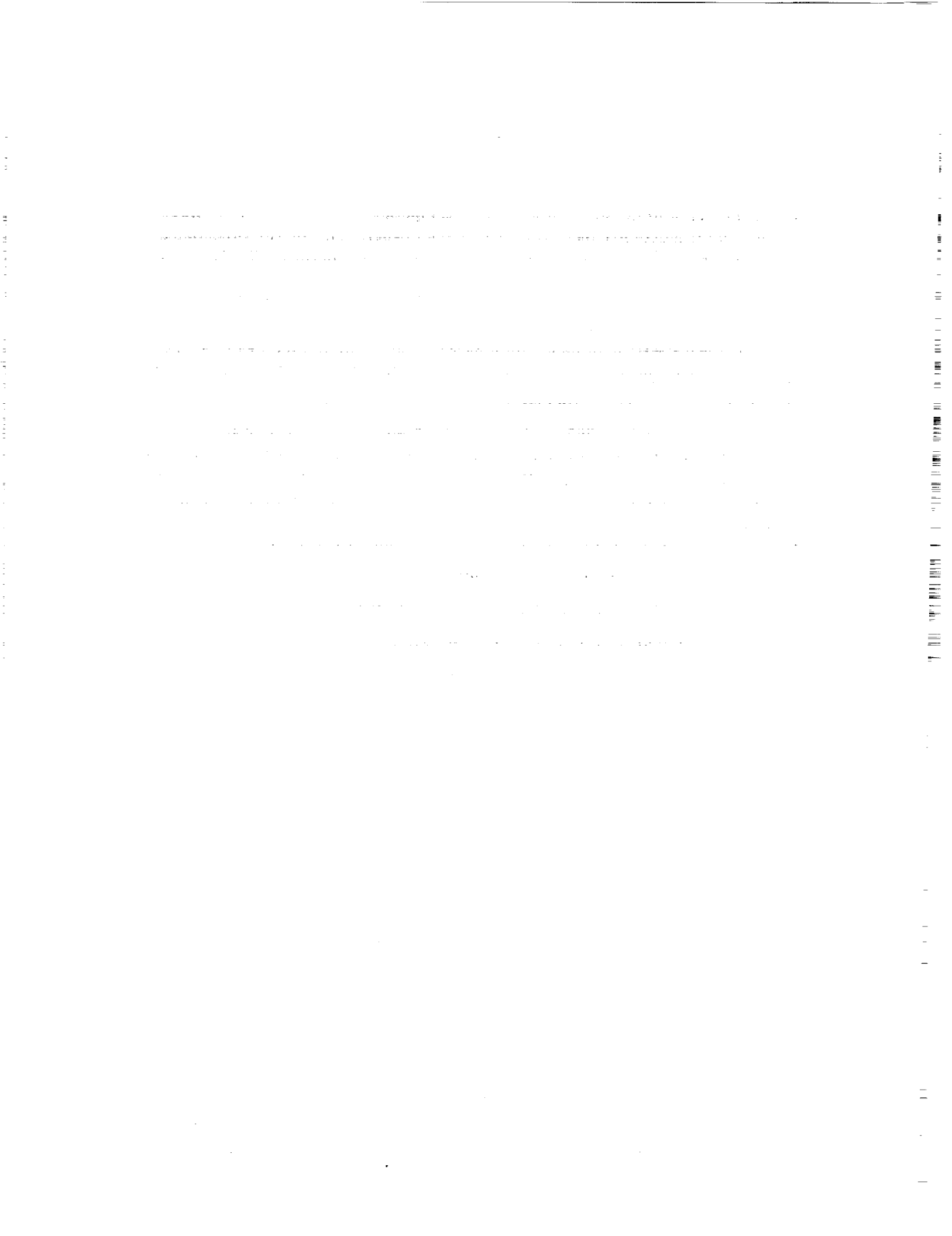

ACKNOWLEDGMENTS

We thank Gary Strand for his assistance in archiving the satellite data sets. His programming skills were invaluable to the project. We also thank Bruce Briegleb, Dennis Shea, Kevin Trenberth and Warren Washington for their suggestions and comments. The manuscript was substantially improved as a result of their input. We thank the staff of NCAR's Graphics Services and the Copy Center for their assistance in producing the color diagrams on the cover of this report, and Ann Modahl for formatting and editing the text. G. Garrett Campbell's permanent affiliation is with Colorado State University in Fort Collins.

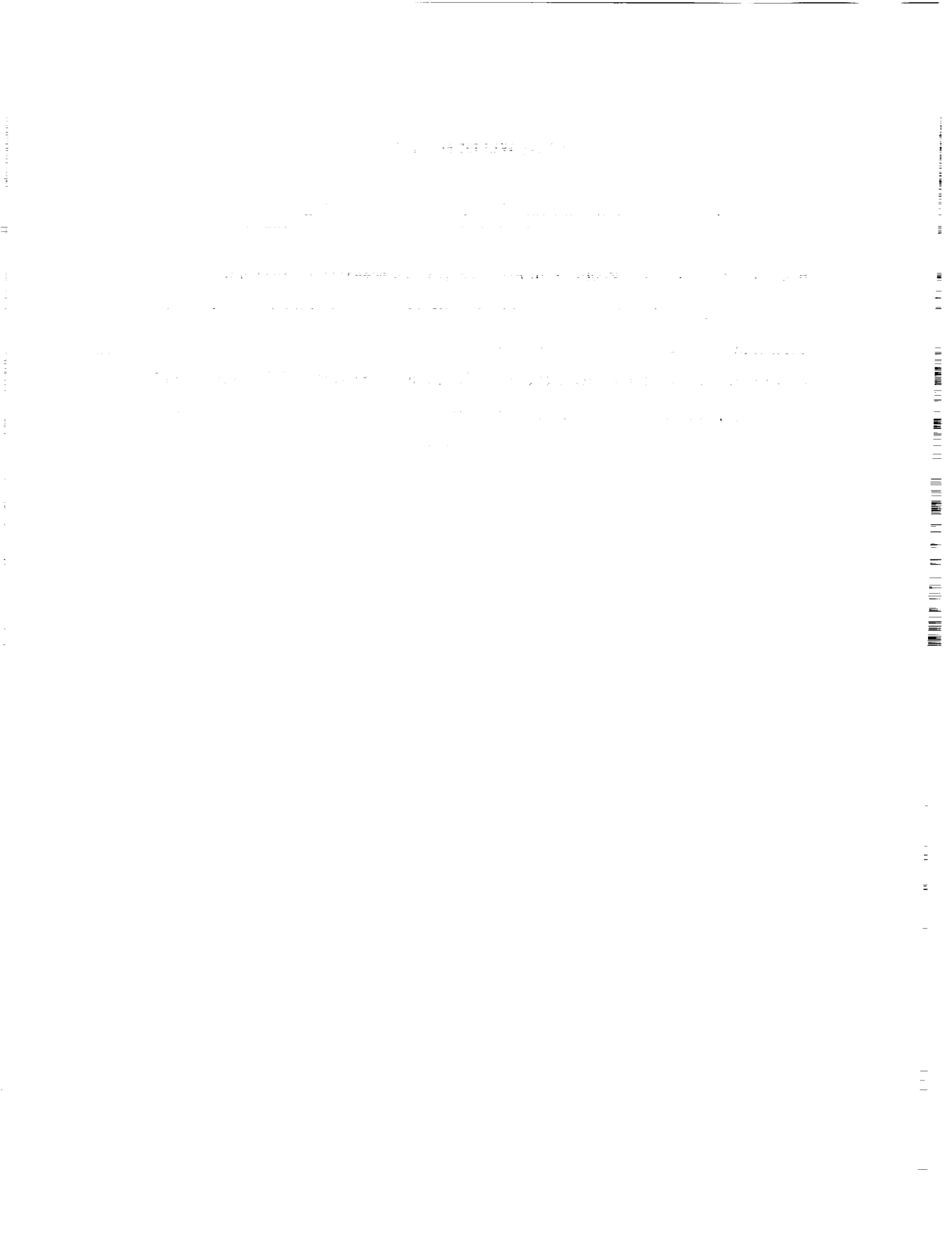

1. INTRODUCTION

Satellite data for climate monitoring have become increasingly important over the past decade or two, especially with increasing concern for inadvertent anthropogenic climate change. Although most satellite-based data are of short record, satellites can provide the global coverage that traditional meteorological observational networks lack. In addition, satellite data are invaluable for the validation of climate models, and they are useful for many diagnostic studies.

In this report, several satellite data sets have been processed and transformed into "history tape" format for use with the Community Climate Model (CCM) modular processor. Only a few of the most widely used and best documented data sets have been selected at this point, although future work will expand the number of data sets examined as well as update (when possible) the archived data sets. An attempt has been made to include data of longer record and only monthly averaged data have been processed. Most of the data have been archived at their original resolution and also transformed to a triangular wavenumber 42 (T42) truncation Gaussian grid to facilitate more direct comparison to CCM output. Gaussian grids are used for the horizontal representation of fields in many spectral transform general circulation models (GCMs).

For studies using satellite data over an extended period, it is important to recognize the impact of changes in instrumentation, drift in instrument calibration, errors introduced by retrieval algorithms and other sources of error such as those resulting from insufficient space and/or time sampling. A detailed documentation of such biases for each data set is not the focus of this report. However, the major known shortcomings will be discussed and demonstrated, and references for more detailed error analyses will be given. All users of the archived data should consult the given references for more thorough descriptions of the data and their quality. Future work will include examinations of the archived data that extend beyond the scope of this report, and appropriate atlases of the archived data may be produced. The purpose of this technical note is simply to introduce the data available for use with the CCM processor.

Because of biases, temporal and spatial discontinuities and the shortness of records, it is difficult to establish climatologies for some of the data. Nonetheless, an attempt has been made to archive some appropriate climatological products. Also, individual months common to several or all data sets will be discussed

and compared in order to highlight the types of data available and some of the major similarities and differences.

A description of each satellite data set follows in section 2, including brief summaries of data sources, inversion techniques and known limitations of the data. The data-processing methods used to archive the satellite data in CCM history tape format on both rectangular and Gaussian grids are described in section 3, and a few parameters necessary to access the archived data with the processor are defined. A few intercomparisons of archived data are presented in section 4, and section 5 concludes with a description of future planned activities. Appendices describe how to access the data (including sample CCM processor job decks) and provide additional details about the data processing. Some of the terminology relating to the CCM processor in the Appendices may be confusing without first consulting section 3.

2. DATA SET DESCRIPTIONS

2.1 Microwave Sounding Unit (MSU)

The technical aspects of the MSU data retrievals have been described by Spencer et al. (1990), and the data specifically archived here have been described in detail by Spencer and Christy (1992a,b). The individual channels in the MSU measure a vertically averaged atmospheric thermal emission, or brightness temperature, by molecular oxygen in the atmosphere at different spectral intervals in the oxygen-absorption complex near 60 GHz. Oxygen is a very good temperature tracer for climate monitoring because it is uniformly mixed and its concentration is very stable in time. The deep-layer nature of the MSU measurements is illustrated by the channel-weighting functions shown in Fig. 1 for channels 2 (53.74 GHz), 4 (57.95 GHz) and 2R. Channel 2R brightness temperatures are described by Spencer and Christy (1992b) and will be discussed later.

A concern is the proportion of the signal that arises from nonoxygen emission. For channel 2 data, the theoretical calculations of Spencer et al. (1990) predict small contaminating influences from interannual variations in precipitation-size ice in deep convection, cloud water, water vapor and surface emissivity. The magnitudes of these errors, however, are difficult to quantify. Spencer et al. estimate that the monthly brightness temperature anomaly signal in regional areas might be contaminated by 0.1°C or more, although the value would be reduced to about 0.01°C for globally averaged monthly anomalies. They also found that the

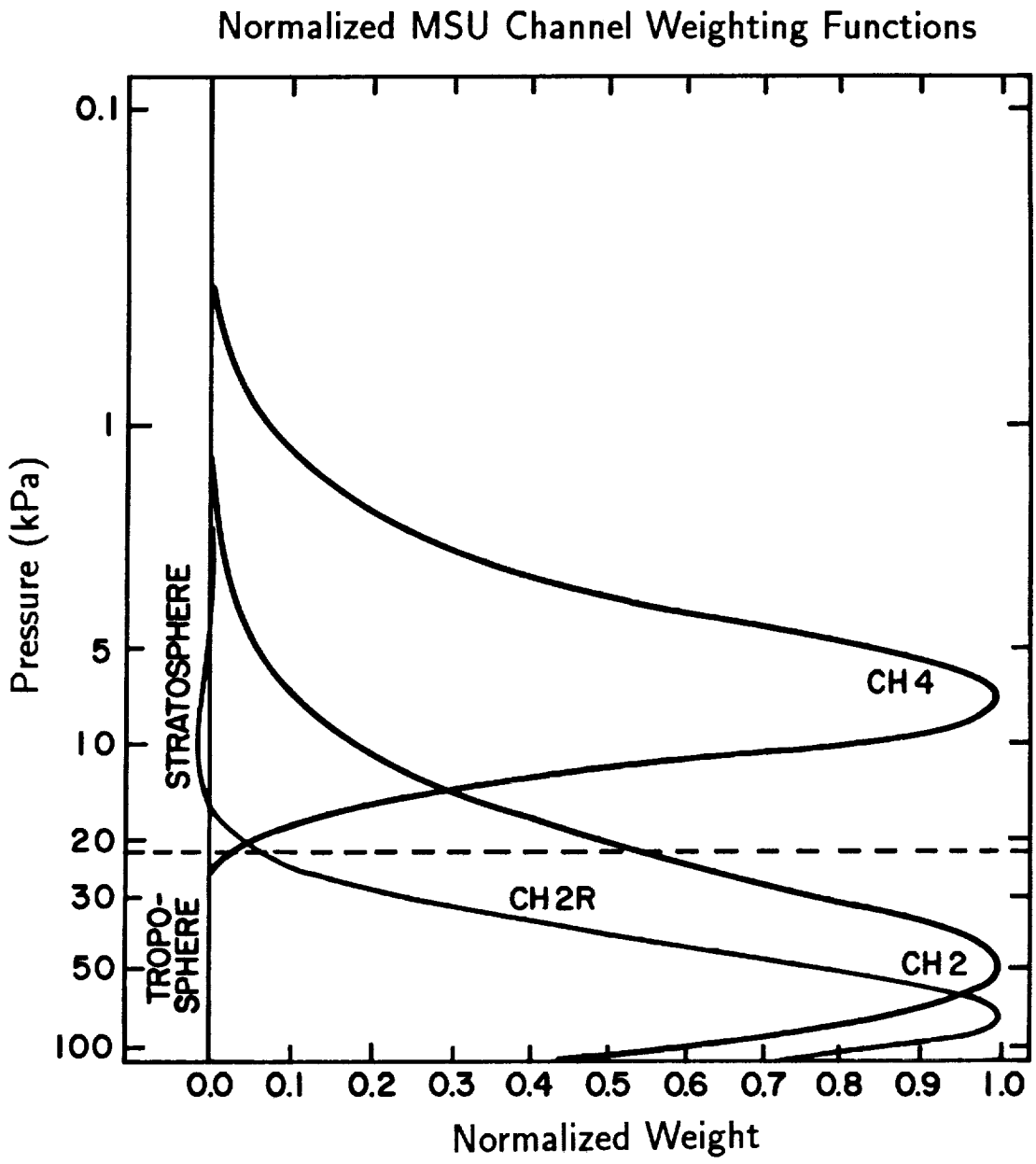

Figure 1. Normalized weighting functions for MSU channels 2 (53.74 GHz), 4 (57.95 GHz) and 2R for a 22° view angle through a U.S. Standard Atmosphere. The dashed line represents the level of the tropopause.

largest contamination results from precipitation-size ice in deep convection, which can cause brightness temperature depressions of up to several degrees. Therefore, the MSU data have been filtered to remove this particular contamination (Spencer et al. 1990). The surface emissivity has a noticeable effect in mountainous regions but, because it is systematic, the interference can mostly be eliminated when the mean annual cycle is removed.

Probably the most limiting factor influencing the interpretation of the channel 2 MSU data in terms of a tropospheric temperature, however, is the small, but nontrivial, signal received from the lower stratosphere. The magnitude of this contamination is difficult to estimate, but Spencer et al. (1990) state that perhaps a few percent of a stratospheric brightness temperature will be included in a tropospheric channel 2 measurement. This is especially true at high latitudes where the height of the tropopause is lower. The stratospheric influence on the channel 2 data is addressed by Spencer and Christy (1992b), who propose a retrieval technique to remove it. Essentially, the off-nadir data, which have a somewhat different vertical weighting function, can be used to remove the stratospheric influence and thus provide an adjusted vertical weighting function (channel 2R) that peaks slightly lower in the troposphere (Fig. 1). It should be noted, however, that the reproducibility of brightness temperatures between different satellites is about a factor of three better with the channel 2 data than with the adjusted channel 2R data (Spencer and Christy 1992b). Measurements made close in frequency to the 60 GHz absorption peak (e.g., MSU channel 4) are dominated by the stratosphere since the absorption and emission by oxygen are so strong at those altitudes that the signal received from the troposphere is small.

The MSUs sample globally twice daily from each of two satellites with different equator-crossing times, although periods exist when only one satellite is in operation. The MSUs have been on NOAA satellites since late 1978. The main intervals when only one satellite was operating were February 1980–January 1981 (NOAA 6), April 1983–December 1984 (NOAA 7) and April 1987–September 1988 (NOAA 10). Figure 2 illustrates the history of satellite coverage for the MSU data. The data have been binned into 2.5° grid squares from 88.75°S to 88.75°N. Over the tropics, about 40 observations per operating satellite are collected over a month for each individual grid square, while regions poleward of 45° have well over 100 observations. The data are then averaged in each grid square after outliers are removed, and anomalies are constructed from a base annual cycle which

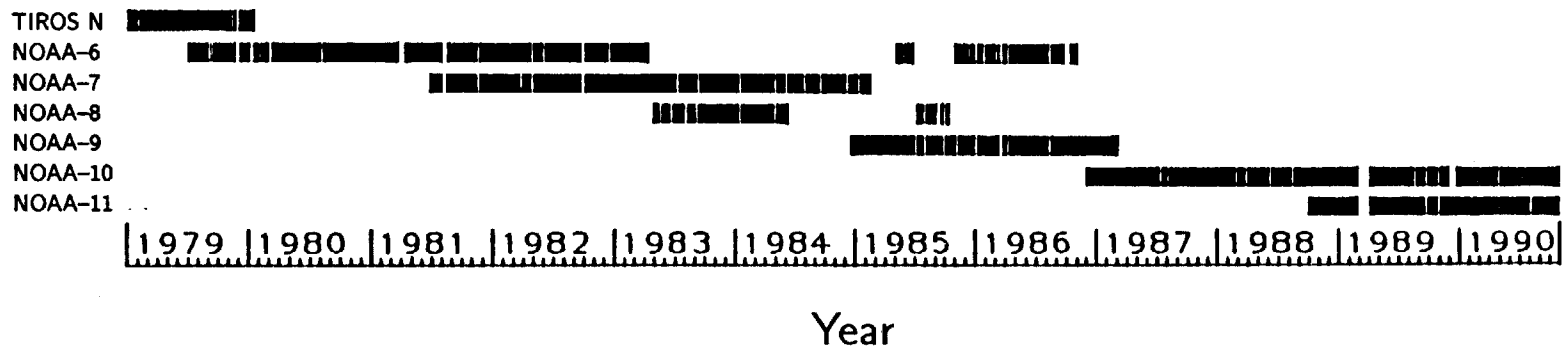

Figure 2. Periods of operation and overlap between MSUs from 1979 through 1990 (from Christy, personal communication). Gaps indicate one or more days of less than 85% global coverage.

is itself dependent on the equator-crossing time of the satellite so that systematic diurnal effects are effectively removed.

The stability of the MSU channel 2 data from one satellite to another is a key issue. Spencer and Christy (1992a) describe how the multisatellite data have been merged, and they evaluate instrument stability. Monthly mean channel 2 brightness temperatures averaged over the hemispheres are reproduced from different satellites to within approximately 0.01°C, indicating a significant lack of instrument drift. In fact, the monthly reproducibility at the 2.5° gridpoint resolution was generally better than 0.1°C in the tropics and 0.2°C at higher latitudes. In comparisons with radiosonde data over the decade, Spencer and Christy (1992a) show that no significant spurious trends are present in the satellite data. Moreover, they conclude that the accuracy of the MSU data approaches the precision of individual radiosonde stations in their ability to measure monthly mean temperature anomalies, which they estimated, from intercomparisons of closely spaced oceanic stations in the tropical Pacific, to be 0.2°C.

In evaluating the ability of the MSUs to measure tropospheric temperature fluctuations, Spencer and Christy (1992a) found that both monthly and annual MSU anomalies from the last decade correlated from 0.90 to 0.98 with those from vertically weighted radiosonde temperature profiles. Root-mean-square (rms) differences generally ranged from 0.15°C in the tropics to 0.25°C at high latitudes and improved to 0.10°C and 0.20°C for radiosonde data composited into regional profiles. Correlations of the satellite data with radiosonde-measured thickness values were only slightly lower and were best for the 1000- to 200-mb layer. These results were somewhat limited, however, to stations from the continental United States, Alaska, Hawaii, the Caribbean basin and the tropical west Pacific. Hurrell and Trenberth (1992) examined the relationship between the apparent climate records as depicted by the MSU data and the European Centre for Medium-Range Weather Forecasts (ECMWF) analyses on a global scale and found very good agreement over most regions.

The above results seem to indicate that the MSUs are highly suitable for monitoring intraseasonal to interannual temperature variations with global coverage. Channel 2, 4 and 2R monthly brightness temperatures have been archived from January 1979 through December 1991 (Appendix 3).

2.2 International Satellite Cloud Climatology Project (ISCCP)

The ISCCP was established as part of the World Climate Research Program to use operational satellite data to produce a calibrated and normalized infrared (IR) and visible (VIS) radiance data set from which global, reduced-resolution cloud properties could be derived (Rossow and Schiffer 1991). Narrow-band radiances have been collected since July 1983 to estimate the cloud properties. Polar-orbiting and geostationary satellites have contributed data (observations eight times per day) over most of the globe. Global coverage was originally to be provided from five geostationary satellites and one polar-orbiting satellite but, because of various satellite failures and replacements, actual coverage has ranged from near 70% to greater than 90% through 1990. Figure 3 (Rossow, personal communication) illustrates the history of weather-satellite coverage for ISCCP.

The operational instruments have included geosynchronous narrow-band imagers onboard the Geostationary Operational Environmental Satellites (GOES), Japan's Geostationary Meteorological Satellite (GMS) and the European Space Agency's METEOSAT, as well as the Advanced Very High Resolution Radiometer (AVHRR) imagers on NOAA-7 to NOAA-11. The basic pixel resolution is about 10 km, but a sampled data set with pixel spacing of about 30 km is prepared for the analysis that produces the cloud climatology data. After inclusion of calibration factors, the reduced-resolution radiance data are called Stage B3 data and are described in detail by Rossow et al. (1987). The calibration of the operational instruments was particularly difficult and is described in Rossow and Schiffer (1991).

The data archived here are the Stage C2 data, which consist of monthly averaged cloud properties, so it is relevant to describe the ISCCP cloud-analysis procedure, as detailed in Rossow and Schiffer. The first step is cloud detection, which refers to the separation of individual pixels into clear and cloudy categories. Using the B3 data for one month, time composite background clear VIS and IR radiance fields are estimated for each location and time within that month. The key assumptions are that radiances in clear areas are less variable than in cloudy scenes and that clear areas are the "darker" and "warmer" parts of the VIS and IR spectra. Each radiance value from the B3 data is then compared to its corresponding time composite clear estimate. Cloudy pixels are identified as those pixels different from the clear background by some threshold amount. Different thresholds are applied over land and ocean, which leads to some differences in cloud amount between the two different geographic types (illustrated in section 4.1). The thresholds

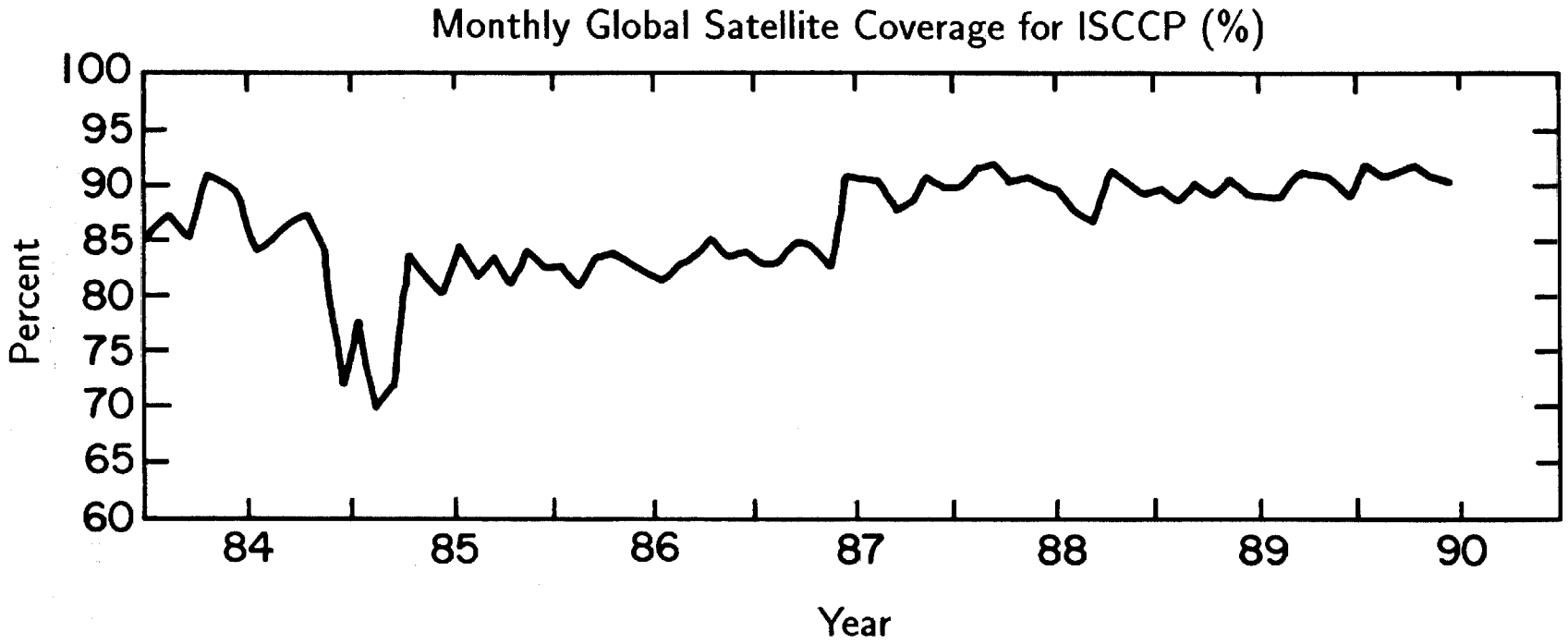

Figure 3. Percent of global coverage provided by geostationary and polar-orbiting satellites for ISCCP from July 1983 (from Rossow, personal communication).

are based upon the noise level of the estimated clear radiances, and each pixel is labeled to indicate the position of its radiance value relative to the magnitude of uncertainty in the clear value. Thus, besides clear and cloudy pixels, marginally cloudy pixels are those barely detected as cloudy and probably represent thin cirrus clouds and low-level broken clouds. This method can be accused of being prone to errors, but it was chosen for simplicity and robustness in the presence of a variety of sensor systems from the different satellites and earth surface geography.

After a pixel is identified as cloudy or clear, the measured radiances are compared to the results of a radiative transfer model. The model simulates the radiances that would ideally be measured by the satellites as a function of surface visible reflectance and temperature for clear scenes and cloud-optical thickness and cloud-top temperature for cloudy scenes. Data from the Television Infrared Operations Satellite (TIROS) Operational Vertical Sounder (TOVS) for each location and time account for the effects of the atmosphere on the radiances. Details of the radiative model and analysis are given in Rossow and Schiffer (1991) and are not summarized further here.

In order to correspond to other climate archives and typical GCM resolutions, the pixel-level estimates are averaged into 280-km equal-area bins by calculating the average values of cloud and surface properties, as well their standard deviations. The results from all satellites are then merged to produce Stage C1 data. The merging of statistics is governed by the rule that only data from one satellite are reported for each grid cell. The criteria for choosing the satellite are based on a preference for continuous time records and on limiting the satellite zenith angle.

Stage C2 data are monthly averaged results from the C1 data. More detailed properties are available in the C1 data if one wishes to prepare different averages. Average cloud, surface and atmospheric properties contained in the C2 data archive are given in Appendix 4. The average spatial and time deviations of the C1 data are also archived. Monthly averages are made for eight 3-hour periods (00, 03, 06, 09, 12, 15, 18 and 21 UTC), and the complete monthly mean is a result of averaging these eight sets. All nine averages have been processed and archived for each available variable given in Appendix 4. Besides total cloud information, average cloud properties for ten different cloud types are also reported. These cloud types are summarized in Fig. 4 (Fig. 4 in Rossow and Schiffer 1991). Low, middle and high clouds are defined solely by cloud-top pressures obtained from

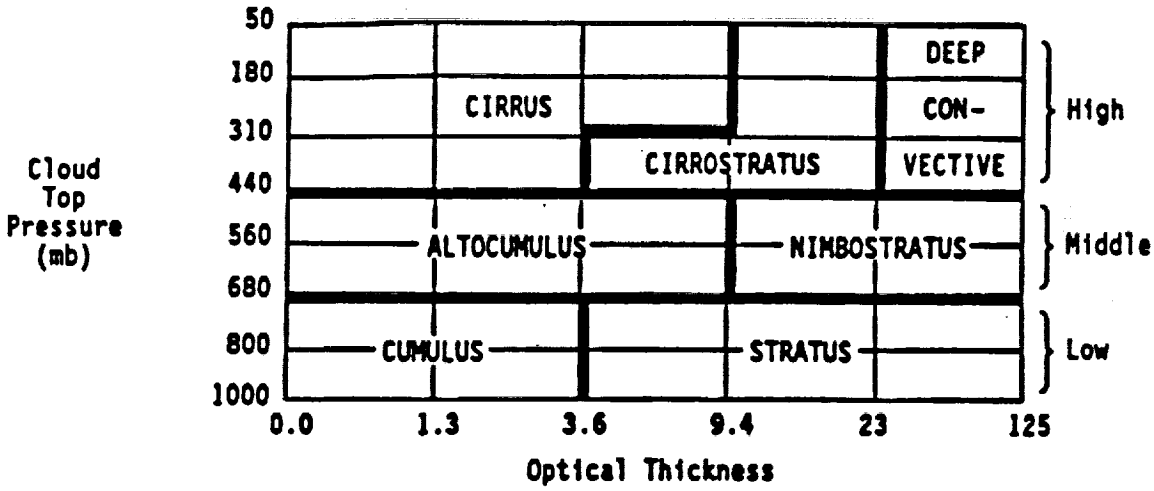

Figure 4. Schematic defining the ten ISCCP cloud types by their cloud-top pressures and optical thicknesses (from Rossow and Schiffer 1991). Low, middle and high clouds are defined by cloud-top pressures from IR data only.

IR data only. Thus, they give the diurnal variations of the vertical distribution of cloudiness. The remaining seven cloud types are for daytime only by combining cloud-top pressure and optical-thickness information. This leads to large areas of missing data in the diurnal resolution products for the daytime-only properties.

The overall absolute accuracy of the cloud data is difficult to assess because the definition of a cloud is inherently an arbitrary threshold test. To help determine the effects of changing the magnitude of the radiance thresholds, the average properties of marginal clouds are also archived. Marginal clouds represent the change in cloud amount that would occur with a change in the temperature threshold.

For studies of interannual variability, it must be recognized that biases are introduced by the movement and failure of some satellites throughout the record. For example, some areas have ranged from a sampling eight times per day by a geostationary satellite to a sampling by two or even one polar-orbiting satellite for different months. This aliasing effect is identifiable in plots of monthly mean data, and variables which document the time sampling of the ISCCP data have been archived (Appendix 4).

Another subtle bias in the analysis is that the cloud amount increases with view zenith angle, an effect of limb darkening or larger optical depth with steep view angles. At low latitudes, the data generally are reported from geostationary satellites. If the primary satellite is not available, the missing data are replaced by an adjacent geostationary satellite (subject to zenith angle restrictions) or, if available at the desired time, a polar-orbiting satellite. Polar orbiters provide all of the data in polar regions.

Daily weather fluctuations provide an additional uncertainty that affects the monthly mean cloud data. An estimate of this bias can be gathered from the within-month variance fields recorded in the archive for several of the variables. It is also possible to estimate the error by comparing the fields derived from IR only with IR plus VIS cloud amounts. These are listed separately in the archive. Cloud estimates near the poles over ice are very inaccurate and are subject to a planned reanalysis of the ISCCP data in the near future (Rossow, personal communication). The basic assumption that clouds are brighter than clear areas often fails over ice. A three-channel method using AVHRR data will be implemented for this improved analysis.

Currently, Stage C2 data have been accessed and archived from July 1983 through June 1988 (Appendix 4). ISCCP data collection and processing will continue through 1995, and the archive will be updated as the data become available.

2.3 Earth Radiation Budget Experiment (ERBE)

The ERBE of NASA is a multisatellite project that is measuring the broadband components of the earth's radiation balance to a high degree of accuracy with diurnal resolution (Barkstrom 1984; Barkstrom et al. 1989). Data collection for ERBE began in early 1985 and involves three satellites: NOAA-9, NOAA-10 and the Earth Radiation Budget Satellite (ERBS). The onboard instrumentation includes both scanner and nonscanner packages. Two wide-field-of-view (WFOV) and two medium-field-of-view (MFOV) radiometers and a solar monitor comprise the nonscanner package. Luther et al. (1986) provide a detailed description of the ERBE instruments. The pairs of radiometers provide simultaneous observations of both the total spectrum (from 0.15 to greater than 200 μm) and the shortwave (0.2 to $\sim$ 4.5 μm) portion. The scanner packages (see Kopia 1986) measure the total and shortwave spectra as well as longwave radiation in the spectral band from about 6 to $\sim$ 35 μm.

The ERBS is in a 57° inclined orbit which allows the satellite to precess over a given location through all hours of the day over a period of roughly 36 days. Consequently, the complete diurnal cycle over that time period can be sampled and, when combined with the sun-synchronous NOAA satellites, more precise estimates can be obtained of regional broadband radiation budgets than has been possible in the past.

Barkstrom et al. (1989) give an overview of the ERBE data reduction, the validation criteria and the types of data archived. The first step in data reduction involves converting telemetry counts to instrument irradiation. Ground and in-flight calibration sources were used in the conversion algorithms. The second step involves computing top-of-the-atmosphere-fluxes using the inversion techniques described by Smith et al. (1986). Finally, the fluxes must be averaged over time and space, as described by Brooks et al. (1986). Instantaneous data are first averaged within geographic regions, and then time series from a single satellite are broken into separate time series for each region. Regional time series between different satellites are merged and, finally, the series for each region are interpolated and averaged in space and time. These averaging procedures are necessary be-

cause of the variety of view angles and observation times of the satellites. While the nonscanner packages are still in operation, the scanners did not operate on all satellites for an extended period. The scanner on ERBS failed at the end of February 1990, and the scanners on NOAA-9 and NOAA-10 failed in January 1987 and May 1989, respectively. This uneven sampling makes it difficult to compare different years of measurement.

The data archived here are the so-called S-4 data products, which are monthly shortwave and longwave fields. The nonscanner data have been excluded because of considerable uncertainty about their interpretation (from minutes of a 1990 ERBE Science Team meeting). Scanner data, which provide an analysis resolution at 2.5° from original nadir radiances at approximately 30-km resolution, have been archived from February 1985 through December 1988. The archived fields are listed in Appendix 5 and represent only a sample of the total number of fields provided by ERBE. The fields most similar to standard GCM-derived fields have been selected.

The clear-sky fluxes listed are averages of radiances screened for the presence of cloud using a maximum likelihood cloud detection scheme (Wielicki et al. 1989). This scheme checks the IR and VIS radiances against a climatology of clear radiances derived from Nimbus-7 Earth Radiation Budget measurements (section 2.4). Therefore, the ERBE clear-sky climatology is constructed by saving data only for those times when no clouds are detected by the retrieval algorithm. Still, the error bounds of the retrieval scheme will allow for some clear-sky radiances that are actually contaminated by clouds, and some truly clear scenes will be excluded in the time-average analysis. An additional problem is that, in areas with large cloud amount, only a few clear radiances may be obtained in a month leading to sampling errors. The clear-sky products are thus less accurate than the mean fluxes. The quality of the clear-sky data is discussed in more detail by Harrison et al. (1990).

Care must be taken when comparing GCM results with ERBE clear-sky composites. As discussed by Cess and Potter (1987), one technique in GCMs is to sample the clear-sky radiation whether or not cloudiness actually occurs. They refer to this as "Method II," while "Method I" is based on sampling the clear-sky fluxes only when clouds do not occur. Obviously, the latter more closely corresponds to the ERBE observational approach. When both approaches are tested with GCM output, significant differences can occur (Harshvardhan et al. 1989).

The ERBE data products are complex combinations of data and models and, therefore, their uncertainties are difficult to assess. Barkstrom et al. (1989) estimate that regional monthly averages of scanner data have uncertainties of $\pm$ 5 W m^{-2} for both the shortwave and longwave channels. The uncertainty in the global annual average net radiation is also about $\pm$ 5 W m^{-2}, an estimate based on the differences of four "validation" months (April, July and October 1985; January 1986) that were intensely analyzed by the ERBE Science Team (1986). The fundamental radiometric accuracy of the individual radiances is high, but the need for radiance to flux conversion (inversion) and diurnal and monthly averaging leads to most of the error.

2.4 Nimbus-7

The Nimbus-7 spacecraft flies in a sun-synchronous, near-polar orbit which provides near-local noon and near-local midnight observations of most of the earth. The satellite was launched in October 1978 and has produced several long-term data sets of potential interest: the Earth Radiation Budget (ERB) observations, the cloud amounts derived from the Temperature Humidity Infrared Radiometer (THIR) and the Total Ozone Mapping Spectrometer (TOMS) (both narrow-band instruments), and the solar backscatter ultraviolet (SBUV) ozone measurements. The ERB and THIR/TOMS cloud estimates are related since the cloud amounts are derived for the analysis of ERB data. These two data sets are discussed below. The ozone data set may be incorporated later into this archive.

- Earth Radiation Budget (ERB)

Like the ERBE instruments, the Nimbus-7 ERB system incorporated a scanner to provide high-resolution radiances and a separate WFOV instrument to provide fluxes at satellite altitude. The experiment is described in detail by Jacobowitz et al. (1984). The scanner operated between November 1978 and June 1980. Because of this short duration, the scanner data have not been included in this archive. The WFOV radiometers are still operating on Nimbus-7 and are capable of measuring the shortwave (0.2–3.8 μm) and total longwave (0.2–50 μm) outgoing components of the Earth's radiation budget at satellite altitude. Kyle et al. (1984) describe the ERB WFOV calibration adjustments. Observations of ERB WFOV fluxes have been analyzed from November 1978 to October 1987 and are included in this archive (Appendix 6).

The basic spatial resolution of the WFOV measurements is about 1500 km, which provides a smoothed version of the earth's radiation budget. The basic measurement is flux at satellite altitude ($\approx$ 955 km), which is then inverted to the top-of-the-atmosphere flux by the simplest $(R_E + h)^2 / (R_E + h_o)^2$ adjustment, where R_E is the radius of the earth, h is the satellite altitude and h_o is the altitude at the top of the atmosphere. Deconvolution methods are available, but they amplify the noise.

The accuracy of Nimbus-7 ERB measurements is not as good as with ERBE data because the calibration of the detectors is not as accurate and the analysis scheme is much simpler (Jacobowitz et al. 1989). Also, there has been a systematic degradation of the response of the short-wave flux observations because the transmission of the filter window has decayed over time. This effect has been removed by calculating the trend in the global mean fields and appropriately adjusting the data. Trend detection on the large scale from this instrument, therefore, is not possible. Despite these problems, comparisons of monthly mean fluxes between simultaneous ERBE and Nimbus-7 ERB measurements are very good (Kyle et al. 1990), except for the resolution differences (Campbell et al. 1987). Examples are presented in section 4.2. The Nimbus-7 ERB data set may be better than ERBE for estimating the interannual variability of the monthly mean radiation budget because of its longer time interval and consistent viewpoint.

• Cloud-Matrix (CMATRIX)

A global multilevel cloud-climatology data archive for the interval April 1979 through March 1985 has been created from Nimbus-7 THIR and TOMS measurements. The algorithms used to derive the climatology and the validation and description of the data set have been comprehensively described by Stowe et al. (1988, 1989). Cloud data have been produced for ascending (local noon) and descending (local midnight) passes of the satellite and have been averaged into monthly means. Thus, diurnal variations about these two times can be studied, but the diurnal resolution is less than for ISCCP data.

As for the ISCCP data set, a brief description of the algorithms used in estimating the cloud climatology is relevant. The 11.5 μm THIR radiances and the 0.36 μm and 0.38 μm TOMS ultraviolet (UV) reflectivities, together with concurrent Air Force surface temperature measurements, are the primary data sources for the cloud-detection algorithms. For sunlight overpasses, two independent estimates

of total cloud amount are produced from both a UV reflectivity algorithm and an IR algorithm, which are then combined to form a composite estimate. At nighttime, only the IR algorithm is used.

In the IR algorithm, each THIR 11.5 μm radiance observation (pixel) is classified depending on its magnitude relative to concurrent radiance thresholds. The final classifications include clear sky and low-, middle- and high-altitude cloud. The threshold technique is based on surface temperature estimates to within one-half hour of a Nimbus-7 overpass obtained from time interpolation of Air Force surface temperature analyses archived every three hours. Adjustments are made for errors due to variations in water-vapor attenuation, known systematic biases in the attenuation adjustment, horizontal gradients in the surface temperature field, and for partially cloudy radiometer fields of view (see Fig. 3 in Stowe et al. 1988). Pixels with radiative temperature differences that exceed the threshold criteria are labeled cloudy.

The definitions of low, middle and high clouds differ from the ISCCP definitions, so direct comparisons of the data sets are difficult. In the Nimbus-7 CMATRIX data, an altitude of 2 km separates low- from middle-level clouds. The middle- to high-cloud altitude separation is 7 km equatorward of 30° latitude, but it varies with latitude farther poleward. These definitions are consistent with those in the *International Cloud Atlas* (WMO 1956).

A primary weakness of the IR algorithm is its inability to detect low-altitude clouds, which have very little thermal contrast with the surface. The TOMS reflectance measurements are used largely to offset this weakness. UV reflectivities measured by TOMS are very low and highly uniform for both land and ocean scenes which are clear and snow-free, an advantage over visible reflectance which is highly variable over land. The UV algorithm is very simple and is based on a linear relationship between UV reflectivity and cloud amount (Stowe et al. 1988). For middle- and high-altitude clouds, UV reflectivities are highly variable because they are very sensitive to cloud-thickness variations as well as to changes in cloud amount. Due to the large thermal contrast of these types of clouds from the surface, the IR scheme is, therefore, more accurate. However, low cloud is easier for the UV algorithm to detect accurately because of the large contrast in reflectance between the low cloud and the snow-free surface.

Once the clear-sky and low-, middle- and high-cloud classifications have been made, the TOMS reflectivity data, together with the IR scheme, can be used to produce estimates of cirrus and deep convective clouds. Essentially, cirrus clouds are defined by low TOMS reflectivities in the presence of a substantial amount of cold high-altitude cloud detected by the IR threshold technique. A shortcoming is that only cirrus without underlying cloud can be detected. From this same principle, deep convective clouds are identified when the IR scheme detects a large amount of cold cloud and the TOMS reflectivities are high.

Several methods have been used to validate the Nimbus-7 cloud climatology, as well as the auxiliary meteorological data used in the IR and UV detection schemes (Stowe et al. 1988). From cloud amounts derived by an analyst using geostationary images, systematic errors in the Nimbus-7 cloud estimates were estimated to be less than 10%, and random errors ranged from 7% to 16%. These empirical error estimates were consistent with results obtained from a theoretical sensitivity analysis, although it must be remembered that the analyst also contributed systematic and random error to the comparison. Combining cloud estimates from the UV algorithm with those obtained from the IR algorithm changed the IR estimates by 10% or less; thus, the nighttime estimates should only be slightly less accurate than the daytime estimates outside the geographical regions where low clouds are prevalent. Cloud amounts over humid tropical regions were overestimated even when the UV agorithm was used, and cloud amounts over polar regions were less reliable because of the frequent presence of snow. A few limited comparisons with simultaneous monthly mean ISCCP observations will be presented in section 4.1.

The CMATRIX monthly mean data have been prepared in history tape format for April 1979 to March 1985. Many variables have been included in this archive, and they are listed in Appendix 6.

2.5 Outgoing Longwave Radiation (OLR) Data from NOAA

Estimates of the earth's total longwave emittance have been derived from several NOAA polar-orbiting satellites since June 1974. These data have been used extensively in many diagnostic and climate sensitivity studies and are perhaps most widely used for examining changes in tropical cloudiness and implied rainfall. Unfortunately, the quality of the data has been compromised by changes in satellites, their orbits, instrumentation and data-reduction procedures. Gruber

and Krueger (1984), Janowiak et al. (1985) and Chelliah and Arkin (1992) highlight many of these changes, and Gruber et al. (1983) give a detailed description of the data-reduction procedures, radiometric characteristics and orbital parameters.

One shortcoming of the NOAA OLR record is the sampling problem introduced by the changes in equator-crossing times of each spacecraft since June 1974. Table 1 lists the various NOAA satellites that have been used in constructing the data record, as well as their equator-crossing times. Notice that, after the scanning radiometer (SR) series from June 1974 to February 1978, no data were collected from March 1978 through December 1978. Biases introduced by sampling at different times of the day can be illustrated by a day-minus-night plot globally averaged OLR for each satellite. Such a plot is presented in Fig. 1 of Gruber and Krueger (1984) and shows diurnal differences on the order of 5-6 W m^{-2} for the TIROS-N and NOAA-7 portions of the record, but only 1-2 W m^{-2} for NOAA-6 observations which were near sunrise and sunset. In addition, the equator-crossing times for individual satellites have drifted with time. Corrections for these sampling errors are very difficult to determine and have not been applied to the archived data. Evidence indicates that OLR undergoes a diurnal cycle that is a function of geography and circulation regime. To minimize this error, day and night observations have been averaged to form daily values, and the daily values have been averaged into the monthly means archived here. Janowiak et al. (1985) discuss the fact that this approach appears to preserve the main features of the OLR data as well as their variation in space and time.

Changes in the procedures to estimate the total outgoing longwave emittance from the 11.5-μm channel radiometer measurements are another source of error in the data. This spectral channel is designed to be insensitive to water-vapor changes in the atmosphere, a caveat that should be kept in mind for GCM verification. Originally, an algorithm developed by Wark et al. (1962) was used to convert the window-channel measurements to total OLR, but additional studies by Abel and Gruber (1979) and Ellingson and Ferraro (1983) resulted in new algorithms. More recently, simultaneous measurements from Nimbus-7 of both the total longwave radiation flux (WFOV ERB) and the narrow-band radiance measurements from THIR allowed Ohring et al. (1984) to derive a new algorithm that was introduced 1 March 1983. They estimated that the previous alrogithms introduced a positive bias of 13 W m^{-2} in the OLR record with respect to the ERB data. Gruber and Krueger (1984) and Janowiak et al. (1985) present the equations

Table 1. Longwave radiation observations from NOAA satellites (Chelliah and Arkin 1992).

Satellite	Local Equator Crossing Times	Period of Record	Number of Months
NOAA SR Series (NOAA 2,3,4,5)	9:00a–9:00p	June 1974–Feb 1978	45
TIROS N	3:30a–3:30p	Jan 1979–Jan 1980	13
NOAA 6	7:30a–7:30p	Feb 1980–Aug 1981	18
NOAA 7	2:30a–2:30p	Sep 1981–Feb 1985	21
NOAA 9*	2:30a–2:30p	Feb 1985–Nov 1988	46
NOAA 11**	2:30a–2:30p	Nov 1988–present	

*At launch, NOAA 9 had equator-crossing times at 2:20a and 2:20p.
**At launch, NOAA 11 had equator-crossing times at 1:40a and 1:40p.

used to relate the adjusted flux values to the original flux values for each satellite, and these adjusted data have been archived here. While this approach corrects for different window-channel measurements between satellites, it does not, however, correct biases introduced by instrument drift on individual satellites.

The archived monthly NOAA OLR data exist in history tape format from June 1974 through December 1991 (March through December 1978 are missing). Updates of these widely used data will continue.

3. PROCESSING TECHNIQUES

The satellite data sets have been put into history tape format for use with the CCM modular processor. The CCM processor is a large set of software written for post-processing history tapes written by the CCM. It allows for the quick computation of many of the general circulation statistics commonly used for the analysis of CCM data. Output may be in the form of graphics, printed values and binary data written to a number of different types of save files. A comprehensive description of the capabilities of the CCM processor can be found in Wolski (1987, 1989).

All of the satellite data sets mentioned in section 2, with the exception of Nimbus-7 data, have been placed in CCM history tape format at a resolution of 2.5°, and they have also been transformed to a triangular wavenumber 42 (T42) truncation Gaussian grid ($\sim$ 2.8° resolution). The transformation was appropriately handled by passing each field through a cubic spline interpolation to the 128×64 grid. However, none of the fields was spectrally transformed or truncated at T42. Placing the data on the T42 grid facilitates comparisons with CCM output and other archived observational data [e.g., the ECMWF and National Meteorological Center (NMC) analyses described in Trenberth and Olson 1988a,b,c].

The ISCCP data were originally on equal-area grids so as to maintain a nearly constant statistical weight for results at all locations. Since data manipulation and graphical display are easier with rectangular arrays, however, the ISCCP data were transformed to 2.5° rectangular grids by replication, which preserves all of the original statistics (Rossow and Garder 1984). CCM history tapes of the 2.5° data were then produced, and the 2.5° analyses were used to interpolate to the T42 grid.

The Nimbus-7 ERB data were originally on 500-km equal-area grids. Since the ERB data are oversampled on this grid, however, it was decided to interpolate the equal-area analyses onto 4.5° rectangular grids. The relatively coarse 4.5° data were not, however, further interpolated to higher-resolution grids such as T42. Before comparing the ERB data with higher-resolution model data, the model data should be smoothed, perhaps by truncating to triangular wavenumber 15 (T15). For consistency, the CMATRIX data were treated in the same manner. Thus, the archived ERB and CMATRIX data provide smoother estimates of the radiation budget and cloud statistics than ERBE and ISCCP.

In cases of missing data, gridpoints were flagged by assigning a special value (1.E+36) that is well outside the normal range of values for any of the archived fields. Most of the computational algorithms within the CCM processor check for this special value and, when it is encountered, take appropriate action. For example, in the contoured graphics produced by the processor, missing data are ignored and appear as "holes" in the pattern of contour lines. When no data were available for an entire month, the month was still archived but with all gridpoints set to the special value. This simplifies the accessing and cataloging of the data. Users of the CCM processor can control how missing data affect further computations.

In addition to the basic fields for each data set, surface flags were made for T42, 2.5° and 4.5° resolution grids. The surface flags can be easily accessed from the Mass Store as described in Appendix 8. Certain algorithms in the CCM processor, such as horizontal area averaging with surface-type masking, allow the user to limit the processed data to points above a particular surface type. The typical surface-type data sets used with models such as the CCM flag land, ocean and sea-ice surfaces. For the type of data archived in this note, however, it did not seem useful to estimate climatological sea-ice distributions. Therefore, only land and ocean surfaces have been flagged.

Each individual archived month of data can be called and processed in the CCM processor with the Input Control Parameter (ICP) "DAYSc." For users unfamiliar with the processor, this terminology may be confusing. Since the archived satellite data consist of monthly means, each "day" actually refers to a month. It is desirable that each "day" have a unique and consistent label. Since the NOAA OLR data begin in June 1974, it was decided to set DAYSc = 1 to January 1974. For example, January 1984 data can be called by DAYSc = 121 and so on. Updates

will continue this format. A complete list of the "day" for each month of data is given in Appendix 2.

The archived monthly mean satellite data are in the form of CCM1 history tapes (ICP TYPEc = "CCM1"). A complete list of the fields for each satellite data set, their names (ICP FIELDcn) and units are listed in Appendices 3–7. The Mass Store pathnames and volume names for each monthly data set are also listed. Note that the smaller data sets (MSU, ERBE, Nimbus-7 ERB and NOAA OLR) are contained on single volumes, while individual months of the larger ISCCP and Nimbus-7 CMATRIX data sets are contained on separate volumes on the Mass Store.

Individual monthly mean time-average climatologies have been constructed for some of the data, and they have been written on separate volumes as time-average save tapes (TYPEc = "SAVTAV"). Appendices 3–7 provide a list of volume and pathnames on the Mass Store, the fields available and the names assigned in the archive. For some of the fields, climatologies were inappropriate to construct. Details are given in the Appendices.

4. RESULTS

The main purpose of this section is to intercompare some common months and variables from different data sets in order to highlight the types of data available and a few main issues of data quality. No attempt will be made to present all the data types or describe all possible intercomparisons. Some difficulties encountered when comparing the observed data with model data will be discussed. Future reports will present more detailed evaluations of the monthly satellite data, isolating biases and inhomogeneities in the data. It is possible that several atlases may be created.

For presentation purposes, global maps and time series of fields have been plotted with software outside of the CCM processor, and all of the fields in the global maps have been slightly smoothed. Essentially, the same plots can easily be reproduced using the processor examples in Appendix 9, but their publication quality is generally not as good.

4.1 Intercomparison of ISCCP and Nimbus-7 CMATRIX Cloud Statistics

• Spatial Distributions

The two largest data sets archived are the monthly ISCCP and Nimbus-7 CMATRIX cloud statistics (Appendices 4 and 6). As mentioned in section 2.2 and illustrated in Fig. 4, the ISCCP low-, middle-, and high-cloud types are defined by cloud-top pressure from IR data only, and cloud-top pressure and optical-thickness information from daytime-only satellite passes are combined to define the remaining seven cloud types. These definitions fundamentally differ from those of CMATRIX, where predefined altitudes are used to separate low-, middle- and high-cloud amounts (section 2.4). Thus, intercomparisons of the two data sets are difficult.

One field that is more comparable is total cloud cover. Figure 5 illustrates the zonally averaged total cloud cover, as depicted by ISCCP and Nimbus-7 CMATRIX, for July 1984 and January 1985. In July 1984, both data sets indicate zonal peaks in the middle latitudes of both hemispheres, and a maximum is also evident just north of the equator close to the mean latitude of the Intertropical Convergence Zone (ITCZ). Minima are associated with Hadley circulation subsidence in each hemisphere. In polar latitudes, the total cloud estimates are less reliable since the surface is often covered by snow and there is normally little thermal contrast between the surface and even high clouds. Satellite retrieval of polar cloud amount is difficult and requires further study (Stowe et al. 1989). The zonal plot for January 1985 (Fig. 5b) reflects a shift of the monsoon circulations to the summer hemisphere and a broadening due to increased convection in the northwest-to-southeast oriented South Atlantic and South Pacific convergence zones (SACZ and SPCZ). A seasonal (equatorial) movement of the Northern Hemisphere (NH) middle-latitude total cloudiness maximum is also observed.

Figures 6 and 7 show the global spatial distribution of the total cloud cover for July 1984 and January 1985. In the tropics, the ITCZ in July 1984 is marked by maximum cloud amounts over and near equatorial land masses, especially off the west coasts of Africa and America. Both the ISCCP and the CMATRIX data indicate maxima greater than 90% associated with the Asian monsoon, and high total cloud amounts are present over the west Pacific. Maxima are also observed in the storm tracks of the North Atlantic and North Pacific, in the coastal stratus region west of South America and in the Southern Hemisphere (SH)

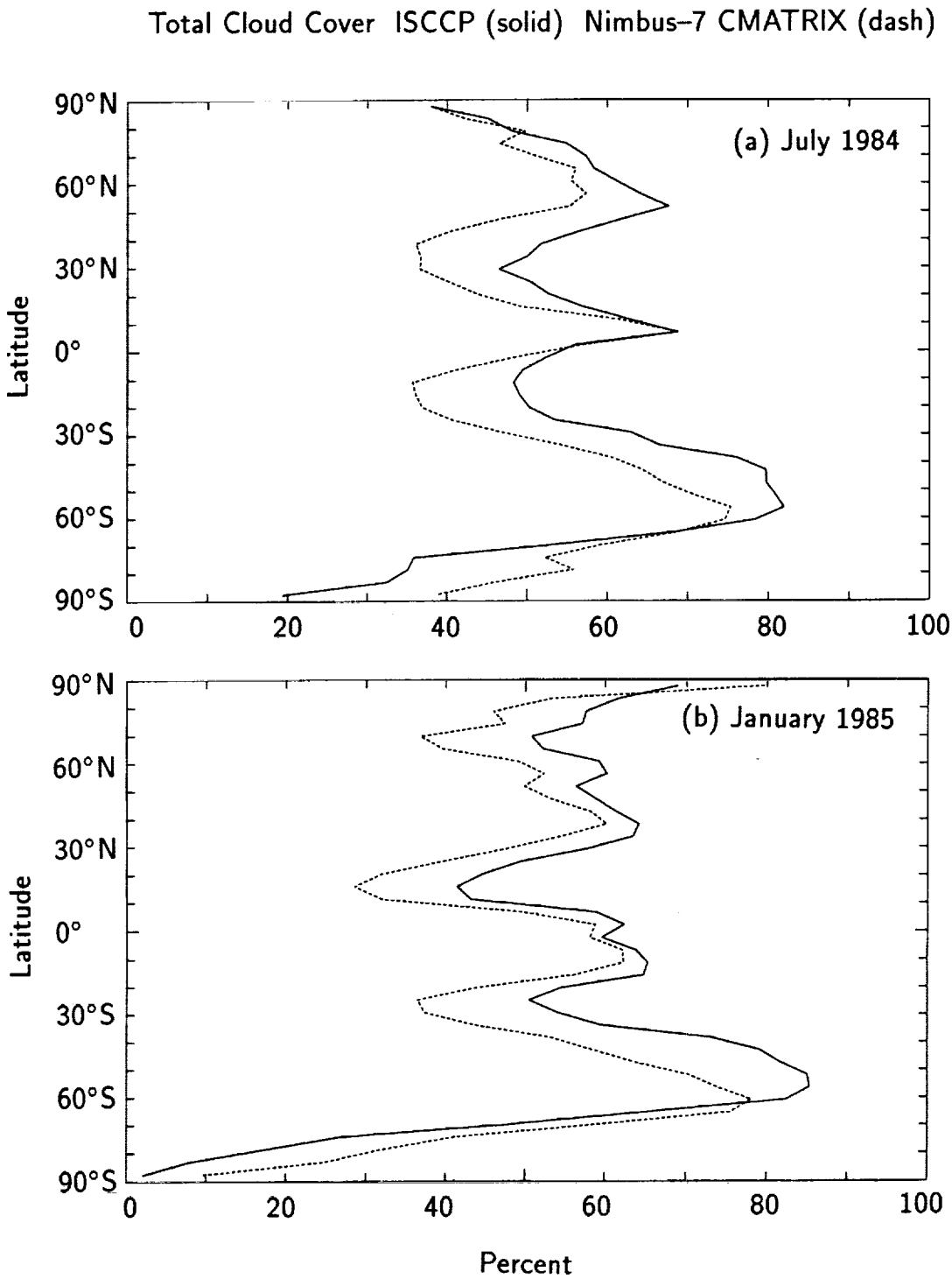

Figure 5. Zonally averaged total cloud cover from ISCCP (solid) and Nimbus-7 CMATRIX (dash) expressed in percent for (a) July 1984 and (b) January 1985.

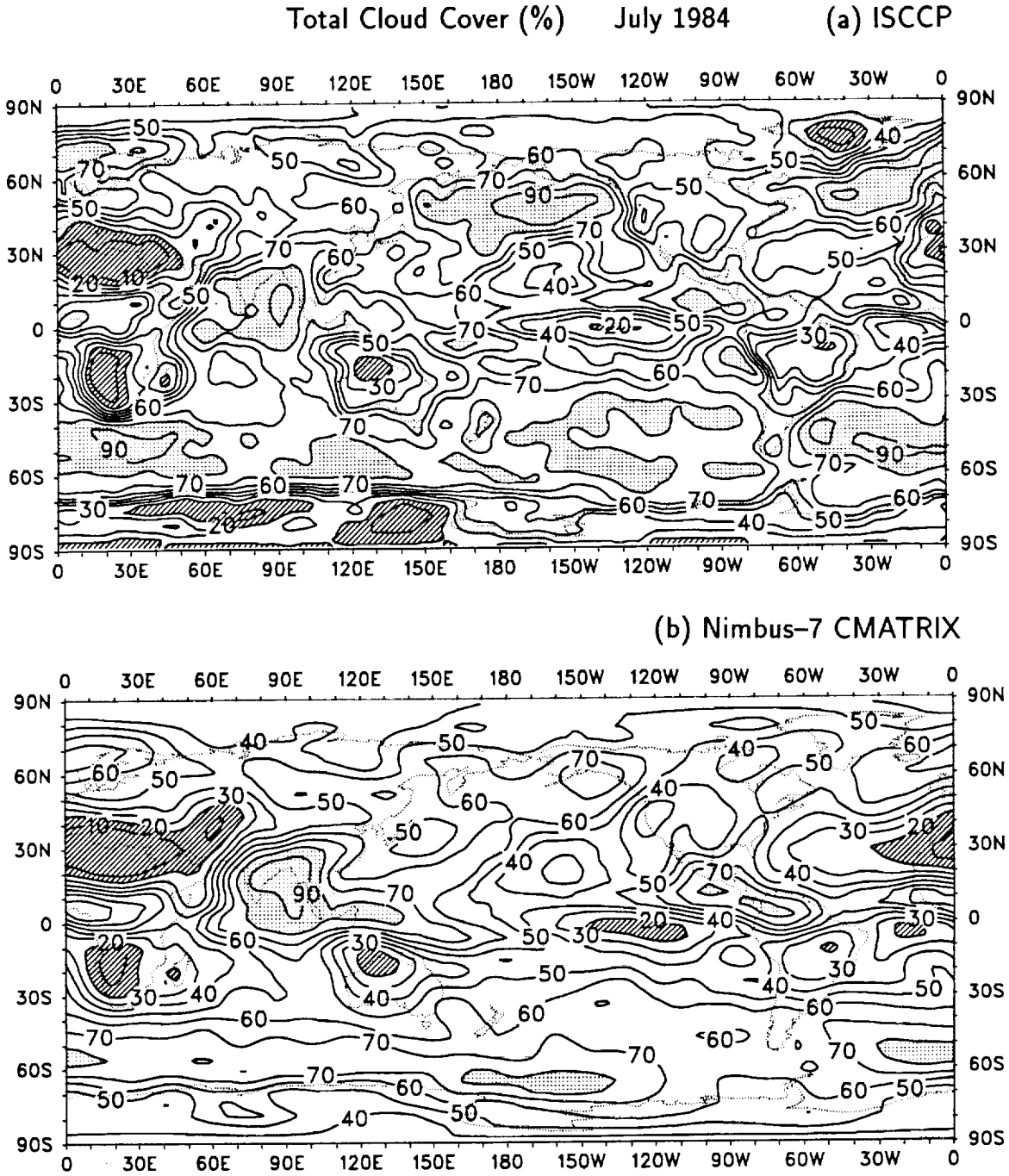

Figure 6. Total cloud cover in percent for July 1984 from (a) ISCCP and (b) Nimbus-7 CMATRIX. Cloud cover less than 20% is indicated by hatching and cloud cover greater than 80% is indicated by stippling. The contour increment is 10%.

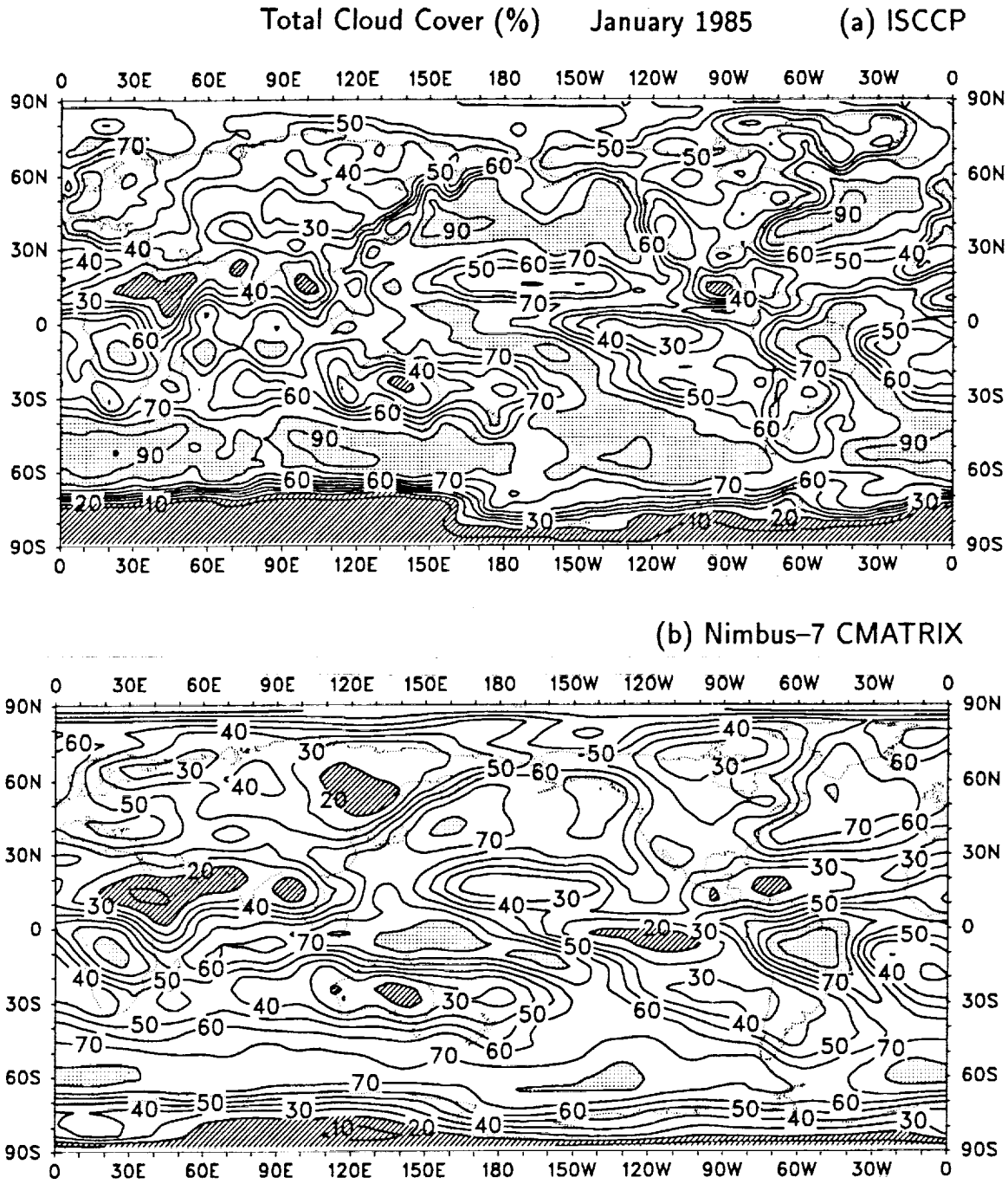

Figure 7. As in Fig. 6 except for January 1985.

between 40° and 60°S. Minimum total cloud amounts are associated with the semipermanent subtropical high-pressure zones in the NH subtropics over the Atlantic and Pacific oceans, the African, Middle Eastern and Australian deserts, the western United States, and the dry zone over the eastern Pacific near the equator.

Both the ISCCP and CMATRIX total cloud estimates reflect major seasonal circulation transitions. In January 1985 (Fig. 7), extensive cloudiness from the SPCZ and SACZ is evident in the tropics and SH subtropics, and the total cloud cover increased substantially from July 1984 over South Africa. Cloudiness is much lower over the Asian monsoon region, and the subtropical high-pressure belts over the NH oceans are farther south. Low cloud percentages are also evident in the areas of the Siberian and Canadian high-pressure centers. Note that the different thresholds applied over land and ocean in the ISCCP analysis (section 2.2) often lead to sharp gradients in cloud cover between the two geographic types.

It is clear from the above figures of total cloud cover that the Nimbus-7 CMATRIX estimates are lower than the simultaneous monthly mean ISCCP observations, and this applies over the entire time span of the data sets as well (see Fig. 12). These differences can be further illustrated by examining different levels of clouds, even though their definitions differ between the two analyses. High and low cloud amounts for July 1984 and January 1985 are shown in Figs. 8–11. Both data sets indicate similar high cloud amounts for July 1984 (Fig. 8), with maxima over the Asian monsoon region and along the ITCZ from west of Central America across the Atlantic into central Africa. By January 1985 (Fig. 9), high clouds are prevalent over the deep convective regions of South Africa, the SPCZ and the SACZ, and high cloud cover has increased in the NH over the Pacific and Atlantic storm tracks. In general, ISCCP high cloud amounts are greater than Nimbus-7 CMATRIX estimates. Large differences are observed over polar regions between the data sets in both months, primarily as a result of large high-cloud percentages over the winter pole in the CMATRIX data. Again, polar cloud amounts should be interpreted with caution.

Poor agreement between the cloud estimates can be seen in plots of low cloud cover (e.g., Figs. 10 and 11), which can often be obscured by higher clouds from the satellite view. Low cloud cover is most prevalent over the oceans, especially in the marine stratus regimes. In general, much more low cloud is detected in the ISCCP algorithms than in CMATRIX. Rossow and Schiffer (1991) discuss this disagreement and suggest that it can be partially traced to differences in the

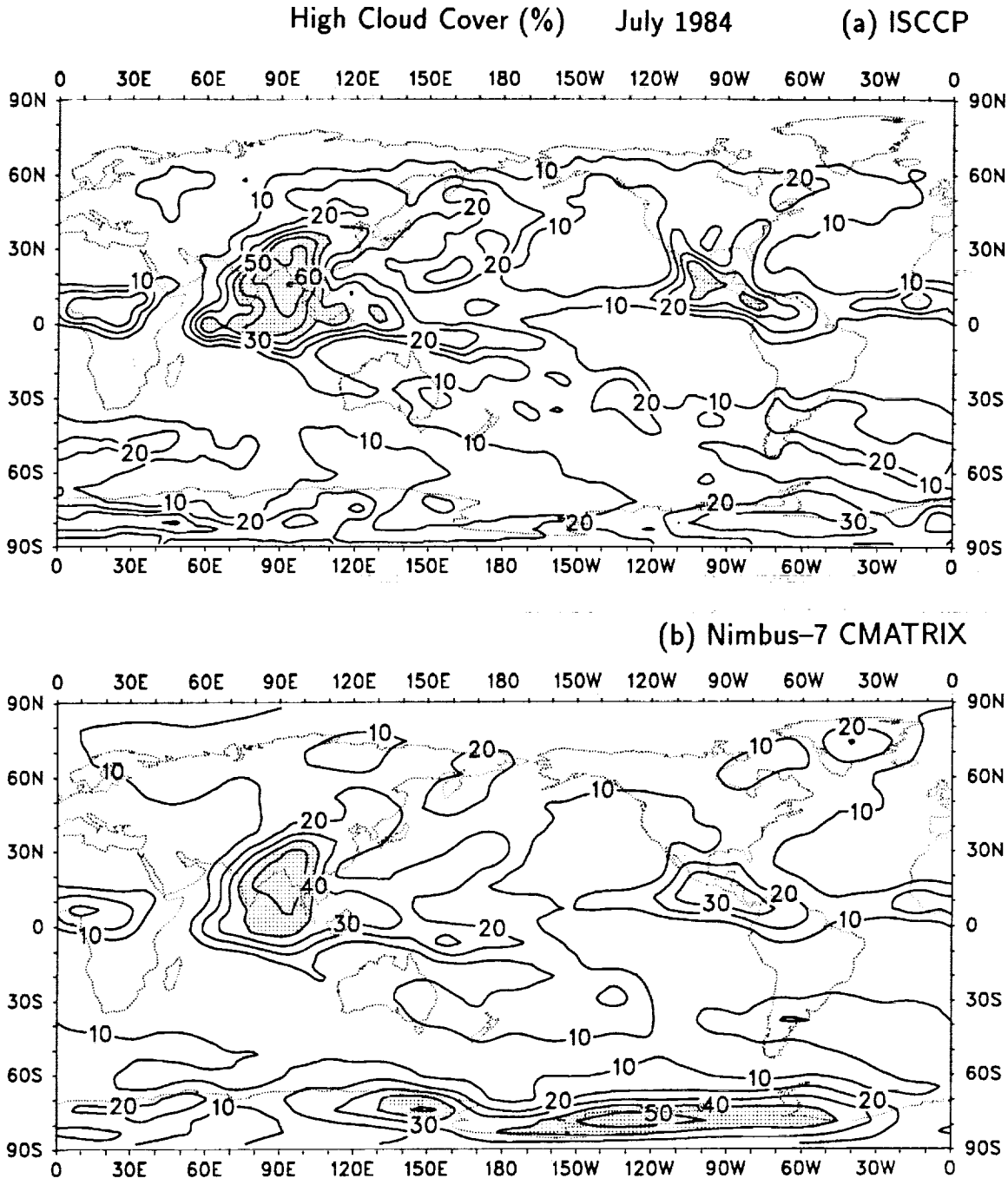

Figure 8. Percent occurrence of high cloud for July 1984 from (a) ISCCP and (b) Nimbus-7 CMATRIX. High cloud cover greater than 40% is indicated by stippling. The contour increment is 10%. The comparison is complicated by different definitions of high cloud between ISCCP and CMATRIX.

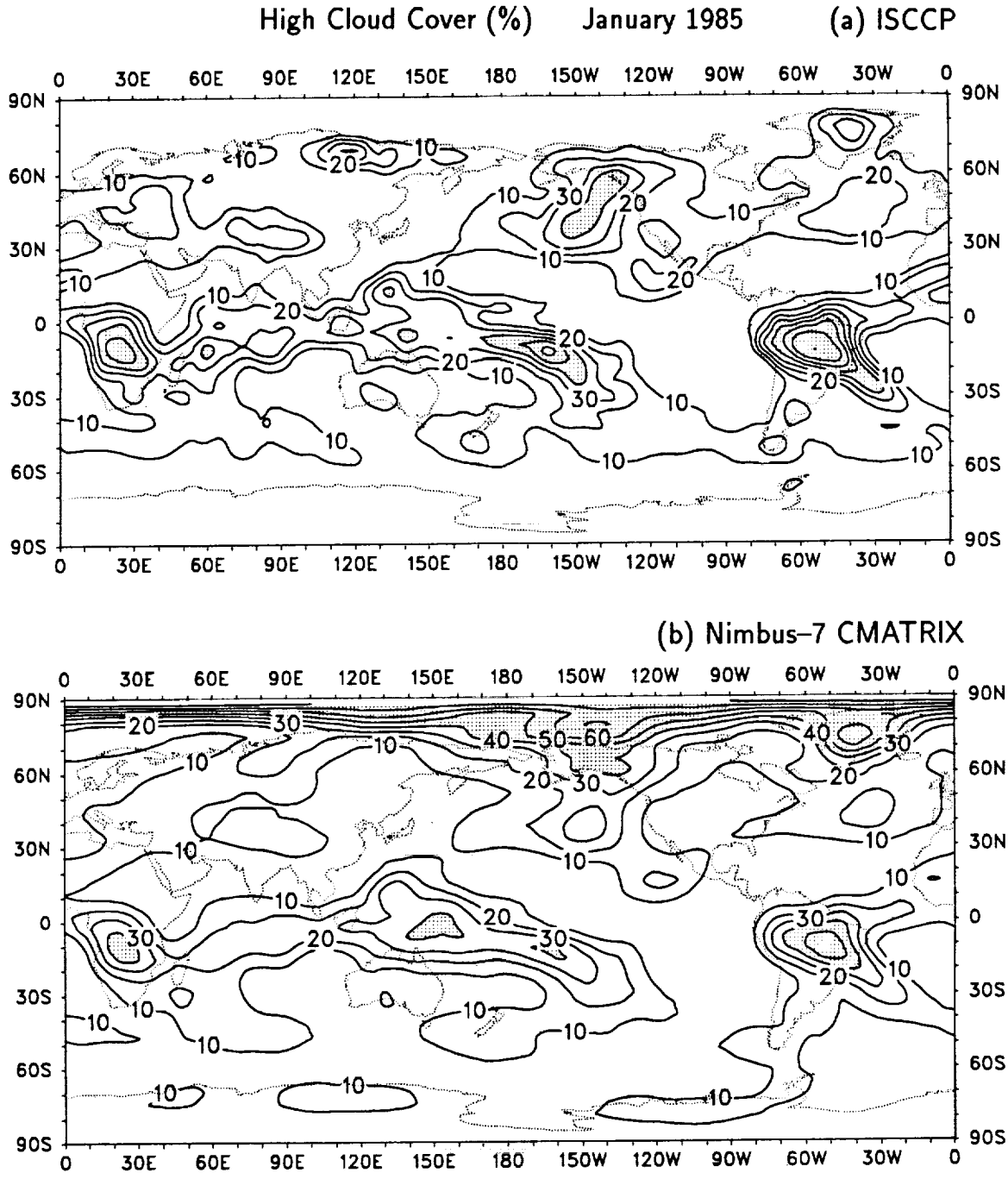

Figure 9. As in Fig. 8 except for January 1985.

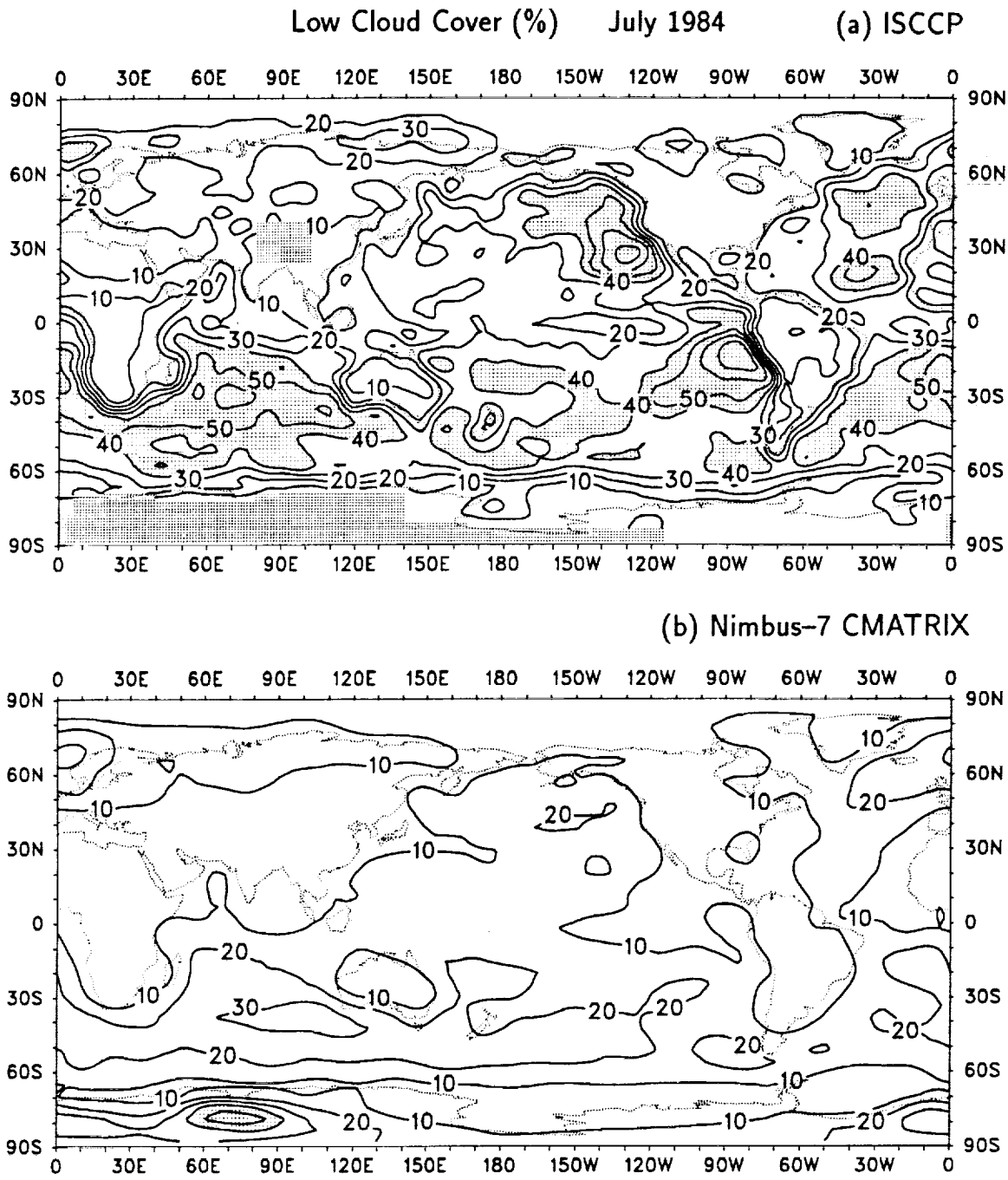

Figure 10. Percent occurrence of low cloud for July 1984 from (a) ISCCP and (b) Nimbus-7 CMATRIX. Low cloud cover greater than 40% is indicated by stippling. The contour increment is 10%. The comparison is complicated by different definitions of low cloud between ISCCP and CMATRIX. Missing data in the ISCCP analysis are also indicated by stippling in high surface elevation regions.

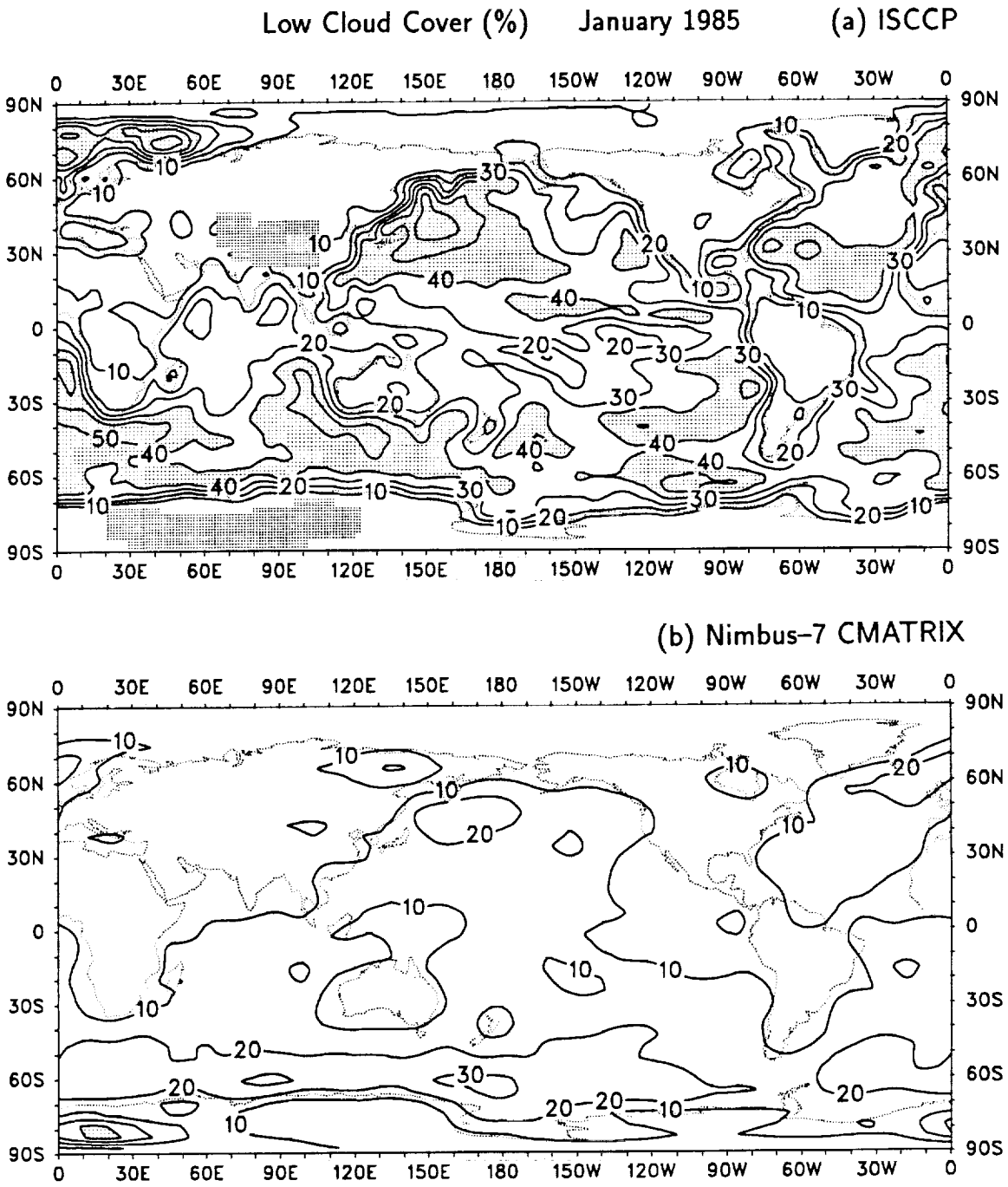

Figure 11. As in Fig. 10 except for January 1985.

magnitudes of the temperature thresholds used in each data set. Namely, the ISCCP analysis employs a much smaller IR threshold, so more cloudiness for simultaneous time periods is recorded, especially at low levels. Rossow and Schiffer report that, if the ISCCP results are modified by using a threshold closer to that of the Nimbus-7 analysis, differences lessen and become more random. Over land, the two cloud analyses have closer thresholds and show better agreement for all cloud types and total cloud cover (see Fig. 13a). Again, such comparisons are difficult because of the different definitions of cloud types between the data sets.

Comparisons of the ISCCP and CMATRIX cloud data with a surface-based cloud analysis (Warren et al. 1986, 1988) indicate a better agreement for the ISCCP data, even in marine stratus regimes (Rossow and Schiffer 1991) . Although it is tempting to conclude that the ISCCP threshold may be more appropriate, such comparisons do not resolve a number of other complexities (e.g., geometry differences, diurnal sampling differences, etc.) and may include some cancellation of errors. Both data sets have weaknesses and strengths, and one should not be viewed as better than the other. A major advantage of the Nimbus-7 data is that the satellite viewpoint has remained consistent with time, which makes the data valuable for studies of interannual variability. The effect of the changing coverage of ISCCP (Fig. 3) on the cloud estimates is difficult to determine without further analysis.

• Area Averages

Another way to examine the satellite data is to compare time series of large regional means. Although mean fields tend to be dominated by the seasonal cycle, it is important that this harmonic be understood and documented. Moreover, for comparisions with model output, it is important that the model be able to accurately simulate the seasonal cycle. A focus of this report is on examining total cloud amounts from ISCCP and Nimbus-7 CMATRIX.

Figure 12 illustrates the globally averaged monthly total cloud amount from ISCCP and CMATRIX. The two solid curves are both ISCCP total cloud estimates. The lower curve is variable "ISCCP72" in the archive and represents the "unadjusted" total cloud amount, while the upper curve is variable "ISCCP08" and represents the "adjusted" total cloud amount. Details are given in Appendix 4, but the adjustments made to ISCCP08 include VIS/IR adjustments applied to the nighttime IR data and some small corrections made to account for incomplete

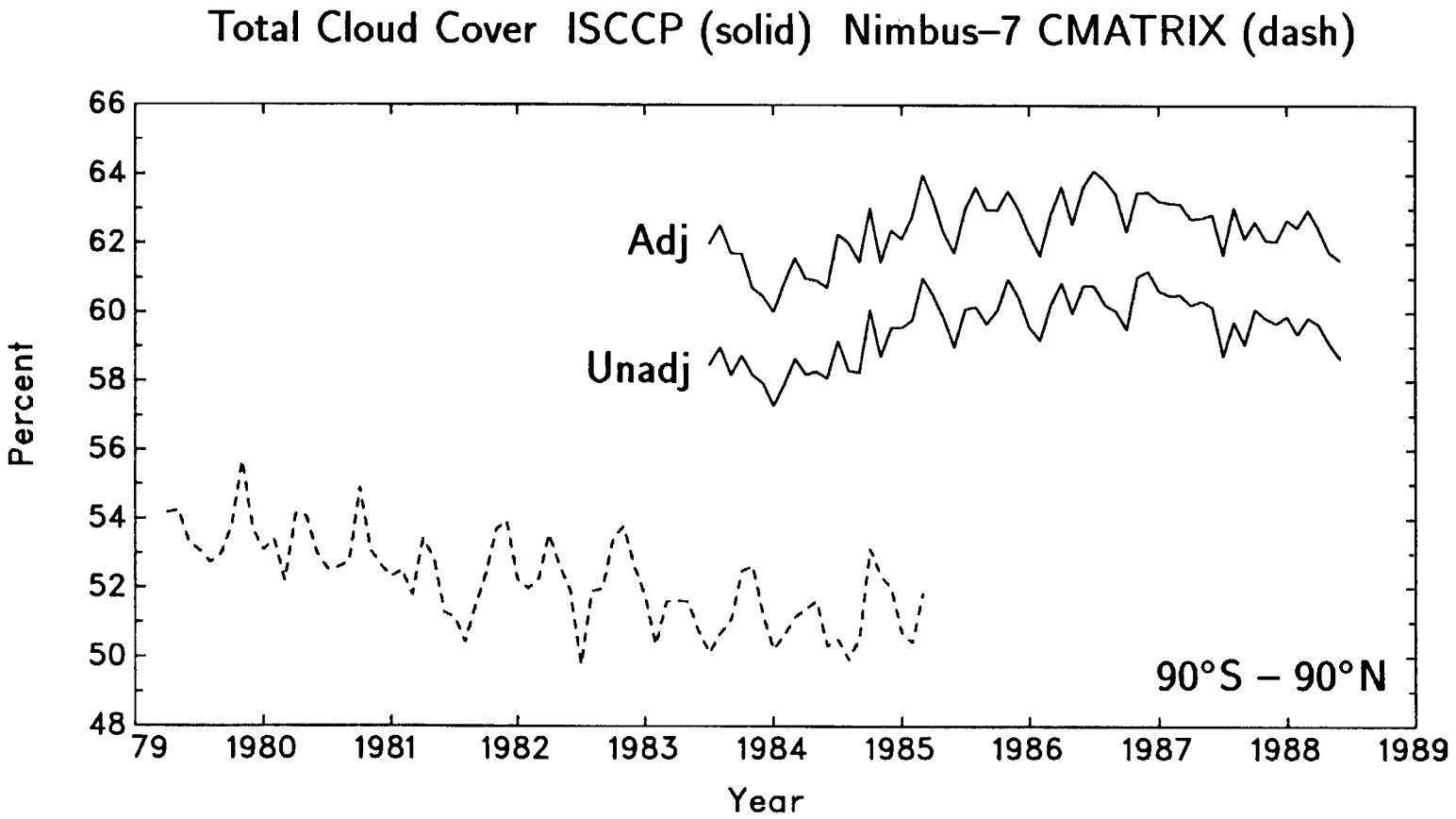

Figure 12. Time series of monthly total cloud cover averaged over the globe from ISCCP (solid) and Nimbus-7 CMATRIX (dash). The lower solid curve from ISCCP represents the "unadjusted" total cloud estimate (see text for details).

sampling of the diurnal cycle. The net effect of these changes is to increase the total cloud estimates by about 3%, except at the polar latitudes of both hemispheres where adjustments are smaller at the summer pole and zero at the winter pole. The unadjusted cloud estimates have been shown in all previous plots only because they are the estimates previously published by Rossow and Schiffer (1991).

The global monthly unadjusted total cloud amount shown in Fig. 12 for ISCCP averages $\approx$ 60% and is clearly about 6 to 8% higher than the Nimbus-7 CMATRIX estimates. Other older climatologies are in better agreement with the lower CMATRIX estimates (Hughes 1984). However, these earlier estimates may be lower partly because of incomplete global coverage, especially over portions of the SH oceans. The lower sensitivity of the CMATRIX algorithm has already been discussed. The newer ground-based climatology described by Warren et al. (1986, 1988) reports a global annual mean cloud amount of $\approx$ 63%, closer to the adjusted ISCCP estimate.

Time series of total cloud estimates are shown in Fig. 13 averaged over land only and ocean only areas (an option of area averaging in the CCM processor). Both ISCCP and CMATRIX estimate higher cloud percentages over marine regions than over land. Also, the estimated total cloud coverage over land is in general agreement in the two data sets, while over oceans differences are on the order of 10–12%. This illustrates the similarity of the thermal thresholds over land between ISCCP and CMATRIX, while larger threshold differences occur between the schemes over ocean.

The total cloud estimates averaged over both hemispheres are shown in Fig. 14, and averages over the tropical western Pacific (15°S–15°N, 120–180°E), tropical eastern Pacific (15°S–15°N, 180–90°W) and the Indian summer monsoon region (0–30°N, 70–100°E) are shown in Fig. 15. The annual cycle is evident in both hemispheres (Fig. 14), with maximum cloud amounts in summer. Higher percentages in the SH are consistent with fewer landmasses. During overlapping months, the two cloud data sets exhibit similar fluctuations over the limited tropical regions (Figs. 15a,b). The 1982-83 El Niño shows up clearly in the CMATRIX total cloud data, while the ISCCP data appear to capture a cloud maximum in the eastern Pacific associated with increased convection during the 1987 warming event. Both cloud estimates capture the very strong signal of the summer monsoon circulation over India (Fig. 15c), with area-averaged seasonal cloud amounts varying from approximately 30% in winter to over 80% in summer.

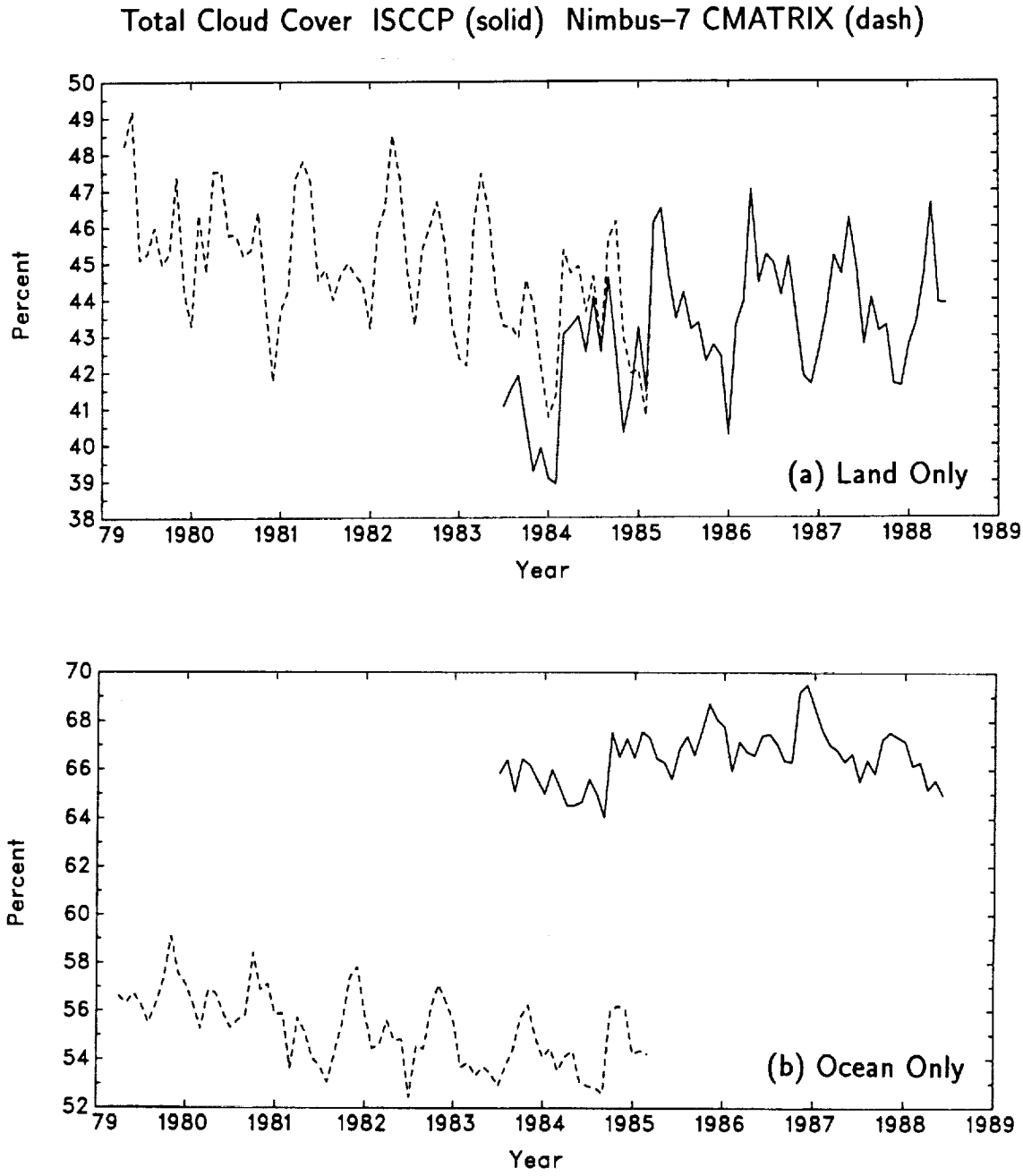

Figure 13. Time series of monthly total cloud cover from ISCCP (solid) and Nimbus-7 CMATRIX (dash) averaged over (a) global land areas and (b) global ocean areas.

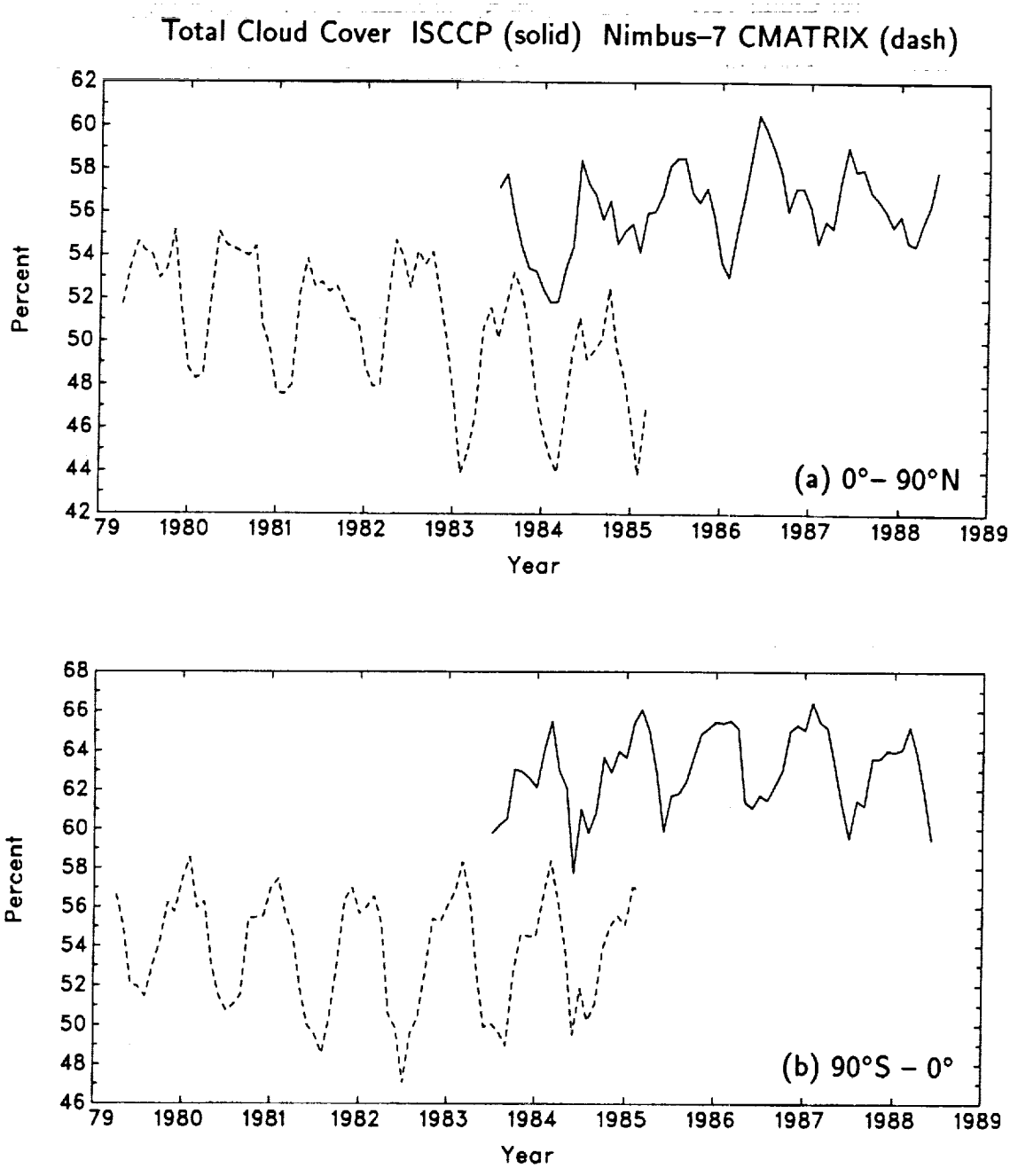

Figure 14. Time series of monthly total cloud cover from ISCCP (solid) and Nimbus-7 CMATRIX (dash) averaged over (a) the Northern Hemisphere and (b) the Southern Hemisphere.

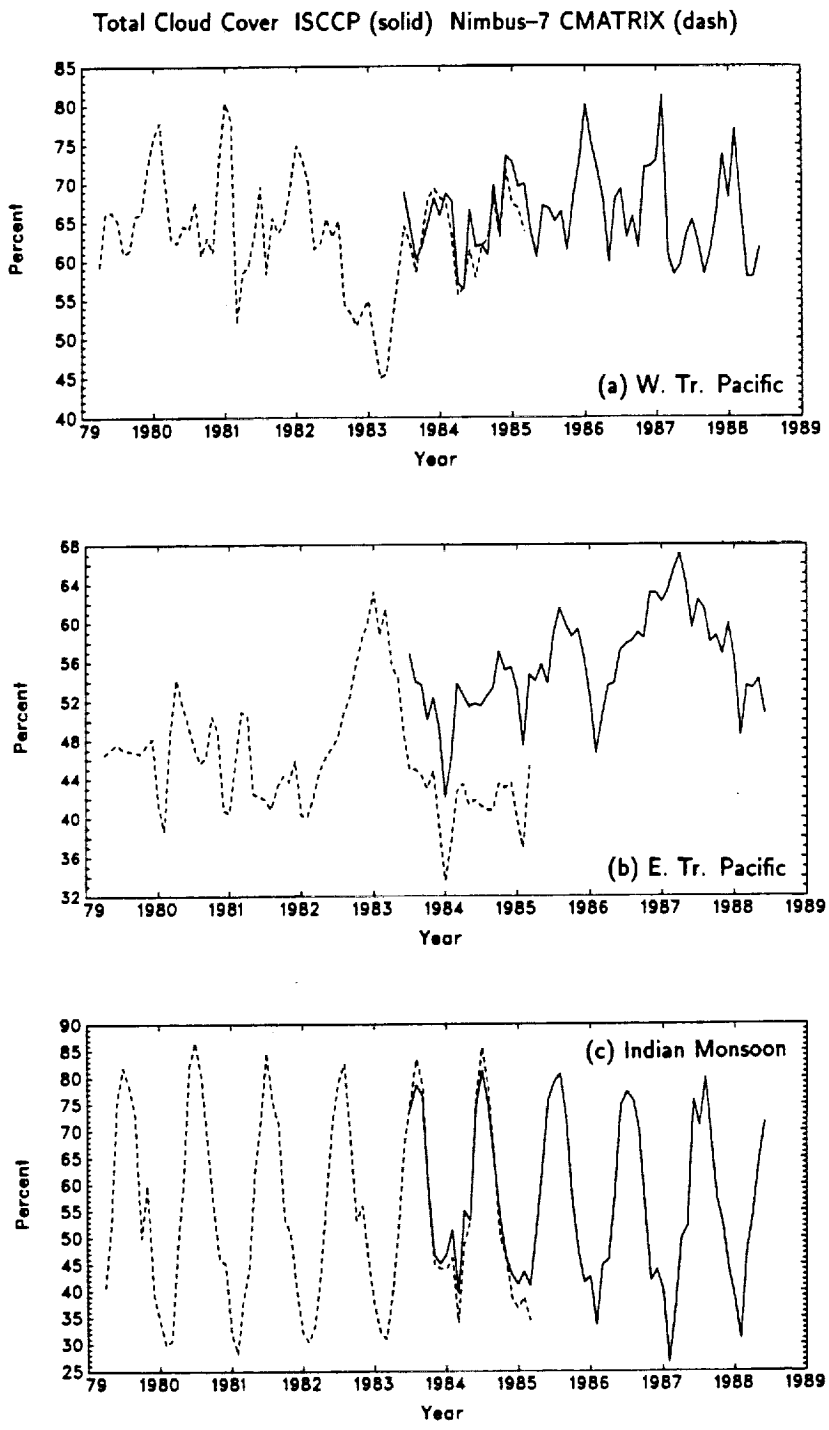

Figure 15. Time series of monthly total cloud cover from ISCCP (solid) and Nimbus-7 CMATRIX (dash) averaged over (a) the western tropical Pacific, (b) the eastern tropical Pacific and (c) the Indian summer monsoon region. The regions are defined in the text.

4.2 Intercomparison of ERBE, Nimbus-7 ERB, and NOAA OLR data

• Spatial Distributions

As with the cloud products, ERBE and ERB have a variety of products that can be intercompared. Here, OLR has been chosen since it is a commonly examined variable and is also available from the NOAA satellites. Figure 16 illustrates the OLR fields for July 1985 from ERBE, NOAA and ERB, and Fig. 17 illustrates the fields for January 1986. In tropical regions, low values ($\approx$ 225 W m^{-2} and less) of OLR are often used to indicate the presence of cold high cloud tops associated with deep convection and precipitation. In July 1985 (Fig. 16), deep convection is implied over the Asian monsoon and tropical western Pacific, and low OLR values are also in the vicinity of the ITCZ just north of the equator from the eastern Pacific across the Atlantic into Africa. Higher values ($\geq$ 275 W m^{-2}) are observed in the subtropical dry zones of both hemispheres. By January 1986 (Fig. 17), the major tropical convective centers have shifted to south of the equator and extend from central Africa across the Indian Ocean into the western Pacific and SPCZ, and strong convection is also implied in the SACZ. Again, regions of subsidence are marked by the higher tropical OLR values.

The spatial distributions of OLR in Figs. 16 and 17 are similar in all three data sets. The Nimbus-7 ERB data are much smoother because of the large field of view of the sensor. For a more consistent comparison of the large-scale circulation features, the ERBE and NOAA OLR fields were truncated to T15 and placed on the ERB 4.5° rectangular grid. The results are shown in Fig. 18 for July 1985 and Fig. 19 for January 1986. Although the general spatial patterns agree, differences in the magnitudes of OLR are evident among the three data sets. Before comparisons are made between Nimbus-7 ERB data and higher-resolution model data, a similar approach should be adopted by truncating the model output.

A more quantitative comparison between the OLR fields from ERBE, NOAA and Nimbus-7 ERB is given by the scatter plots in Figs. 20 and 21. Each point in a scatter plot represents an individual gridpoint value from the two data sets compared. Each data set was sampled from 70°S to 70°N, and the ERBE and NOAA data were sampled from the T42 archived data. Comparisons of OLR from ERBE with Nimbus-7 ERB were made using the truncated ERBE data shown in Figs. 18a and 19a. The superimposed fit lines are from an area-weighted least-squares fit between the two data sets. Three lines are plotted: one minimizes

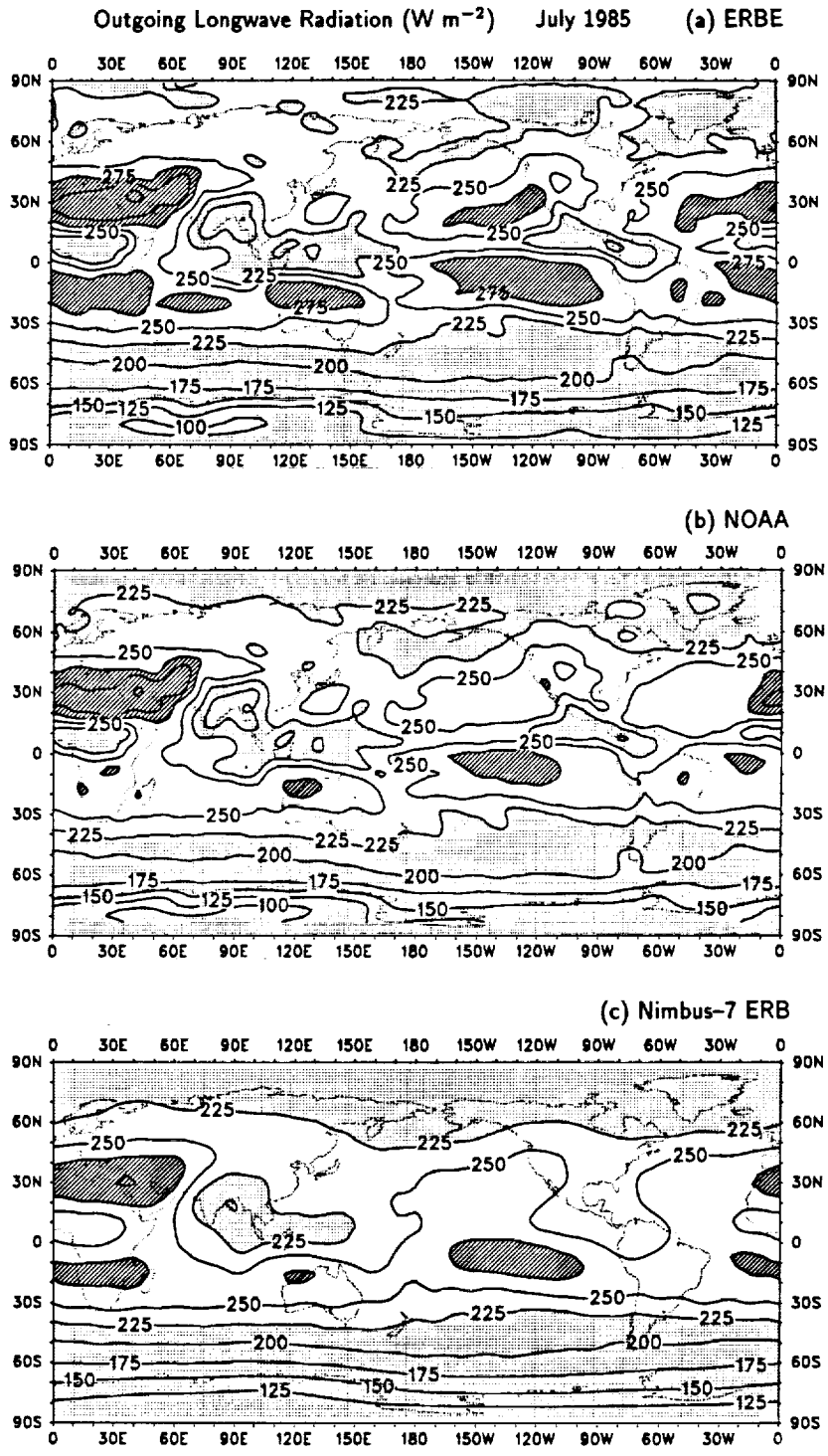

Figure 16. Outgoing longwave radiation in W m^{-2} for July 1985 from (a) ERBE, (b) NOAA and (c) Nimbus-7 ERB. Values less than 225 W m^{-2} are indicated by stippling, and values greater than 275 W m^{-2} are hatched. The contour increment is 25 W m^{-2}.

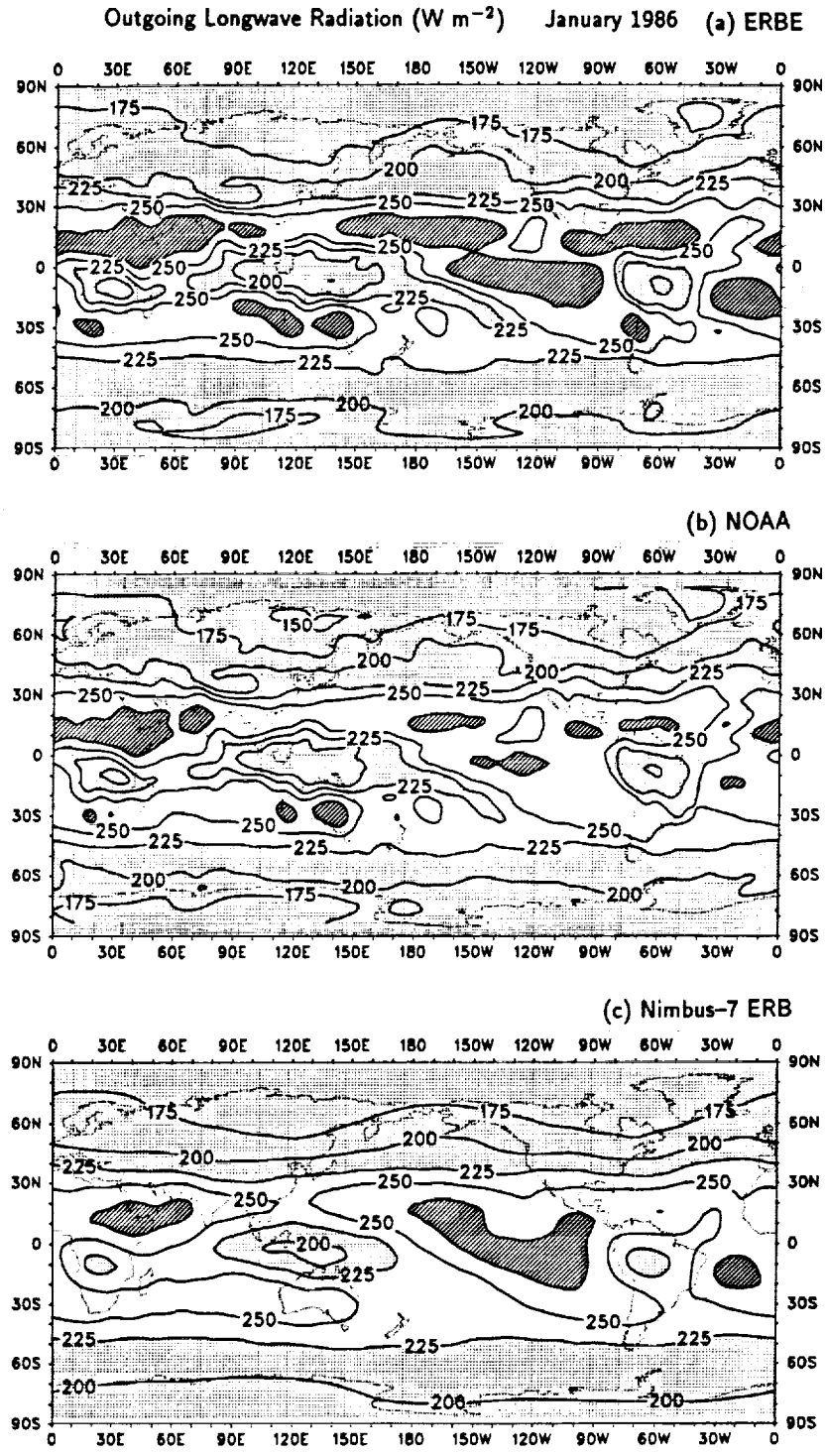

Figure 17. As in Fig. 16 except for January 1986.

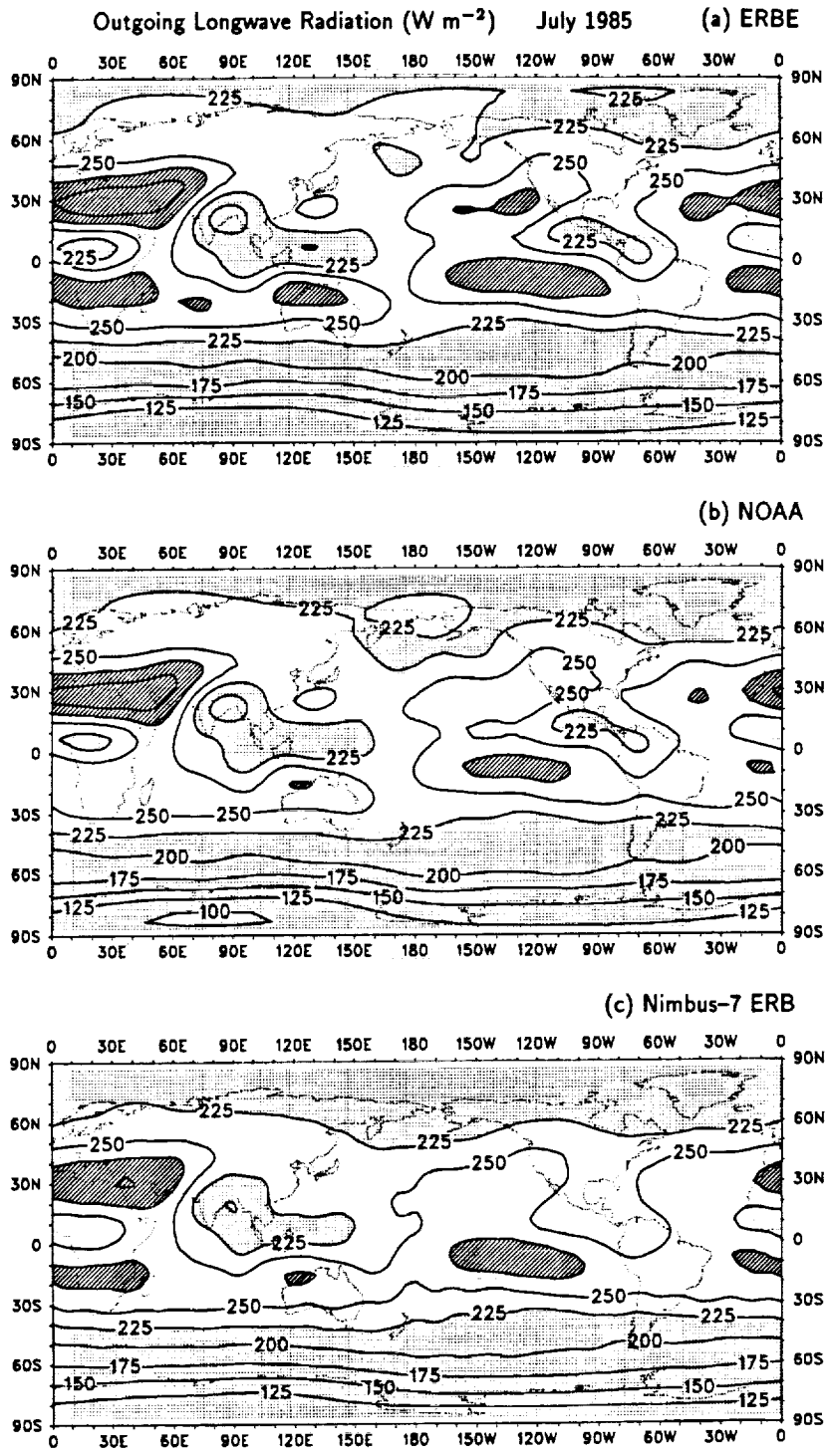

Figure 18. As in Fig. 16 (July 1985) except the (a) ERBE and (b) NOAA OLR data have been truncated to T15 and placed on a 4.5° rectangular grid for a more direct comparison with the (c) Nimbus-7 ERB measurement.

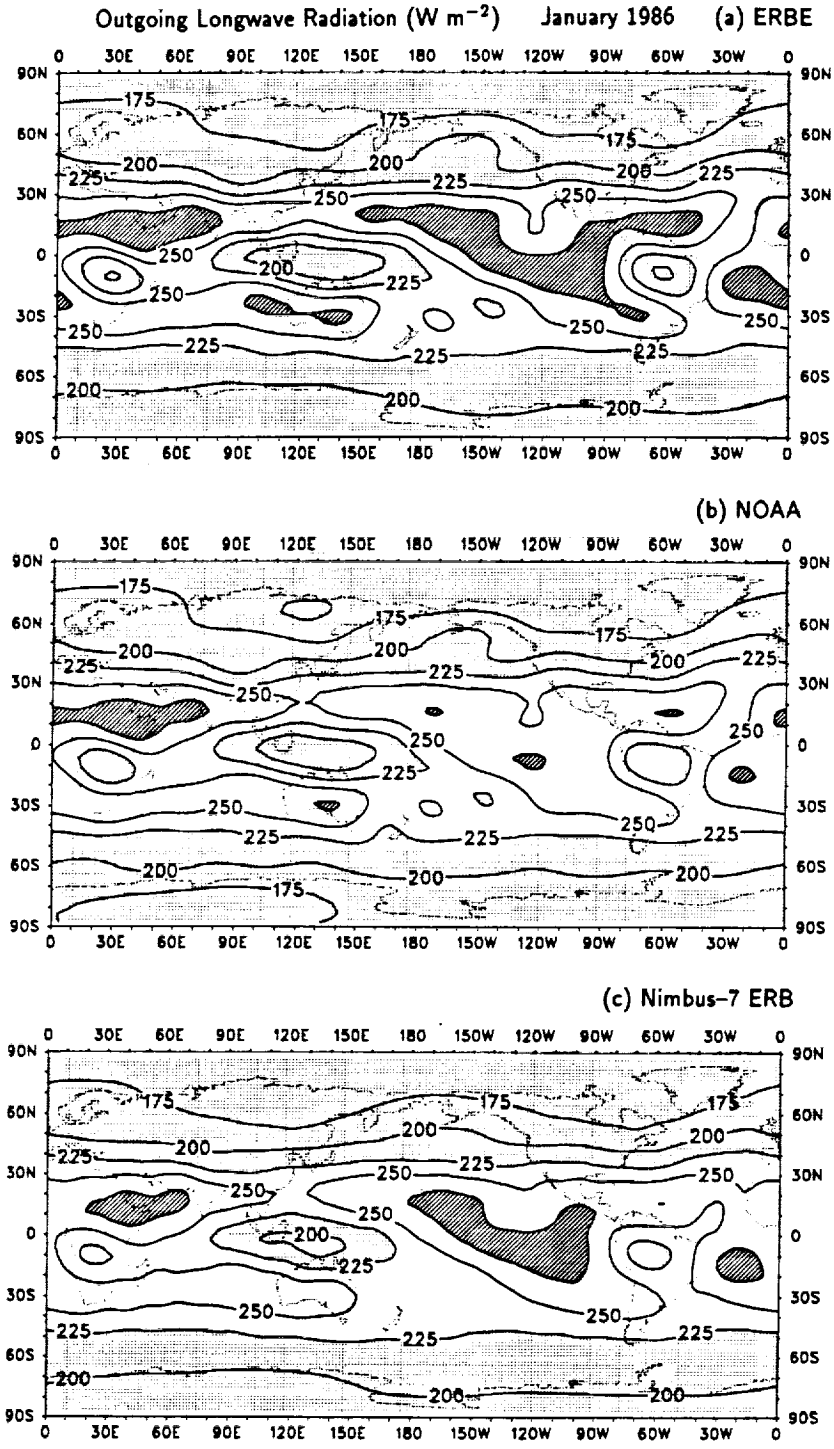

Figure 19. As in Fig. 18 except for January 1986.

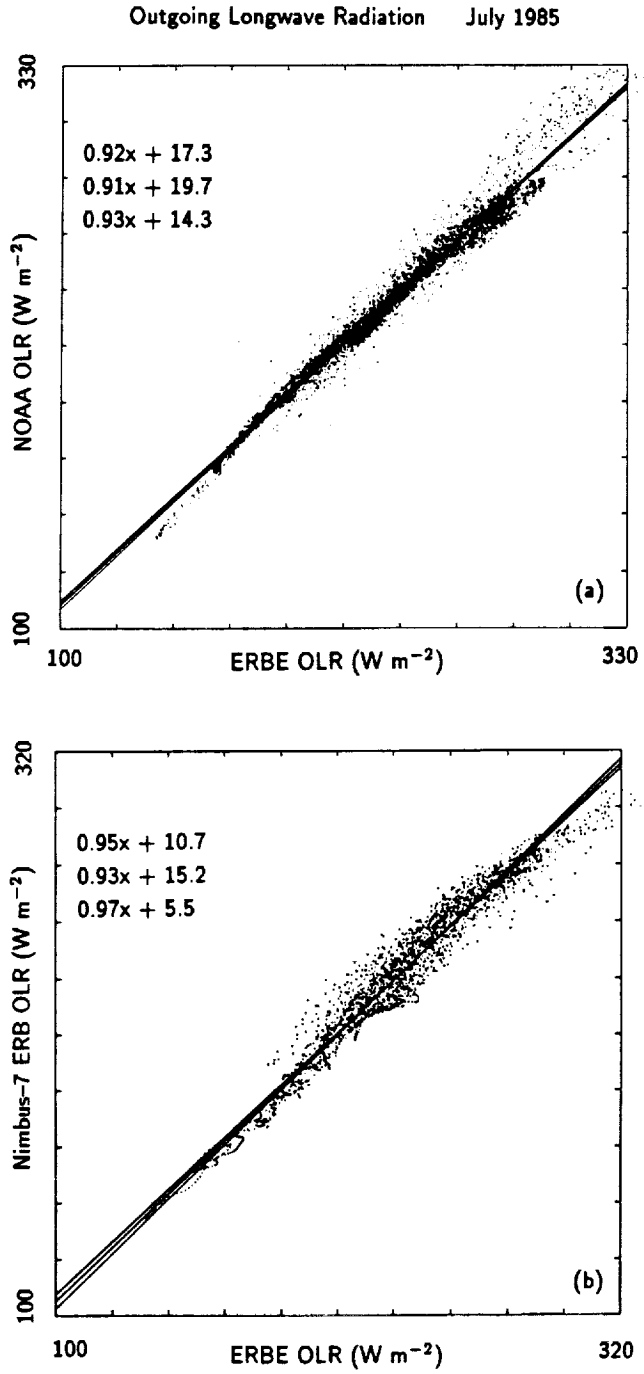

Figure 20. Scatter plot of outgoing longwave radiation for July 1985 from (a) ERBE and NOAA and (b) ERBE and Nimbus-7 ERB. Each point in (a) represents a gridpoint on the T42 grid sampled between 70°S and 70°N, while each point in (b) is sampled between 70°S and 70°N from the 4.5° resolution grid with ERBE data truncated to T15.

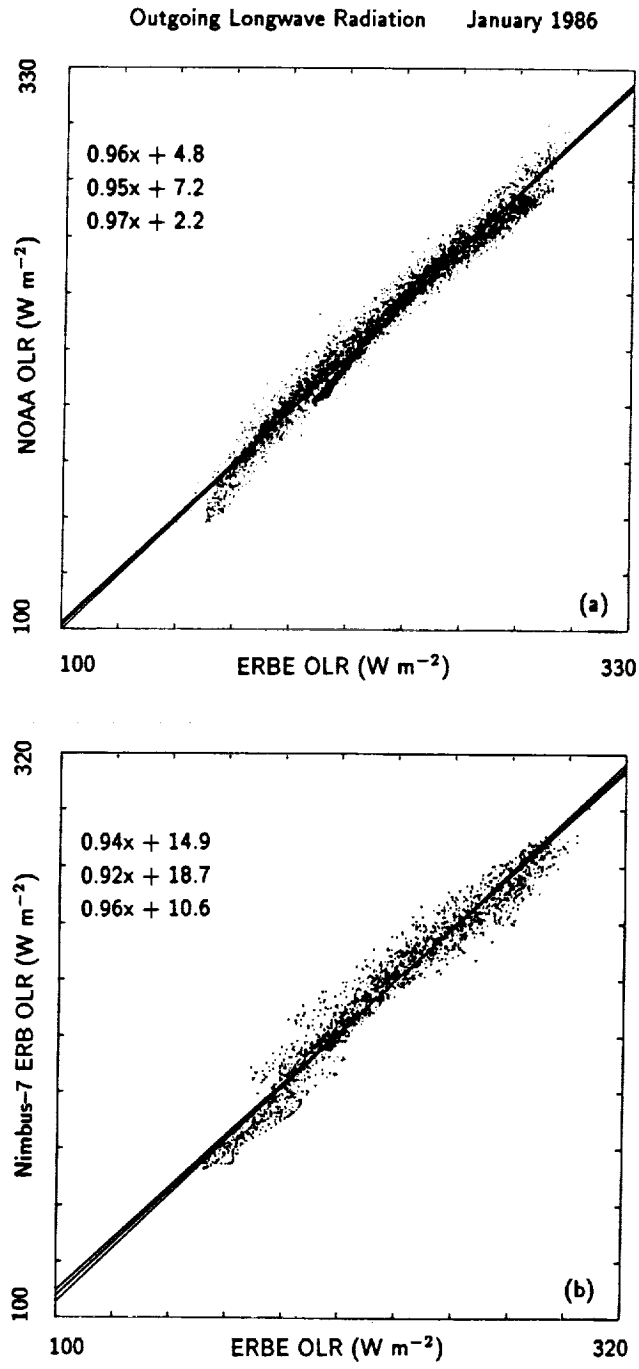

Figure 21. As in Fig. 20 except for January 1986.

the perpendicular distance (top), one minimizes the sum of x^2 deviations (middle) and the third minimizes the sum of y^2 deviations (bottom). The slope and intercept of the three lines are shown in the upper left corner of each plot.

The scatter between the NOAA and ERBE OLR fields for July 1985 (shown in Fig. 20a) is relatively narrow. However, the slopes are different from 1.0, which illustrates that the two OLR estimates have been calibrated differently. The NOAA data have been empirically calibrated from narrow-band radiances into broadband fluxes by a comparison to simultaneous measurements from Nimbus-7 of both total longwave fluxes (ERB WFOV) and narrow-band radiances from THIR (section 2.5). This process is inherently inaccurate since the NOAA 11.5-μm channel radiometer measurements are more sensitive to surface temperature and are relatively insensitive to water-vapor changes. Standard model output includes broadband OLR, so a comparison to ERBE or Nimbus-7 is most appropriate. The slope difference between OLR from ERBE and Nimbus-7 ERB (Fig. 20b) is primarily a result of the different resolutions of the sensors. The smoothing produced by the ERB WFOV sensor eliminates extreme values and produces an an apparent rotation in the regression, although this effect was considerably reduced by truncating the ERBE OLR field. Similar plots for January 1986 are shown in Fig. 21.

Figure 22 shows a scatter plot of ERBE T42 OLR data from July 1985 and July 1986. The main point to emphasize is the considerable variability in the year-to-year climate. Comparisons between individual monthly model results and satellite observations should recognize such interannual variations.

• Area Averages

The ERBE, Nimbus-7 ERB and NOAA OLR data can be further studied with regional mean plots. As with the cloud data, the total field will be examined. The NOAA OLR measurements have a clear discontinuity with the end of the scanning radiometer data in February 1978, so only data from 1979 and later have been plotted. The data after 1978 are remarkably consistent in view of the different satellites and equator-crossing times that make up the record (Table 1). Other discontinuities that are evident in the regional mean plots include a change in the Nimbus-7 ERB data in July 1980 as a result of a change in the analysis method and a transition in the ERBE data in January 1987 as a result of the failure of the scanner on NOAA-9 and its subsequent replacement by the NOAA-10 scanner.

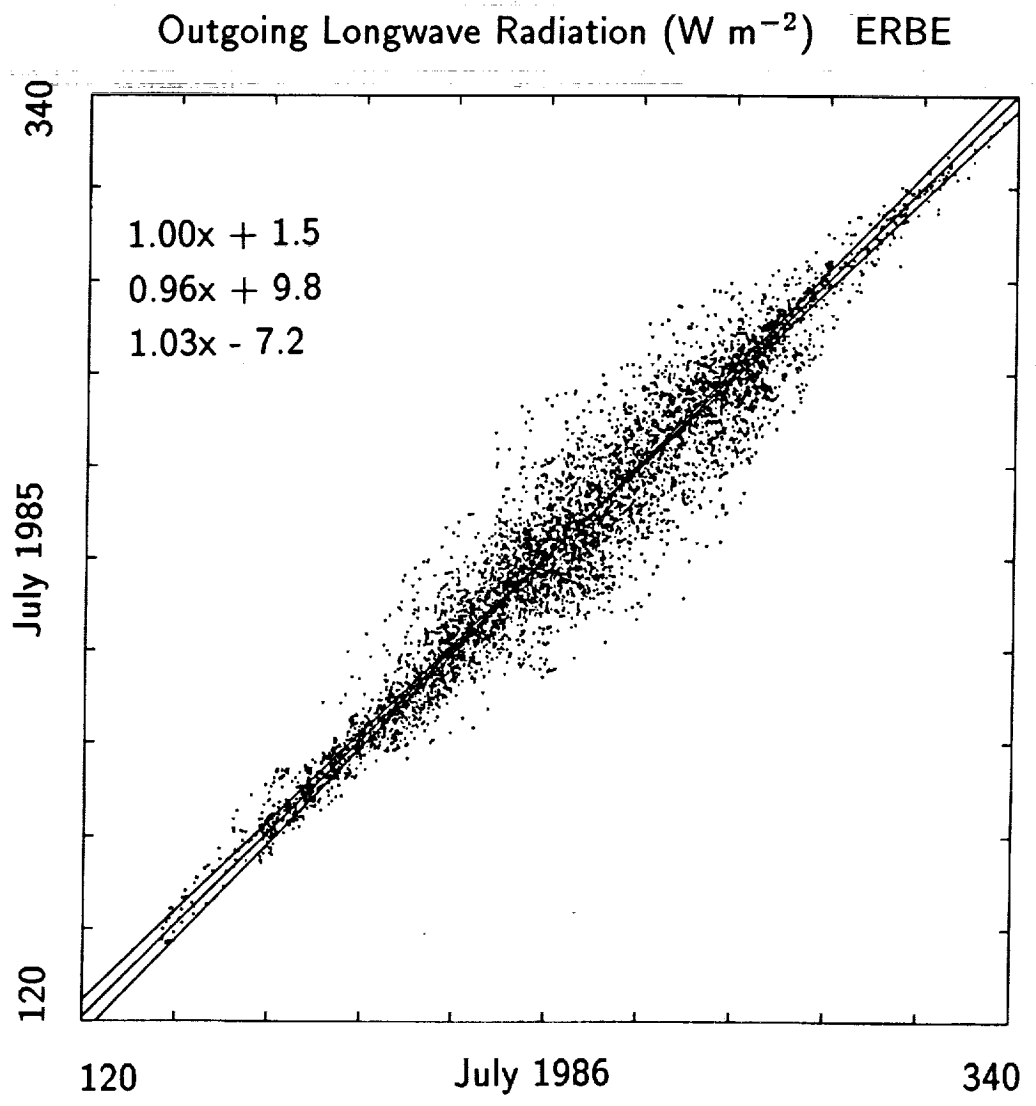

Figure 22. Scatter plot of outgoing longwave radiation measurements from ERBE from July 1985 and July 1986. Each point represents a gridpoint on the T42 grid sampled between 70°S and 70°N.

The globally averaged (70°S–70°N) OLR time series from all three data sets is presented in Fig. 23, and Figs. 24 and 25 show the NH and SH (0–70° latitude) averages as well as tropical (0–25° latitude) and extratropical (25–70° latitude) averages for each hemisphere. The global series is dominated by the NH extratropical annual cycle (Fig. 24c), which exhibits a very strong difference between winter and summer. In the NH tropics (Fig. 24b), the annual cycle is out of phase with that of the NH extratropics. Lowest values occur in summer and indicate the movement of the monsoon circulations to north of the equator. Similar features are seen in the SH plots (Fig. 25); however, since the annual cycle in the SH extratropics is weaker than its counterpart in the NH, averaging with the opposite phase in the SH tropics produces a nearly constant large-scale mean for the SH (0–70°S) as a whole (Fig. 25a).

Over such large regions, the resolution differences between Nimbus-7 ERB and ERBE are not as important, and both data sets agree fairly well when they overlap in time. This is not always the case when intercomparing the NOAA OLR data, however, and this probably results from errors introduced in the conversion of the narrow-band measurements to broadband fluxes. Perhaps the worst agreement is in the SH (Fig. 25) because the empirical adjustment is dominated by the signal of the NH deserts.

The 1982–83 El Niño event is clearly evident, even in the mean OLR fields over the tropical western Pacific (15°S–15°N, 120–180°E) and eastern Pacific (15°S–15°N, 180–90°W) (Fig. 26). Comparisons with the cloud statistics (Fig. 15) show that the OLR changes are produced by large-scale changes in cloud cover and not directly by changes in sea-surface temperatures (SST). The detailed response of clouds to changes in SST and the resulting changes of OLR are important areas of research and should be carefully examined in tropical simulations with models. In the western Pacific (Fig. 26a), onsets of the Australian monsoon are given by the sharp decreases in OLR at the beginning of each year. The 1987 El Niño is evident in the eastern Pacific series (Fig. 26b), and perhaps the 1991–92 warming event can be seen at the tail end of the series in the NOAA OLR data.

4.3 MSU Data

The brightness temperatures from the MSU data have been very carefully calibrated over the 13 years of data collection, as described in section 2.1. Because of this consistency, it is possible to form anomaly fields. Monthly

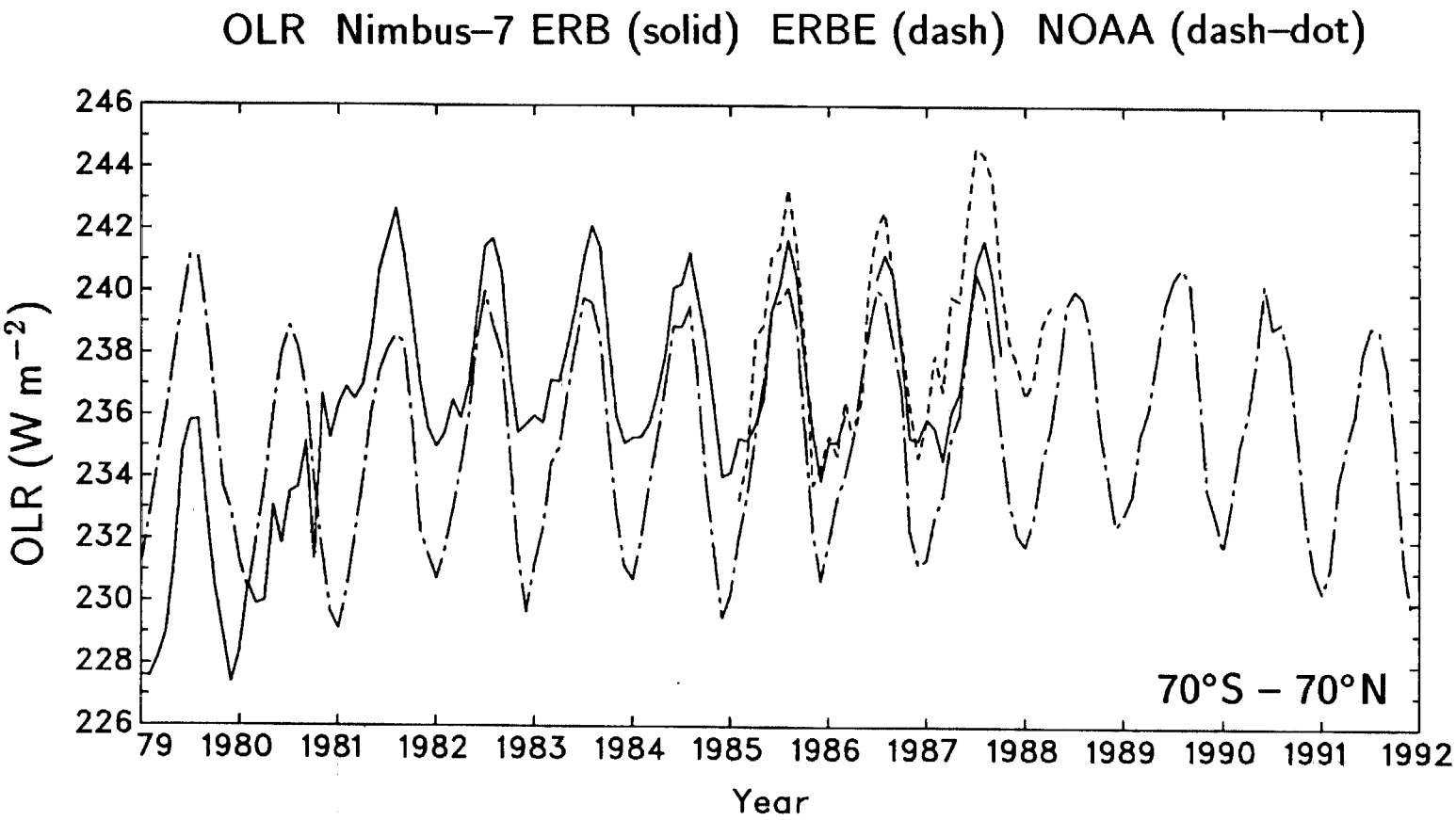

Figure 23. Time series of monthly outgoing longwave radiation from Nimbus-7 ERB (solid), ERBE (dash) and NOAA (dash-dot) averaged from 70°S to 70°N.

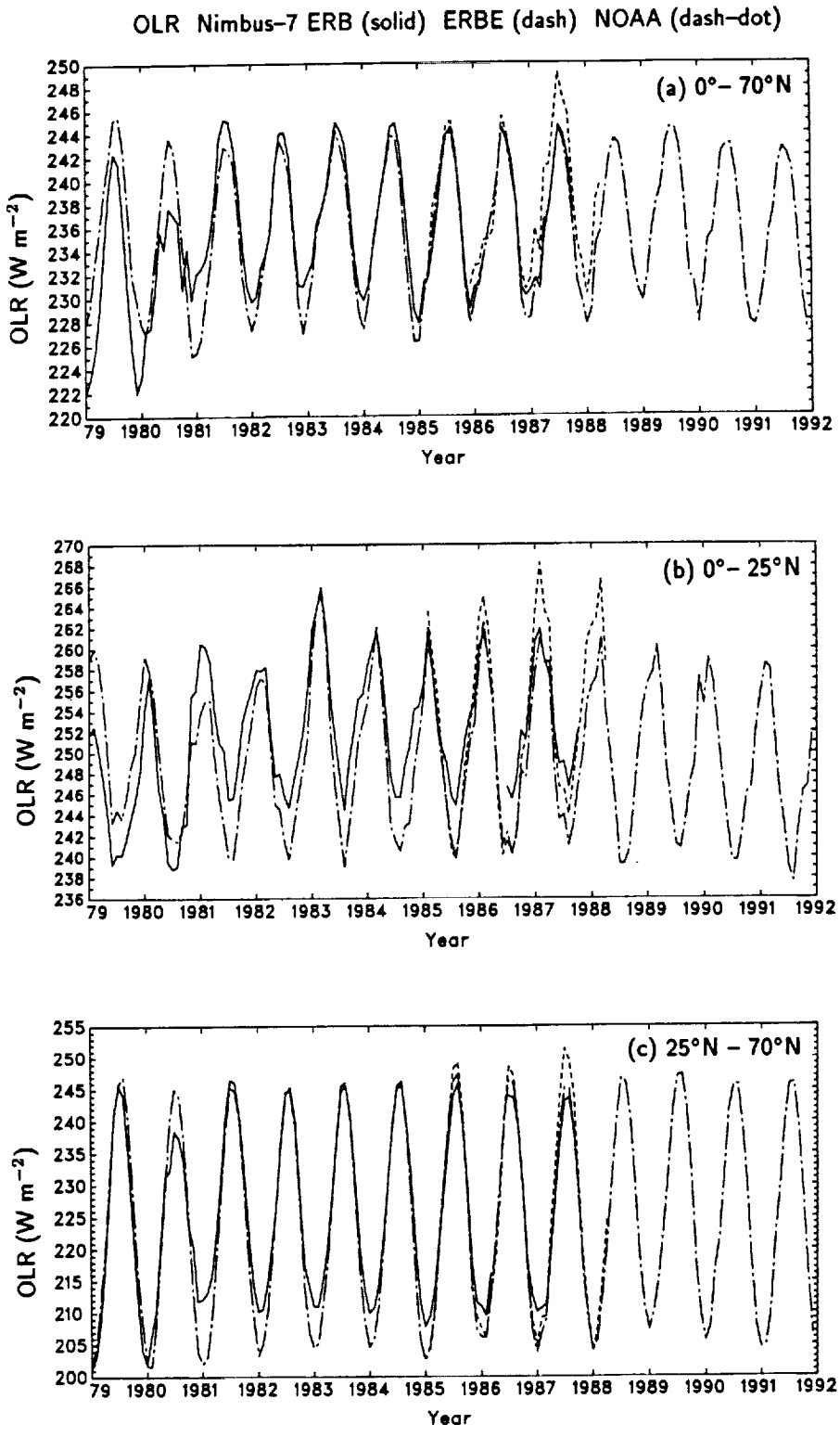

Figure 24. As in Fig. 23 except averaged from (a) 0° to 70°N, (b) 0° to 25°N and (c) 25°N to 70°N.

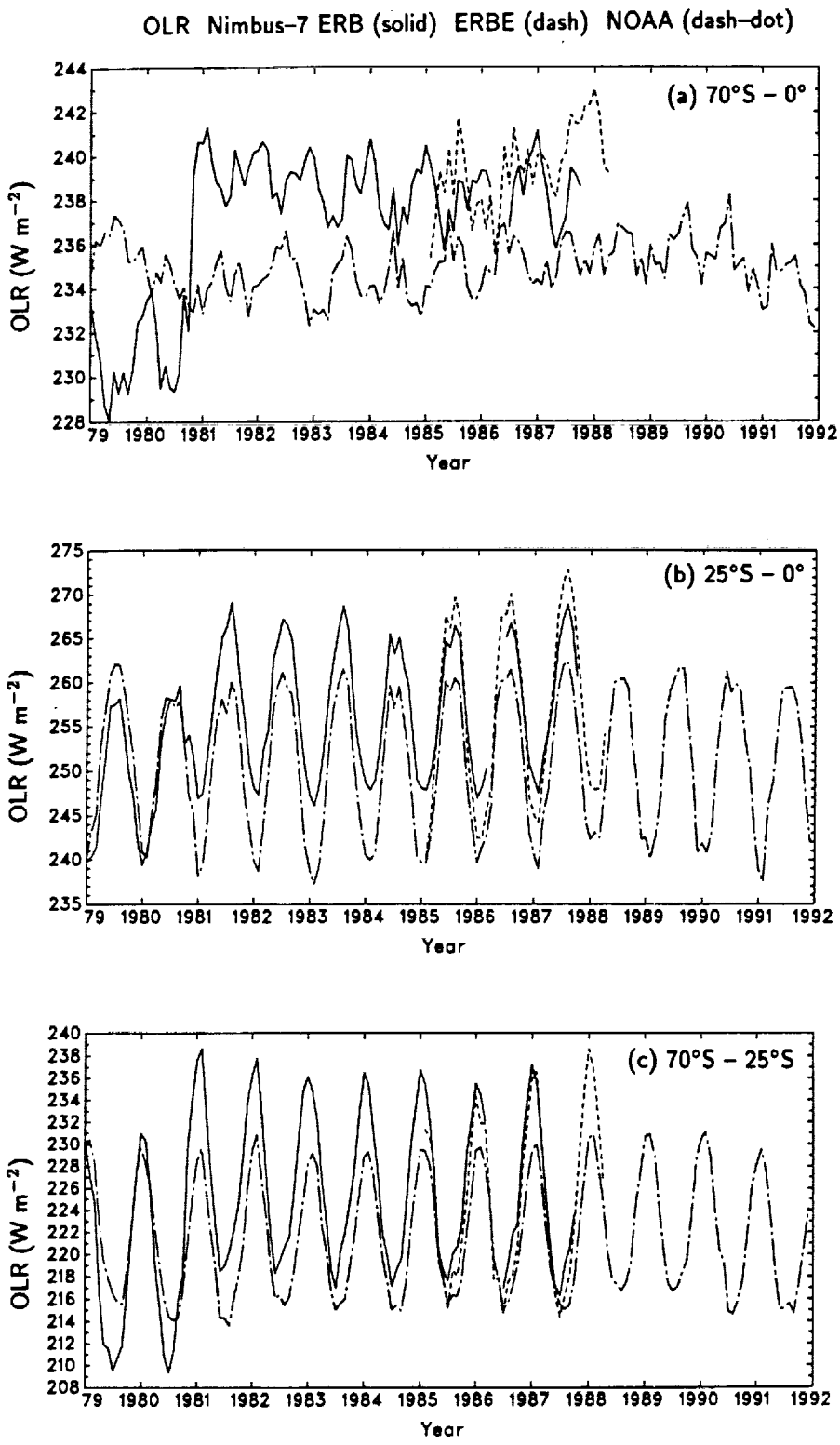

Figure 25. As in Fig. 23 except averaged over (a) 0° to 70°S, (b) 0° to 25°S and (c) 25°S to 70°S.

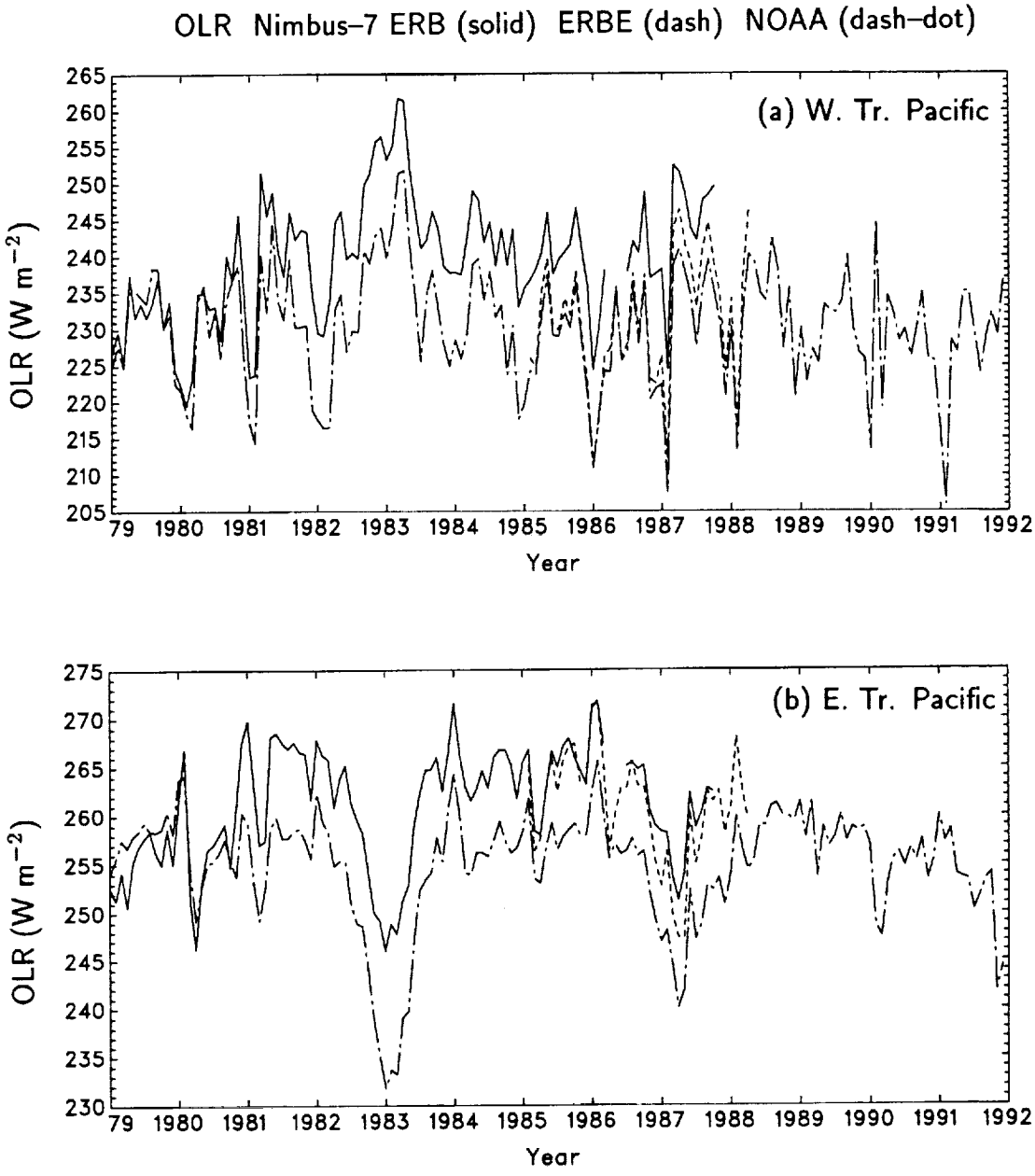

Figure 26. As in Fig. 23 except averaged over (a) the western tropical Pacific and (b) the eastern tropical Pacific. The regions are defined in the text.

anomalies were computed by subtracting the ten-year annual cycle from 1982–1991 from the monthly brightness temperatures. The anomalies have been archived and are further described in Appendix 3.

Anomalies from channels 2R, 2 and 4 are shown averaged over the globe (Fig. 27), both hemispheres (Figs. 28 and 29) and the tropical (20°S-20°N) belt (Fig. 30). For the channel 4 data, two strong warming events superimposed on an overall cooling trend are evident in the regional plots. The 1982–83 warming is generally attributed to the solar heating of volcanic dust injected by an African volcano in December 1981 and El Chichon in early 1982, while the rapid July–September 1991 heating can be attributed to the eruption of Mt. Pinatubo. The 1982-83 stratospheric warming occurred at generally the same time as the El Niño event evident in the tropospheric (channels 2R and 2) brightness temperature anomaly data. To the extent that the weighting functions of channels 2 and 4 overlap (Fig. 1), it is possible that the channel 2 1982–83 warming might be partially due to the stratospheric event. However, comparisons with channel 2R data indicate that the stratospheric influence on channel 2 was probably quite small. It is interesting to compare the channel 2R and 2 anomaly fluctuations shown in Figs. 27–30 with those obtained by more sporadically sampled surface temperature estimates. This has been done in some detail by Trenberth et al. (1992).

Figure 31 illustrates the spatial distribution of channel 2R brightness anomalies for the Januaries of 1982–1984. It is evident that the MSU data are very coherent on large spatial scales. The El Niño warming of January 1983 exceeded 1°C over much of the eastern tropical Pacific, with warmest temperatures in excess of 2°C on either side of the equator between 150°W and 120°W. Similar comparisons could be made with appropriately weighted model temperature data, and the natural variability of model temperatures could be compared to the observed variability of the MSU brightness temperatures.

4.4 Climatologies

The focus of this work has not been to document extensively the quality of each archived satellite data set. Inconsistencies are introduced into the data from a wide range of sources, many of which were discussed for each data set in section 2. Without such an effort, it is difficult to establish accurate monthly averages. Nonetheless, an attempt has been made to archive monthly climatologies for some fields. Details are given in the Appendices as to which fields were

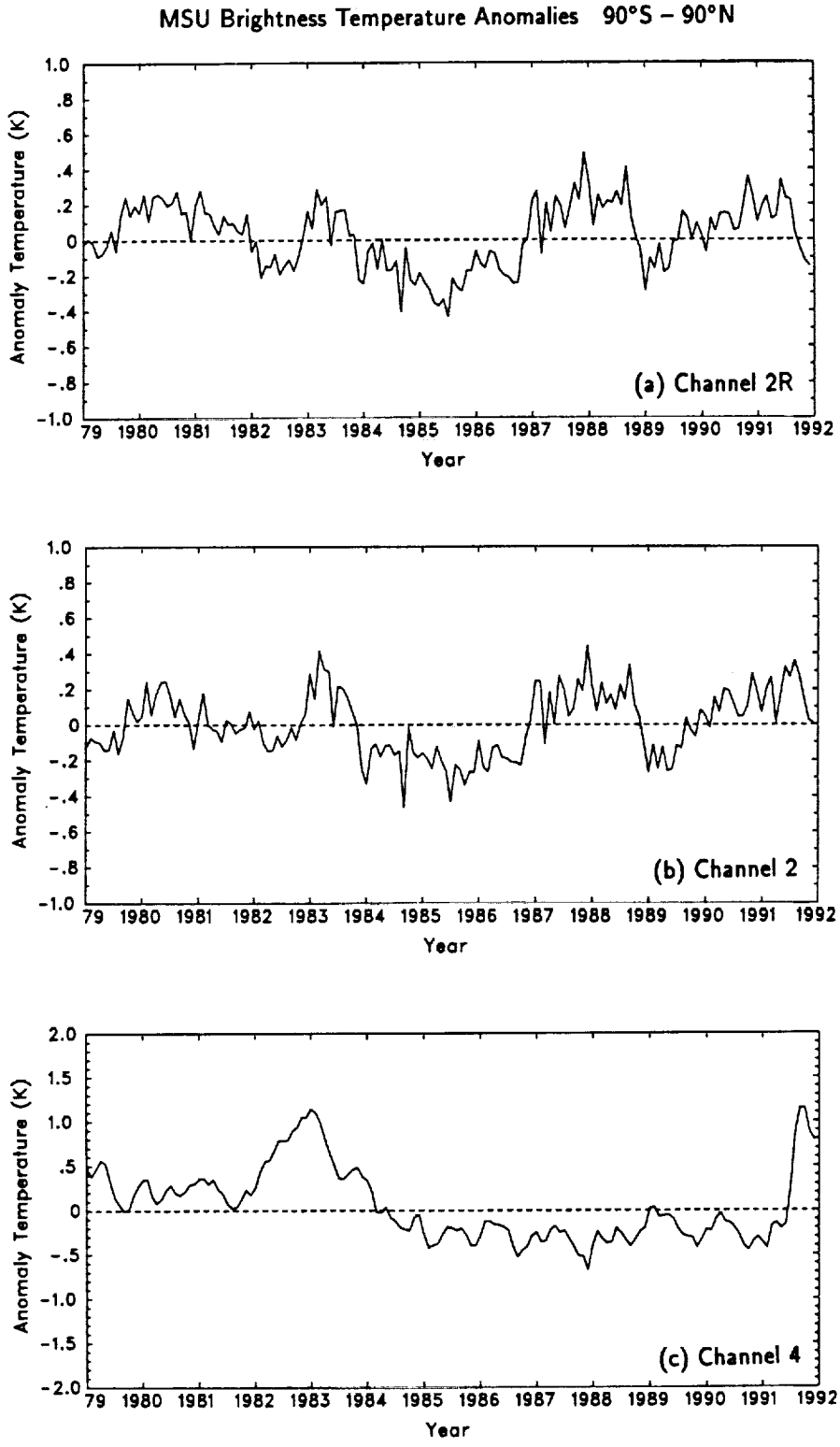

Figure 27. Time series of monthly global MSU brightness temperature anomalies, defined relative to the 1982–1991 annual cycle, for (a) channel 2R, (b) channel 2 and (c) channel 4.

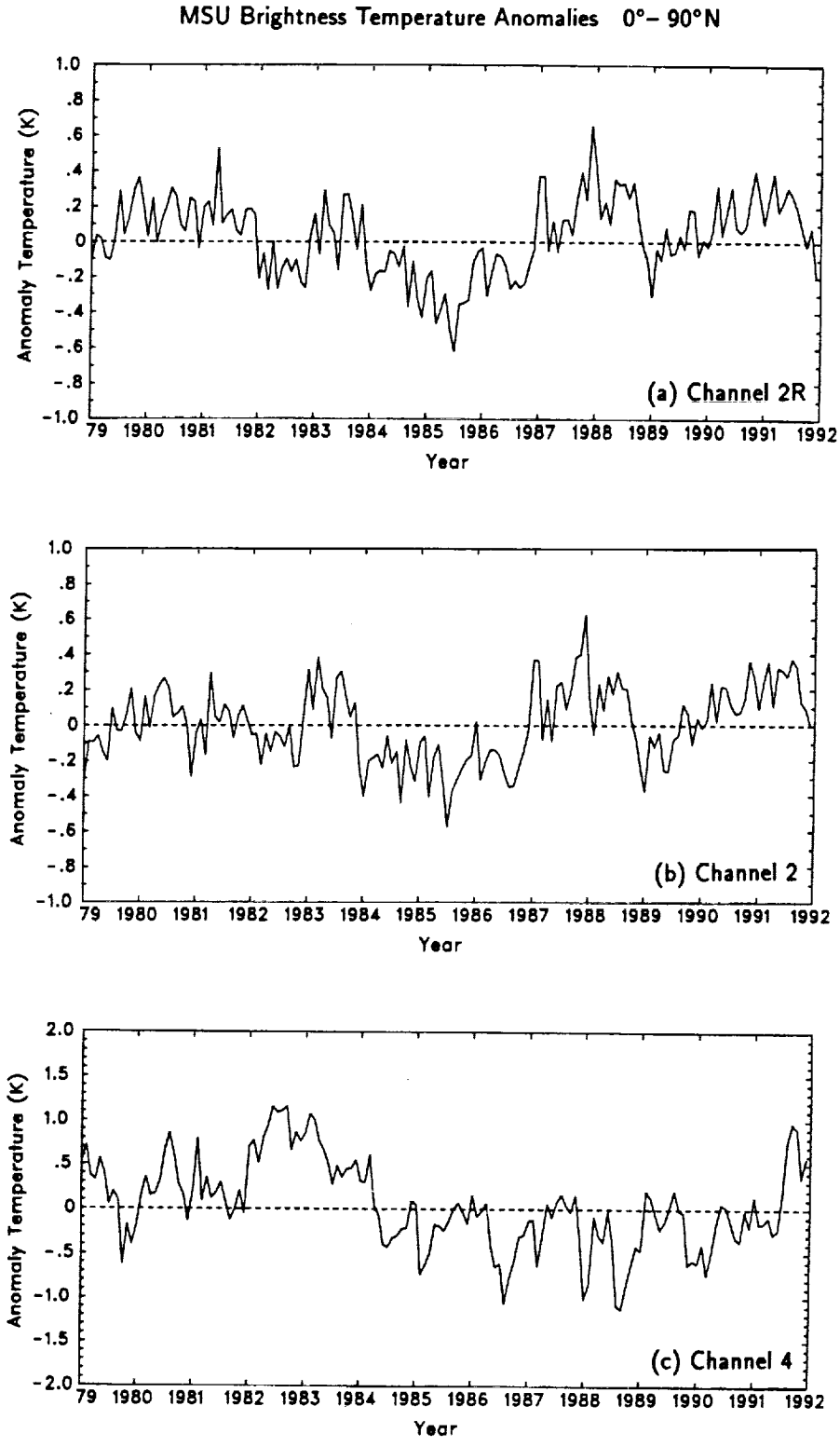

Figure 28. As in Fig. 27 except for Northern Hemisphere averages.

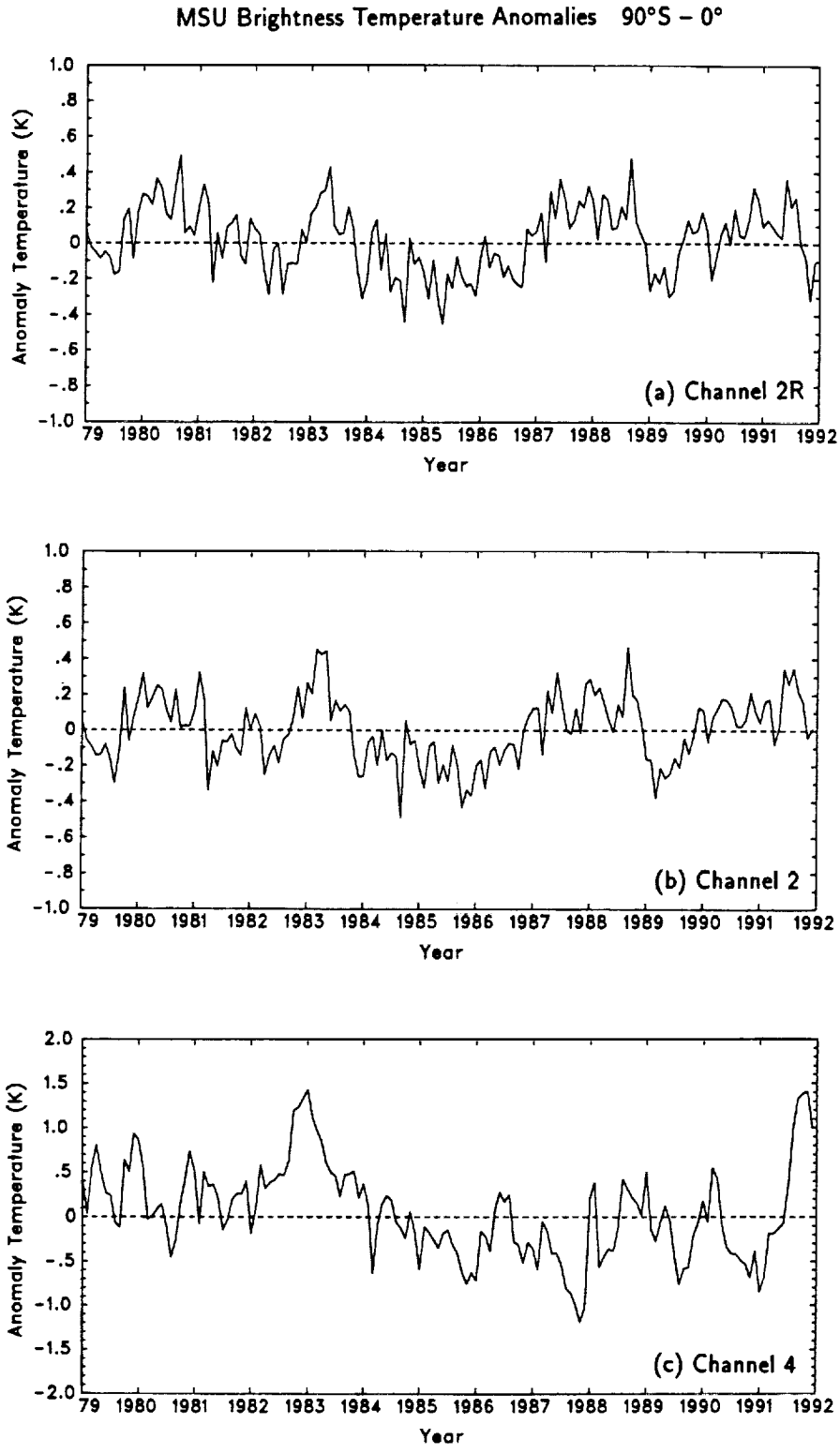

Figure 29. As in Fig. 27 except for Southern Hemisphere averages.

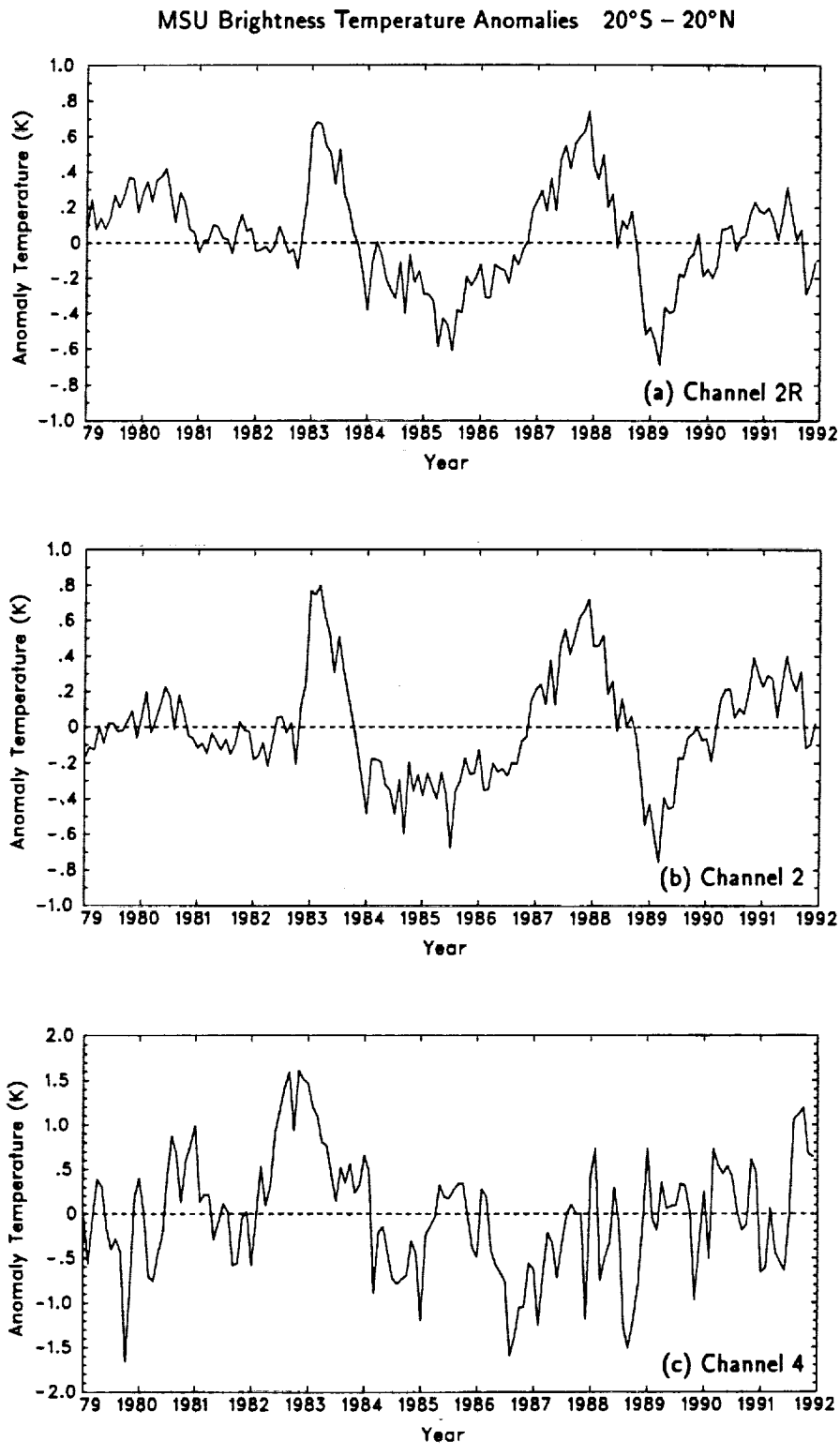

Figure 30. As in Fig. 27 except for tropical (20°S to 20°N) averages.

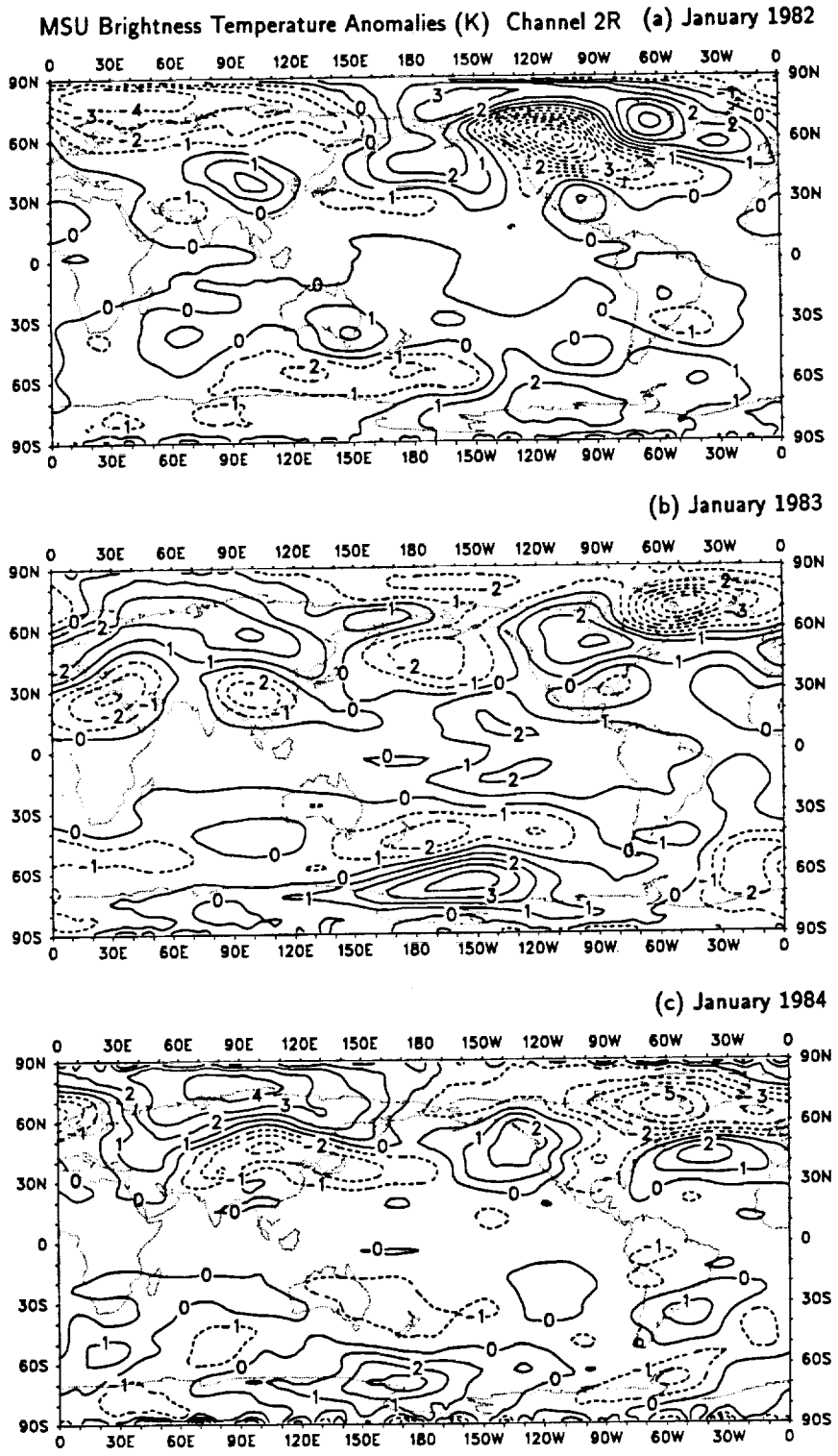

Figure 31. Brightness temperature anomalies from MSU channel 2R for (a) January 1982, (b) January 1983 and (c) January 1984. The contour increment is 1 K and negative values are indicated by the dashed lines.

chosen. Sample January and July climatologies of total cloud cover from ISCCP and OLR from NOAA satellites are given in Figs. 32 and 33. Climatologies for many more fields have been produced and are listed in the Appendices. Users of the climatologies should keep in mind that their accuracy has not been evaluated in this report.

5. SUMMARY AND FUTURE WORK

Several satellite data sets have been archived in CCM1 history tape format for use with the CCM modular processor. Data sets with longer records have been acquired, so only monthly averaged data have been processed. These data are useful for a wide range of diagnostic studies as well as for intercomparisons with model output. The purpose of this note is to draw attention to this resource.

The archived data sets contain similar fields. For instance, ISCCP and Nimbus-7 CMATRIX contain monthly estimates of global cloud properties, and ERBE and Nimbus-7 ERB both contain monthly estimates of the global radiation budget. However, fundamental differences exist in the definitions of the fields, the analysis schemes that produced the data, the periods of coverage and the sampling resolutions, to name but a few. An objective of this work was to document some of these differences, provide references for more detailed descriptions of the data, give some simple examples of the types of products available and highlight some of the issues that need to be considered when using the data, for example, in model validation and diagnostics.

Current and future work will include more detailed evaluations of the archived satellite data, updates of the archived data and the archival and description of other relatively long-term satellite data sets, such as some ocean and sea-ice satellite data. Detailed intercomparisons with model output will also be a future emphasis.

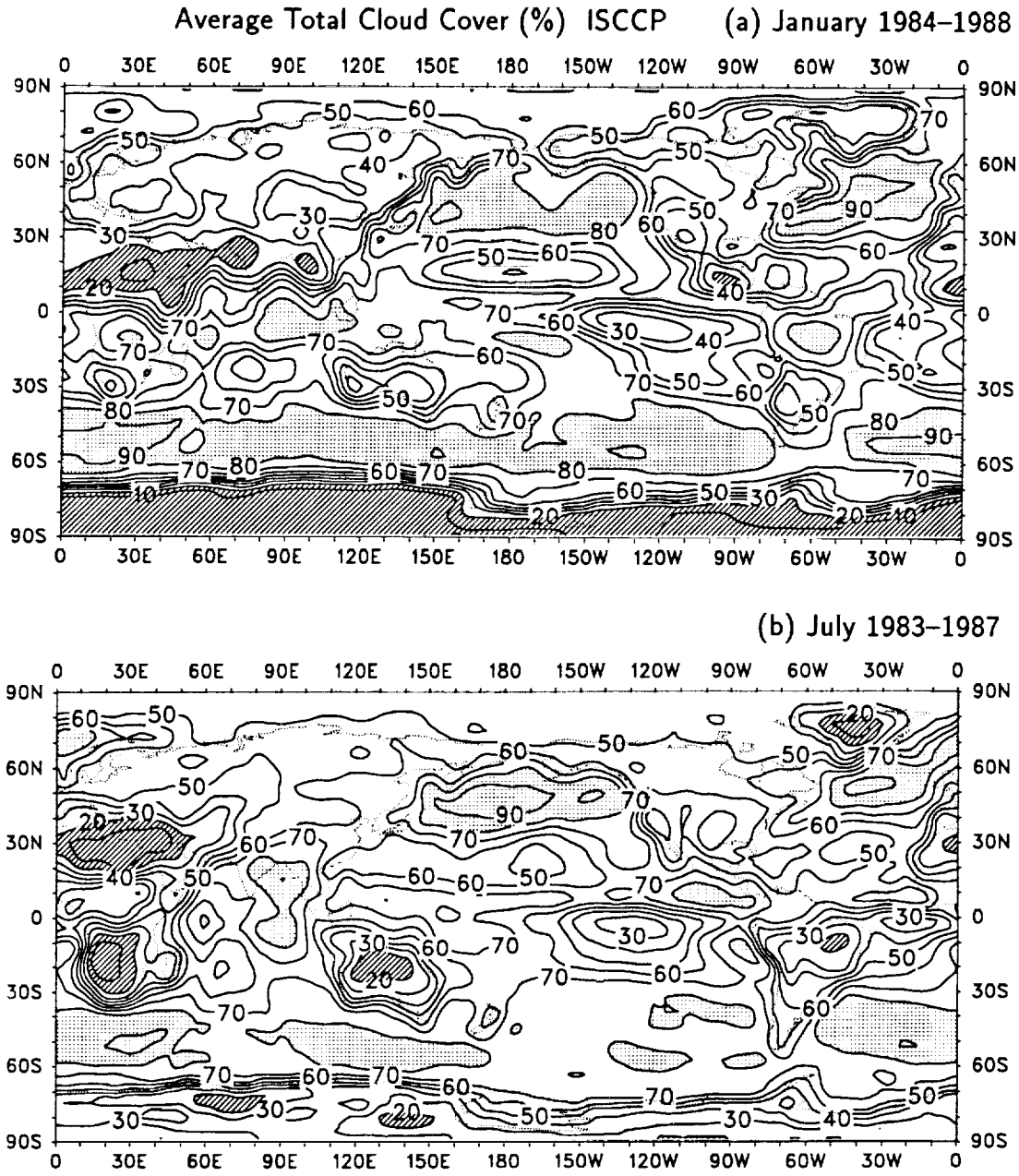

Figure 32. Average total cloud cover in percent from ISCCP for (a) January 1984–1988 and (b) July 1983–1987. Cloud cover less than 20% is indicated by hatching and cloud cover greater than 80% is indicated by stippling. The contour increment is 10%.

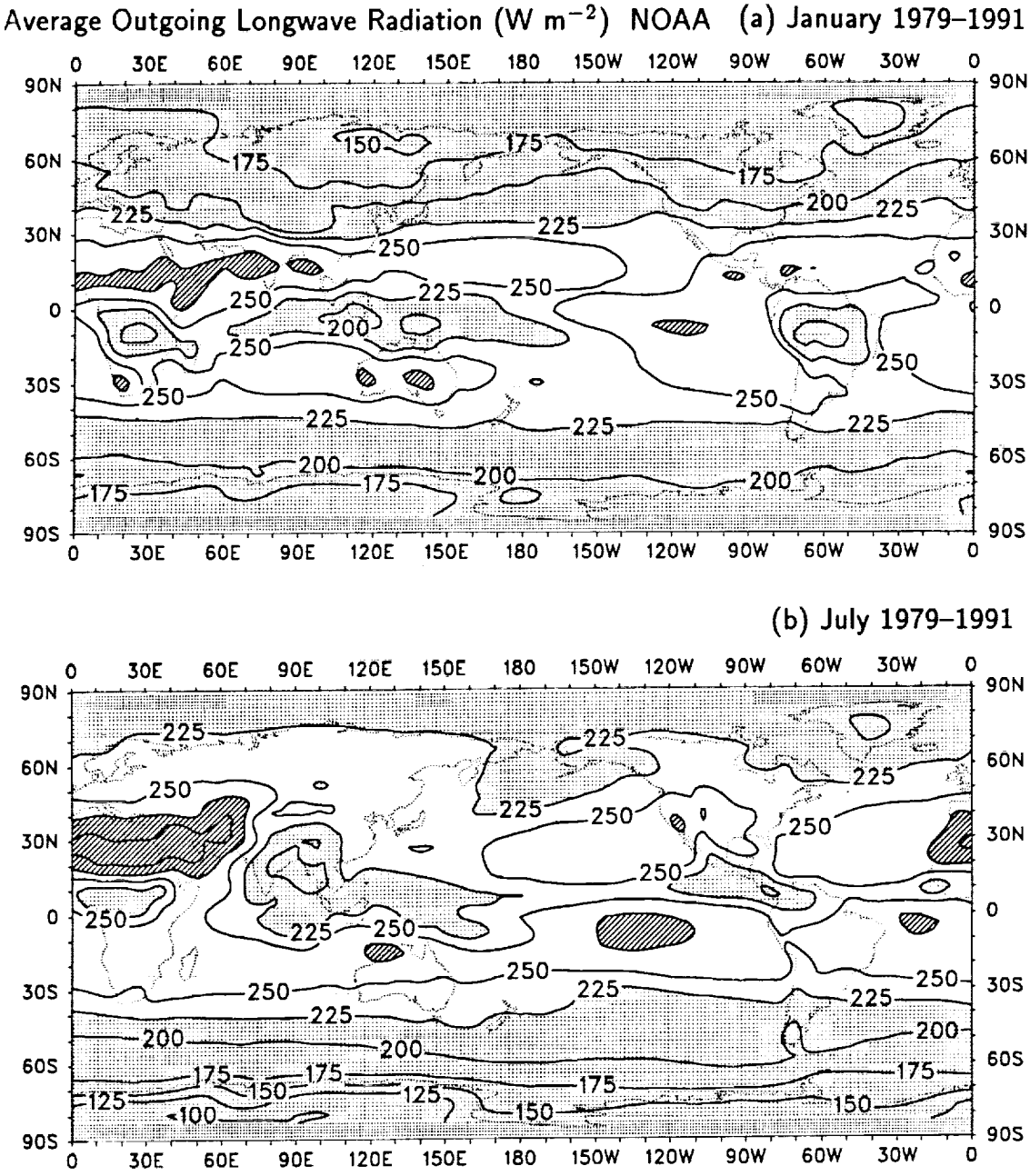

Figure 33. Average outgoing longwave radiation from NOAA for 1979–1991 for (a) January and (b) July. Values less than 225 W m^{-2} are indicated by stippling, and values greater than 275 W m^{-2} are hatched. The contour increment is 25 W m^{-2}.

REFERENCES

Abel, P., and A. Gruber, 1979: An improved model for the calculation of longwave flux at 11 μm. NOAA Tech. Report NESS 106, Washington, D.C., 24 pp.

Barkstrom, B.R., 1984: The Earth Radiation Budget Experiment (ERBE). *Bull. Amer. Meteor. Soc.*, **65**, 1170–1185.

——, E. Harrison, G. Smith, R. Green, J. Kibler, R. Cess, and the ERBE Science Team, 1989: Earth Radiation Budget Experiment (ERBE) archival and April 1985 results. *Bull. Amer. Meteor. Soc.*, **70**, 1254–1262.

Brooks, D.R., E.F. Harrison, P. Minnis, J.T. Suttles, and R.S. Kandel, 1986: Development of algorithms for understanding the temporal and spatial variability of the earth's radiation balance. *Rev. Geophys*, **24**, 422–438.

Campbell, G.G., T.H. Vonder Haar, D.L. Hartmann, R. Kandel, G.E. Hunt, A. Mecherinkunnel, F. House, A. Ingersoll, H.L. Kyle, R. Maschhoff, and L.L. Stowe, 1986: Comparison of Nimbus 7 and ERBE radiation budget measurements. *Proc. Sixth Conference on Atmospheric Radiation,* Williamsburg, Virginia, Amer. Meteor. Soc., Boston, Massachusetts.

Cess, R.D., and G.L. Potter, 1987: Exploratory studies of cloud radiative forcing with a general circulation model. *Tellus*, **39A**, 460–473.

Chelliah, M., and P. Arkin, 1992: Large scale interannual variability of monthly outgoing longwave radiation anomalies over the global tropics. *J. Climate*, (in press).

Ellingson, R.G., and R.R. Ferraro, Jr., 1983: An examination of a technique for estimating longwave radiation budget from satellite radiance observations. *J. Clim. Appl. Meteor.*, **22**, 1416–1423.

ERBE Science Team, 1986: First data from the Earth Radiation Budget Experiment (ERBE). *Bull. Amer. Meteor. Soc.*, **67**, 818–824.

Gruber, A., and A.F. Krueger, 1984: The status of the NOAA outgoing longwave radiation data set. *Bull. Amer. Meteor. Soc.*, **65**, 958–962.

——, I. Ruff, and C. Earnest, 1983: Determination of the planetary radiation budget from TIROS–N satellites. NOAA Tech. Rept. NESDIS 3, U.S. Dept. Commerce, NOAA/NESDIS, Washington, D.C., 12 pp. [NTIS PB84 100916].

Harrison, E.F., P. Minnis, B.R. Barkstrom, V. Ramanathan, R.D. Cess, and G.G. Gibson, 1990: Seasonal variation of cloud radiative forcing derived from the Earth Radiation Budget Experiment. *J. Geophys. Res.*, **95**, 18687–18703.

Harshvardhan, D. A. Randall, T.G. Corsetti, and D.A. Dazlich, 1989: Earth radiation budget and cloudiness simulations with a general circulation model. *J. Atmos. Sci.*, **46**, 1922–1942.

Hughes, N.A., 1984: Global cloud climatologies: A historical review. *J. Climate Appl. Meteor.*, **23**, 724–751.

Hurrell, J.W., and K.E. Trenberth, 1992: An evaluation of monthly mean MSU and ECMWF global atmospheric temperatures for monitoring climate. *J. Climate*, (in press).

Jacobowitz, H.H., H.V. Soule, H.l. Kyle, F.B. House, and Nimbus–7 ERB Experiment Team, 1984: The Earth Radiation Budget (ERB) experiment: An Overview. *J. Geophys. Res*, **89**, 5021–5038.

Janowiak, J.E., A.F. Krueger, and P.A. Arkin, 1985: Atlas of outgoing longwave radiation derived from NOAA satellite data. NOAA Atlas No. 6, U.S. Dept. of Commerce, NOAA/NESDIS, Washington, D.C., 44 pp.

Kopia, L.P., 1986: Earth Radiation Budget Experiment scanner instrument. *Rev. Geophys*, **24**, 400–406.

Kyle, H.L., F.B. House, P.E. Ardanuy, H. Jacobowitz, R.H. Maschhoff, and J.R. Hickey, 1984: New in-flight calibration adjustment of the NIMBUS 6 and 7 Earth Radiation Budget wide field of view radiometers. *J. Geophys. Res.*, **89**, 5057–5076.

——, A. Mecherikunnel, P. Ardanuy, L. Penn, B. Groveman, G.G. Campbell, and T.H. Vonder Haar, 1990: A comparison of two major earth radiation budget data sets. *J. Geophys. Res.*, **95**, 9951–9970.

Luther, M.R., J.E. Cooper, and G.R. Taylor, 1986: The Earth Radiation Budget Experiment nonscanner instrument. *Rev. Geophys*, **24**, 391–399.

Ohring, G., A. Gruber, R.G. Ellingson, 1984: Satellite determination of the relationship between total longwave radiation flux and infrared window radiance. *J. Clim. Appl. Meteor.*, **23**, 416–425.

Rossow, W.B., and L.C. Garder, 1984: Selection of a map grid for data analysis and archival. *J. Climate Appl. Meteor.*, **23**, 1253–1257.

——, E. Kinsella, and A. Wolf, 1987: International Satellite Cloud Climatology Project (ISCCP). Description of reduced resolution radiance data. July 1985 (revised July 1987). WMO/TD–No.58, World Meteorological Organization, Geneva, 143 pp.

——, and R.A. Schiffer, 1991: ISCCP cloud data products. *Bull. Amer. Meteor. Soc.*, **72**, 2–20.

——, and A.W. Walker, 1991: International Satellite Cloud Climatology Project (ISCCP): Description of monthly mean cloud data (Stage C2). Appendix C, WMO/ICSU, 29 pp.

Smith, G.L., R.N. Green, E. Raschke, L.M. Avis, J.T. Suttles, B.A. Wielicki, and R. Davies, 1986: Inversion methods for satellite studies of the earth's radiation budget: Development of algorithms for the ERBE mission. *Rev. Geophys*, **24**, 407–421.

Spencer, R.W., and J.R. Christy, 1990: Precise monitoring of global temperature trends from satellites. *Science*, **247**, 1558-1562.

——, and ——, 1992a: A satellite-derived global tropospheric temperature data set, Part I: Radiosonde validation. *J. Climate*, (in press).

——, and ——, 1992b: A satellite-derived global tropospheric temperature data set, Part II: An improved method and trends for 1979-1990. *J. Climate*, (in press).

——, ——, and N.C. Grody, 1990: Global atmospheric temperature monitoring with satellite microwave measurements: Method and results 1979–1984. *J. Climate*, **3**, 1111-1128.

Stowe, L.L, C.G. Wellemeyer, T.F. Eck, H.Y.M. Yeh, and the Nimbus–7 Cloud Data Processing Team, 1988: Nimbus–7 global cloud climatology, Part I: Algorithms and validation, *J. Climate*, **1**, 445–470.

——, H.Y.M. Yeh, T.F. Eck, C.G. Wellemeyer, H. L.Kyle, and the Nimbus–7 Cloud Data Processing Team, 1989: Nimbus–7 cloud climatology, Part II. *J. Climate*, **2**, 671–709.

Trenberth, K.E., and J.G. Olson, 1988a: *Evaluation of NMC Global Analyses.* NCAR Technical Note NCAR/TN–299+STR, National Center for Atmospheric Research, Boulder, Colorado, 82 pp.

——, and ——, 1988b: *ECMWF Global Analyses 1979-1986: Circulation Statistics and Data Evaluation.* NCAR Technical Note NCAR/TN-300+STR, National Center for Atmospheric Research, Boulder, Colorado, 94 pp and 12 fiche.

——, and ——, 1988c: An evaluation and intercomparison of global analyses from the National Meteorological Center and the European Centre for Medium Range Weather Forecasts. *Bull. Amer. Meteor. Soc.*, **69**, 1047–1057.

——, J.R. Christy, and J.W. Hurrell, 1992: Monitoring global monthly mean surface temperatures. *J. Climate*, (in press).

Wark, D.Q., G. Yamomoto, and J. Lienesch, 1962: Infrared flux and surface temperature determination from TIROS radiometer measuremennts. MSL report No. 10, U.S. Dept. of Commerce, Weather Bureau, Washington, D.C., 85 pp.

Warren, S. G., C. J. Hahn, J. London, R. M. Chervin and R. L. Jenne, 1986: *Global Distribution of Total Cloud Cover and Cloud Type Amounts over Land.* NCAR Technical Note NCAR/TN-273+STR, National Center for Atmospheric Research, Boulder, Colorado, 229 pp.

——, ——, ——, ——, and ——, 1988: *Global Distribution of Total Cloud Cover and Cloud Type Amounts over Ocean.* NCAR Technical Note NCAR/TN-317+STR, National Center for Atmospheric Research, Boulder, Colorado, 212 pp.

Wielicki, B.A., and R.N. Green, 1989: Cloud identification for ERBE radiative flux retrieval. *J. Appl. Meteor.*, **28**, 1133–1146.

WMO, 1956: *International Cloud Atlas*, Vol. 1. World Meteorological Organization, Geneva, Switzerland.

Wolski, R.J., 1987: *CCM Modular Processor Users' Guide (Version PROC02).* NCAR Technical Note NCAR/TN-290+IA, National Center for Atmospheric Research, Boulder, Colorado, 193 pp. plus appendices.

——, 1989: PROC02A: *Enhancements to the PROC02 Version of the CCM Modular Processor.* NCAR Technical Note NCAR/TN-335+IA, National Center for Atmospheric Research, Boulder, Colorado, 32 pp.

Appendix 1. Acronyms.

AVHRR	Advanced Very High Resolution Radiometer
CCM	Community Climate Model
CMATRIX	Cloud-Matrix
ECMWF	European Centre for Medium-Range Weather Forecasts
ERB	Earth Radiation Budget
ERBE	Earth Radiation Budget Experiment
ERBS	Earth Radiation Budget Satellite
GCM	General Circulation Model
GMS	Geostationary Meteorological Satellite
GOES	Geostationary Operational Environmental Satellite
ICP	Input Control Parameter
IR	Infrared
ISCCP	International Satellite Cloud Climatology Project
MFOV	Medium-Field-of-View
MSU	Microwave Sounding Unit
NASA	National Aeronautics and Space Administration
NCAR	National Center for Atmospheric Research
NMC	National Meteorological Center
NOAA	National Oceanic and Atmospheric Administration
OLR	Outgoing Longwave Radiation
SBUV	Solar Backscatter Ultraviolet
SR	Scanning Radiometer
THIR	Temperature Humidity Infrared Radiometer
TIROS	Television Infrared Operations Satellite
TOMS	Total Ozone Mapping Spectrometer
TOVS	TIROS Operational Vertical Sounder
UTC	Coordinated Universal Time
VIS	Visible
WFOV	Wide-Field-of-View

Appendix 2. Table of day number (for use in the CCM Processor)

1974	1975	1976	1977	1978	1979	1980	1981	1982
Jan: 1	Jan: 13	Jan: 25	Jan: 37	Jan: 49	Jan: 61	Jan: 73	Jan: 85	Jan: 97
Feb: 2	Feb: 14	Feb: 26	Feb: 38	Feb: 50	Feb: 62	Feb: 74	Feb: 86	Feb: 98
Mar: 3	Mar: 15	Mar: 27	Mar: 39	Mar: 51	Mar: 63	Mar: 75	Mar: 87	Mar: 99
Apr: 4	Apr: 16	Apr: 28	Apr: 40	Apr: 52	Apr: 64	Apr: 76	Apr: 88	Apr: 100
May: 5	May: 17	May: 29	May: 41	May: 53	May: 65	May: 77	May: 89	May: 101
Jun: 6	Jun: 18	Jun: 30	Jun: 42	Jun: 54	Jun: 66	Jun: 78	Jun: 90	Jun: 102
Jul: 7	Jul: 19	Jul: 31	Jul: 43	Jul: 55	Jul: 67	Jul: 79	Jul: 91	Jul: 103
Aug: 8	Aug: 20	Aug: 32	Aug: 44	Aug: 56	Aug: 68	Aug: 80	Aug: 92	Aug: 104
Sep: 9	Sep: 21	Sep: 33	Sep: 45	Sep: 57	Sep: 69	Sep: 81	Sep: 93	Sep: 105
Oct: 10	Oct: 22	Oct: 34	Oct: 46	Oct: 58	Oct: 70	Oct: 82	Oct: 94	Oct: 106
Nov: 11	Nov: 23	Nov: 35	Nov: 47	Nov: 59	Nov: 71	Nov: 83	Nov: 95	Nov: 107
Dec: 12	Dec: 24	Dec: 36	Dec: 48	Dec: 60	Dec: 72	Dec: 84	Dec: 96	Dec: 108

1983	1984	1985	1986	1987	1988	1989	1990	1991
Jan: 109	Jan: 121	Jan: 133	Jan: 145	Jan: 157	Jan: 169	Jan: 181	Jan: 193	Jan: 205
Feb: 110	Feb: 122	Feb: 134	Feb: 146	Feb: 158	Feb: 170	Feb: 182	Feb: 194	Feb: 206
Mar: 111	Mar: 123	Mar: 135	Mar: 147	Mar: 159	Mar: 171	Mar: 183	Mar: 195	Mar: 207
Apr: 112	Apr: 124	Apr: 136	Apr: 148	Apr: 160	Apr: 172	Apr: 184	Apr: 196	Apr: 208
May: 113	May: 125	May: 137	May: 149	May: 161	May: 173	May: 185	May: 197	May: 209
Jun: 114	Jun: 126	Jun: 138	Jun: 150	Jun: 162	Jun: 174	Jun: 186	Jun: 198	Jun: 210
Jul: 115	Jul: 127	Jul: 139	Jul: 151	Jul: 163	Jul: 175	Jul: 187	Jul: 199	Jul: 211
Aug: 116	Aug: 128	Aug: 140	Aug: 152	Aug: 164	Aug: 176	Aug: 188	Aug: 200	Aug: 212
Sep: 117	Sep: 129	Sep: 141	Sep: 153	Sep: 165	Sep: 177	Sep: 189	Sep: 201	Sep: 213
Oct: 118	Oct: 130	Oct: 142	Oct: 154	Oct: 166	Oct: 178	Oct: 190	Oct: 202	Oct: 214
Nov: 119	Nov: 131	Nov: 143	Nov: 155	Nov: 167	Nov: 179	Nov: 191	Nov: 203	Nov: 215
Dec: 120	Dec: 132	Dec: 144	Dec: 156	Dec: 168	Dec: 180	Dec: 192	Dec: 204	Dec: 216

Appendix 3. MSU data on the Mass Store.

The following is a list of the single-level monthly mean fields archived for the Microwave Sounding Unit (MSU) data. Each field has been converted into a "TYPEc = CCM1" history tape at 2.5° and T42 resolution. The monthly data are available from January 1979 through December 1991 (156 months). Note that the "day" parameter (ICP "DAYSc") actually refers to monthly means.

FIELD LIST

Field	Processor Name	Units
Channel 2 Temperature	CH2T	K
Channel 2R Temperature	CH2R	K
Channel 4 Temperature	CH4T	K

T42 Data

MS PATHNAME	"DAY" (MONTH) SINCE JAN 74
/CTSAT/MSU/T42/CCM1H/7991T	

2.5° Data

MS PATHNAME	"DAY" (MONTH) SINCE JAN 74
/CTSAT/MSU/2.5DG/CCM1H/7991T	61 - 216

A climatology for each month has been established based on the 10-year period of 1982–1992. A limited number of retrievals during November 1979 and March, April, and August 1981 affected the data and are the reason for the 10-year mean. Monthly anomalies have been formed by subtracting the 10-year mean from the monthly brightness temperatures. The missing data appear to have had a small impact on tropical and summer hemisphere anomalies, but caution should be used when examining the winter hemisphere anomalies during the months of missing retrievals (Christy, personal communication).

The mean temperatures have the same processor names and units as above, but they are in "TYPEc = SAVTAV" format at 2.5° and T42 resolution. Only the T42 data are listed below, but the 2.5° data can be accessed by changing "T42" to "2.5DG" in the Mass Store pathnames.

T42 Data

MS PATHNAME
/CTSAT/MSU/T42/SAVTAV/JAN8291T
/CTSAT/MSU/T42/SAVTAV/FEB8291T
/CTSAT/MSU/T42/SAVTAV/MAR8291T
/CTSAT/MSU/T42/SAVTAV/APR8291T
/CTSAT/MSU/T42/SAVTAV/MAY8291T
/CTSAT/MSU/T42/SAVTAV/JUN8291T
/CTSAT/MSU/T42/SAVTAV/JUL8291T
/CTSAT/MSU/T42/SAVTAV/AUG8291T
/CTSAT/MSU/T42/SAVTAV/SEP8291T
/CTSAT/MSU/T42/SAVTAV/OCT8291T
/CTSAT/MSU/T42/SAVTAV/NOV8291T
/CTSAT/MSU/T42/SAVTAV/DEC8291T

The monthly anomalies have been archived in "TYPEc = CCM1" format at 2.5° and T42 resolution relative to the 1982–1991 annual cycle.

FIELD LIST

Field	Processor Name	Units
Channel 2 Anomalies	CH2TANOM	K
Channel 2R Anomalies	CH2RANOM	K
Channel 4 Anomalies	CH4TANOM	K

T42 Data

MS PATHNAME	"DAY" (MONTH) SINCE JAN 74
/CTSAT/MSU/T42/CCM1H/7991A	61 - 216

2.5° Data

MS PATHNAME	"DAY" (MONTH) SINCE JAN 74
/CTSAT/MSU/2.5DG/CCM1H/7991A	61 - 216

Appendix 4. ISCCP data on the Mass Store.

The Stage C2 data from ISCCP have been archived from July 1983 through June 1988, which gives five full years of monthly analyses. The data include monthly means for 00, 03, 06, 09, 12, 15, 18 and 21 UTC, as well as a complete monthly mean obtained by averaging the eight "hour-monthly" means. The total number of days of observations used in constructing the average values is recorded as a variable. Hour-monthly mean values which consist of less than three daily observations were excluded from the complete monthly mean.

Some adjustments were applied to selected parameters in the C2 data, and it is useful to briefly summarize them. The adjustments have all been made to the general version of the C2 data available to the research community. They are not adjustments made specifically for this archive. Parameters that have been adjusted are so marked in the table which follows. A more detailed discussion of the adjustments and the Stage C2 data can be found in the data set description of Rossow and Walker (1991).

As discussed in section 2.2, cloud amount for nighttime conditions can only be obtained from IR radiances, while daytime cloud conditions are obtained from combined IR and VIS radiance data. This is especially important in regions of low cloud where IR radiances are generally insensitive and, thus, the combined VIS/IR estimates are superior. Similarly for cloud top temperatures and pressures, it is possible to adjust the IR radiance data to be consistent with the value of cloud optical thickness retrieved from the VIS data. This adjustment is labeled "A1" in the following table and is significant only for optically thin clouds which falsely appear to be warmer and at higher pressures since they transmit IR radiation from below.

A second adjustment is derived from the mean differences between the VIS/IR and IR only daytime values of total cloud, cloud-top pressure and cloud-top temperature. The mean differences are used to adjust the nighttime results by linearly interpolating between dusk and dawn values. The interpolated values are then added to the nighttime IR radiances. This adjustment is labeled "A2" in the following table. Values of cloud-optical thickness are also interpolated over the period between dusk and dawn values (A3). Rossow and Walker report that these ajustments are generally small. For cloud amounts, they are nearly uniformly distributed over the globe (see Fig. 12) and are largest in marine stratus regimes and in low latitudes. Cloud-top pressure corrections are positive where low clouds predominate and are negative where there are high thin clouds.

Rossow et al. (1987) describe the procedures used to normalize the radiances from different satellites over the data collection period. However, small residual differences left after the normalization procedure are amplified when physical quantities are retrieved. An attempt to correct for these biases has been made and is labeled as "A4". Essentially, differences in overlapping measurements are compared with reference values from a polar orbiter. The adjusted parameters and the range of the adjustments are cloud-top temperature (± 2.5 K), surface temperature (± 3.0 K), cloud optical thickness and water path (± 0.08%), and surface visible reflectance (± 8%). A second calibration adjustment (A5) is made to the surface reflectance because the spectral response of the METEOSAT "visible" channel differs from the other radiometers used in the analysis. More details are given in Rossow and Walker (1991).

Finally, before the hour-monthly means are combined to form the complete monthly mean, adjustments are made to some parameters to correct for diurnal sampling biases. This adjustment is denoted "A6" in the following table. An incomplete sample is defined to be less than four hour-monthly values in polar regions and less than eight hour-monthly observations elsewhere. The effects of sub-sampling are determined using zonally averaged variations of the variables in local time from locations with all eight hour-monthly mean values available. Obviously, this adjustment affects only the complete monthly mean estimates and not the hour-monthly means.

The six aforementioned adjustments have been applied to the Stage C2 ISCCP data generally available to the research community (i.e., prior to the archival described in this note). In the Stage C2 data, special count values were also included to flag-derived values that were nonphysical. Nonphysical values result from input data errors and model errors. In the ISCCP analyses archived here, the nonphysical values have been removed and replaced with a missing flag (1.0E+36).

The following table lists the single-level monthly-mean fields archived for the ISCCP data. Each field has been converted into a "TYPEc = CCM1" history tape at 2.5° and T42 resolution. A "D" indicates fields that are present only during local daytime. An asterisk denotes fields that should be examined only with the 2.5° data. Other abbreviations include: TAU = optical thickness, PATH = cloud water path, PC = cloud-top pressure, TC = cloud-top temperature, TS = surface temperature, RS = surface reflectance, and SIGMA = standard deviation over space or time domains. These are the same notations used in Rossow and Walker (1991).

Appendix 4 – Continued

FIELD LIST

Field	Processor Name	Units
Latitude index* (equal-area)	ISCCP01	
Longitude index* (equal-area)	ISCCP02	
Lower-longitude index* (2.5°)	ISCCP03	
Upper-longitude index* (2.5°)	ISCCP04	
Land/water/coast code*	ISCCP05	
00-21 UTC: No. of days in average* (day+night)	ISCCPO6	
UTC All: No. of UTCs in average* (day+night)		
00-21 UTC: No. of days in average* (day)	ISCCP07	
UTC All: No. of UTCs in average* (day)		
Mean frequency of cloudy pixels (A2,A6)	ISCCP08	%
00-21 UTC: No. of days with cloudy pixels	ISCCP09	
UTC All: Mean frequency of cloudy days		
Marginal VIS/IR cloud amount	ISCCP10	%
Mean PC for cloudy pixels (A1,A2,A6)	ISCCP11	mb
Time SIGMA PC for IR cloudy pixels	ISCCP12	mb
Mean space SIGMA PC for IR cloudy pixels	ISCCP13	mb
Mean TC for cloudy pixels (A1,A2,A4,A6)	ISCCP14	K
Time SIGMA TC for IR cloudy pixels	ISCCP15	K
Mean space SIGMA TC for IR cloudy pixels	ISCCP16	K
Mean TAU for VIS/IR cloudy pixels (A3,A4,A6)	ISCCP17	
Time SIGMA TAU for VIS/IR cloudy pixels D	ISCCP18	
Mean space SIGMA TAU for VIS/IR cloudy pixels D	ISCCP19	
Mean PATH for VIS/IR cloudy pixels	ISCCP20	gm^{-2}
Time SIGMA PATH for VIS/IR cloudy pixels D	ISCCP21	
Mean space SIGMA PATH for VIS/IR cloudy pixels D	ISCCP22	
Average frequency of low-level cloudiness	ISCCP23	%
Average PC of low-level cloudiness	ISCCP24	mb
Average TC of low-level cloudiness	ISCCP25	K
Average frequency of middle-level cloudiness	ISCCP26	%
Average PC of middle-level cloudiness	ISCCP27	mb
Average TC of middle-level cloudiness	ISCCP28	K
Average frequency of high-level cloudiness	ISCCP29	%
Average PC of high-level cloudiness	ISCCP30	mb
Average TC of high-level cloudiness	ISCCP31	K

Appendix 4 – Continued

Field	Processor Name	Units
Average frequency of cumulus cloudiness D	ISCCP32	%
Average PC of cumulus cloudiness D	ISCCP33	mb
Average TC of cumulus cloudiness D	ISCCP34	K
Average TAU of cumulus cloudiness D	ISCCP35	
Average frequency of stratus cloudiness D	ISCCP36	%
Average PC of stratus cloudiness D	ISCCP37	mb
Average TC of stratus cloudiness D	ISCCP38	K
Average TAU of stratus cloudiness D	ISCCP39	
Average frequency of altocumulus cloudiness D	ISCCP40	%
Average PC of altocumulus cloudiness D	ISCCP41	mb
Average TC of altocumulus cloudiness D	ISCCP42	K
Average TAU of altocumulus cloudiness D	ISCCP43	
Average frequency of nimbostratus cloudiness D	ISCCP44	%
Average PC of nimbostratus cloudiness D	ISCCP45	mb
Average TC of nimbostratus cloudiness D	ISCCP46	K
Average TAU of nimbostratus cloudiness D	ISCCP47	
Average frequency of cirrus cloudiness D	ISCCP48	%
Average PC of cirrus cloudiness D	ISCCP49	mb
Average TC of cirrus cloudiness D	ISCCP50	K
Average TAU of cirrus cloudiness D	ISCCP51	
Average frequency of cirrostratus cloudiness D	ISCCP52	%
Average PC of cirrostratus cloudiness D	ISCCP53	mb
Average TC of cirrostratus cloudiness D	ISCCP54	K
Average TAU of cirrostratus cloudiness D	ISCCP55	
Average frequency of deep convective cloudiness D	ISCCP56	%
Average PC of deep convective cloudiness D	ISCCP57	mb
Average TC of deep convective cloudiness D	ISCCP58	K
Average TAU of deep convective cloudiness D	ISCCP59	
Mean TS from clear sky composite (A4,A6)	ISCCP60	K
Time SIGMA TS from clear sky composite	ISCCP61	K
Mean RS from clear sky composite (A4,AA5)	ISCCP62	%
Mean snow/ice cover	ISCCP63	%
Surface pressure (TOVS)	ISCCP64	mb
Near-surface air temperature (TOVS extrapolated)	ISCCP65	K
Temperature at 500 mb (TOVS)	ISCCP66	K
Tropopause pressure (TOVS)	ISCCP67	mb
Tropopause temperature (TOVS)	ISCCP68	K
Stratosphere temperature at 15 mb	ISCCP69	K
Precipitable water – column (TOVS)	ISCCP70	cm
Ozone – column (TOVS)	ISCCP71	Dobson
Average frequency of cloudy pixels – unadjusted	ISCCP72	%

Appendix 4 – Continued

The following Mass Store pathnames are for the complete monthly means at T42 resolution. Rather than give a complete listing, the 2.5° resolution data can be accessed by changing "T42" to "2.5DG" in the pathname. The hour-monthly mean data can be accessed by changing "ALL" to "00UTC", "03UTC", etc. in the pathnames. Note that the "day" parameter (ICP "DAYSc") actually refers to monthly means.

T42 Data

MS PATHNAME	"DAY" (MONTH) SINCE JAN 74
/CTSAT/ISCCP/T42/CCM1H/ALL/8307	115
/CTSAT/ISCCP/T42/CCM1H/ALL/8308	116
/CTSAT/ISCCP/T42/CCM1H/ALL/8309	117
/CTSAT/ISCCP/T42/CCM1H/ALL/8310	118
/CTSAT/ISCCP/T42/CCM1H/ALL/8311	119
/CTSAT/ISCCP/T42/CCM1H/ALL/8312	120
/CTSAT/ISCCP/T42/CCM1H/ALL/8401	121
/CTSAT/ISCCP/T42/CCM1H/ALL/8402	122
/CTSAT/ISCCP/T42/CCM1H/ALL/8403	123
/CTSAT/ISCCP/T42/CCM1H/ALL/8404	124
/CTSAT/ISCCP/T42/CCM1H/ALL/8405	125
/CTSAT/ISCCP/T42/CCM1H/ALL/8406	126
/CTSAT/ISCCP/T42/CCM1H/ALL/8407	127
/CTSAT/ISCCP/T42/CCM1H/ALL/8408	128
/CTSAT/ISCCP/T42/CCM1H/ALL/8409	129
/CTSAT/ISCCP/T42/CCM1H/ALL/8410	130
/CTSAT/ISCCP/T42/CCM1H/ALL/8411	131
/CTSAT/ISCCP/T42/CCM1H/ALL/8412	132
/CTSAT/ISCCP/T42/CCM1H/ALL/8501	133
/CTSAT/ISCCP/T42/CCM1H/ALL/8502	134
/CTSAT/ISCCP/T42/CCM1H/ALL/8503	135
/CTSAT/ISCCP/T42/CCM1H/ALL/8504	136
/CTSAT/ISCCP/T42/CCM1H/ALL/8505	137
/CTSAT/ISCCP/T42/CCM1H/ALL/8506	138
/CTSAT/ISCCP/T42/CCM1H/ALL/8507	139
/CTSAT/ISCCP/T42/CCM1H/ALL/8508	140
/CTSAT/ISCCP/T42/CCM1H/ALL/8509	141
/CTSAT/ISCCP/T42/CCM1H/ALL/8510	142
/CTSAT/ISCCP/T42/CCM1H/ALL/8511	143
/CTSAT/ISCCP/T42/CCM1H/ALL/8512	144

Appendix 4 – Continued

T42 Data

MS PATHNAME	"DAY" (MONTH) SINCE JAN 74
/CTSAT/ISCCP/T42/CCM1H/ALL/8601	145
/CTSAT/ISCCP/T42/CCM1H/ALL/8602	146
/CTSAT/ISCCP/T42/CCM1H/ALL/8603	147
/CTSAT/ISCCP/T42/CCM1H/ALL/8604	148
/CTSAT/ISCCP/T42/CCM1H/ALL/8605	149
/CTSAT/ISCCP/T42/CCM1H/ALL/8606	150
/CTSAT/ISCCP/T42/CCM1H/ALL/8607	151
/CTSAT/ISCCP/T42/CCM1H/ALL/8608	152
/CTSAT/ISCCP/T42/CCM1H/ALL/8609	153
/CTSAT/ISCCP/T42/CCM1H/ALL/8610	154
/CTSAT/ISCCP/T42/CCM1H/ALL/8611	155
/CTSAT/ISCCP/T42/CCM1H/ALL/8612	156
/CTSAT/ISCCP/T42/CCM1H/ALL/8701	157
/CTSAT/ISCCP/T42/CCM1H/ALL/8702	158
/CTSAT/ISCCP/T42/CCM1H/ALL/8703	159
/CTSAT/ISCCP/T42/CCM1H/ALL/8704	160
/CTSAT/ISCCP/T42/CCM1H/ALL/8705	161
/CTSAT/ISCCP/T42/CCM1H/ALL/8706	162
/CTSAT/ISCCP/T42/CCM1H/ALL/8707	163
/CTSAT/ISCCP/T42/CCM1H/ALL/8708	164
/CTSAT/ISCCP/T42/CCM1H/ALL/8709	165
/CTSAT/ISCCP/T42/CCM1H/ALL/8710	166
/CTSAT/ISCCP/T42/CCM1H/ALL/8711	167
/CTSAT/ISCCP/T42/CCM1H/ALL/8712	168
/CTSAT/ISCCP/T42/CCM1H/ALL/8801	169
/CTSAT/ISCCP/T42/CCM1H/ALL/8802	170
/CTSAT/ISCCP/T42/CCM1H/ALL/8803	171
/CTSAT/ISCCP/T42/CCM1H/ALL/8804	172
/CTSAT/ISCCP/T42/CCM1H/ALL/8805	173
/CTSAT/ISCCP/T42/CCM1H/ALL/8806	174

A climatology for each month has been established from the five archived years of ISCCP data. Only the complete monthly mean data have been averaged. The averaged variables have the same processor names as in the archived monthly data, but not all variables have been included in the climatologies. The included variables are ISCCP08, ISCCP10, ISCCP11, ISCCP14, ISCCP17, ISCCP23 through ISCCP60, and ISCCP62 through ISCCP72.

The following monthly climatologies are in "TYPEc = SAVTAV" format. The 2.5° resolution fields can be accessed by changing "T42" to "2.5DG" in the Mass Store pathnames. Note that the January–June climatologies have been averaged over the years 1984–1988, while the July–December climatologies have been averaged over 1983–1987. No attempt has been made to correct for biases introduced into the data record (e.g., by changes in the satellite coverage as shown by Fig. 3), so the climatologies should be used with caution.

T42 Data

MS PATHNAME
/CTSAT/ISCCP/T42/SAVTAV/ALL/JAN8488
/CTSAT/ISCCP/T42/SAVTAV/ALL/FEB8488
/CTSAT/ISCCP/T42/SAVTAV/ALL/MAR8488
/CTSAT/ISCCP/T42/SAVTAV/ALL/APR8488
/CTSAT/ISCCP/T42/SAVTAV/ALL/MAY8488
/CTSAT/ISCCP/T42/SAVTAV/ALL/JUN8488
/CTSAT/ISCCP/T42/SAVTAV/ALL/JUL8387
/CTSAT/ISCCP/T42/SAVTAV/ALL/AUG8387
/CTSAT/ISCCP/T42/SAVTAV/ALL/SEP8387
/CTSAT/ISCCP/T42/SAVTAV/ALL/OCT8387
/CTSAT/ISCCP/T42/SAVTAV/ALL/NOV8387
/CTSAT/ISCCP/T42/SAVTAV/ALL/DEC8387

Appendix 5. ERBE data on the Mass Store.

The following is a list of the single-level monthly mean fields archived for the Earth Radiation Budget Experiment (ERBE). There are many more fields available from the ERBE S-4 data product; however, only those variables most similar to standard GCM-derived fields have been accessed and archived. The monthly data are available from February 1985 through December 1988 (47 months). Updates will continue in the future. The data are in "TYPEc = CCM1" history tape format at both 2.5° and T42 resolutions. Note that the "day" parameter (ICP "DAYSc") actually refers to monthly means.

FIELD LIST

Field	Processor Name	Units
Net radiation	NETD	$W\ m^{-2}$
Clear sky net radiation	NETCSD	$W\ m^{-2}$
Solar insolation	TSOLRDCS	$W\ m^{-2}$
Outgoing longwave radiation	MLWD	$W\ m^{-2}$
Reflected shortwave radiation	MSWD	$W\ m^{-2}$
Albedo	ALBD	fraction
Clear sky outgoing longwave radiation	MLWCSD	$W\ m^{-2}$
Clear sky reflected shortwave radiation	MSWCSD	$W\ m^{-2}$
Clear sky albedo	ALBCSD	fraction

T42 Data

MS PATHNAME	"DAY" (MONTH) SINCE JAN 74
/CTSAT/ERBE/T42/CCM1H/8588	134 – 180

2.5° Data

MS PATHNAME	"DAY" (MONTH) SINCE JAN 74
/CTSAT/ERBE/2.5DG/CCM1H/8588	134 – 180

Climatologies for each month and field have been produced. All available months were used, so averages were made over four years of data (except January, which was made over three years, 1986–1988). No attempt has been made to correct for inconsistencies introduced into the data record (e.g., by the failure of scanners), and this should be kept in mind when using the climatological data. The mean fields have the same processor names and units as above, but they are in "TYPEc = SAVTAV" format at 2.5° and T42 resolution. Only the T42 climatologies are listed, but the 2.5° data can be accessed by changing "T42" in the Mass Store pathnames to "2.5DG."

T42 Data

MS PATHNAME
/CTSAT/ERBE/T42/SAVTAV/JAN8688
/CTSAT/ERBE/T42/SAVTAV/FEB8588
/CTSAT/ERBE/T42/SAVTAV/MAR8588
/CTSAT/ERBE/T42/SAVTAV/APR8588
/CTSAT/ERBE/T42/SAVTAV/MAY8588
/CTSAT/ERBE/T42/SAVTAV/JUN8588
/CTSAT/ERBE/T42/SAVTAV/JUL8588
/CTSAT/ERBE/T42/SAVTAV/AUG8588
/CTSAT/ERBE/T42/SAVTAV/SEP8588
/CTSAT/ERBE/T42/SAVTAV/OCT8588
/CTSAT/ERBE/T42/SAVTAV/NOV8588
/CTSAT/ERBE/T42/SAVTAV/DEC8588

Appendix 6. 7-Nimbus ERB and CMATRIX data on the Mass Store.

The Nimbus-7 spacecraft has produced several long-term data sets of interest. Two have been archived for use with the CCM modular processor: Earth Radiation Budget (ERB) and Cloud-Matrix (CMATRIX). The data consist of single-level monthly mean fields archived at 4.5° resolution in "TYPEc = CCM1" history tape format. No attempt has been made to place these data on a T42 Gaussian grid because of their coarse resolution.

As for ERBE (Appendix 5), only the most widely used fields from Nimbus-7 ERB have been archived for November 1978 through October 1987. Data are not available for April, May and June 1986, and these months have been coded as missing (1.E+36). The archived Nimbus-7 ERB products are listed below. Ascending (near local-noon) and descending (near local-midnight) observations are given by "A" and "D." Note that the "day" parameter (ICP "DAYSc") actually refers to monthly means.

FIELD LIST

Field	Processor Name	Units
Outgoing longwave radiation A	EMITASC	$W\ m^{-2}$
Outgoing longwave radiation D	EMITDSC	$W\ m^{-2}$
Outgoing longwave radiation Avg of A and D	EMITSAT	$W\ m^{-2}$
Solar insolation at the ground Daily Avg	INSOLAR	$W\ m^{-2}$
Net radiation Daily Avg	NETSAT	$W\ m^{-2}$
Albedo A	ALBEDSAT	fraction

4.5° Data

MS PATHNAME	"DAY" (MONTH) SINCE JAN 74
/CTSAT/N7ERB/4.5DG/CCM1H/7887	59 - 166

Climatologies for each month and field have been produced. The analysis system changed for the Nimbus-7 ERB data in July 1980, so data prior to this time have not been used in the averages. Specifically, data from the last seven years (November 1980 through October 1987) of measurements have been used in the construction of monthly averages. No other attempts have been made to correct for possible biases in the data. The mean fields have the same processor names and units as above, but they are in "TYPEc = SAVTAV" format at 4.5° resolution.

4.5° Data

MS PATHNAME
/CTSAT/N7ERB/4.5DG/SAVTAV/JAN8187
/CTSAT/N7ERB/4.5DG/SAVTAV/FEB8187
/CTSAT/N7ERB/4.5DG/SAVTAV/MAR8187
/CTSAT/N7ERB/4.5DG/SAVTAV/APR8187
/CTSAT/N7ERB/4.5DG/SAVTAV/MAY8187
/CTSAT/N7ERB/4.5DG/SAVTAV/JUN8187
/CTSAT/N7ERB/4.5DG/SAVTAV/JUL8187
/CTSAT/N7ERB/4.5DG/SAVTAV/AUG8187
/CTSAT/N7ERB/4.5DG/SAVTAV/SEP8187
/CTSAT/N7ERB/4.5DG/SAVTAV/OCT8187
/CTSAT/N7ERB/4.5DG/SAVTAV/NOV8086
/CTSAT/N7ERB/4.5DG/SAVTAV/DEC8086

Many different fields have been archived for Nimbus-7 CMATRIX over the period April 1979 through March 1985 (72 months). As for ERB, ascending (near local-noon) and descending (near local-midnight) observations are given by "A" and "D." The radiances listed in the table below are in units of 0.125 W m^{-2} str^{-1}. SIGMA refers to standard deviation.

FIELD LIST

Field	Processor Name	Units
Total percent cloudiness A	TOTCLDUP	%
Mean time SIGMA of total cloudiness A	STOTCLUP	%
Percent low cloudiness A	LOWCLDUP	%
Mean time SIGMA of low cloudiness A	SLOWCUP	%
Percent mid cloudiness A	MIDCLDUP	%
Mean time SIGMA of mid cloudiness A	SMIDCUP	%
Percent high cloudiness A	HICLDUP	%
Mean time SIGMA of high cloudiness A	SHICUP	%
Total percent cloudiness A IR only	TOTCIRUP	%
Mean time SIGMA of total cloudiness A IR only	STOTCIRU	%
Radiance for total cloud A	RADCLDUP	W m^{-2} str^{-1}
Mean time SIGMA of radiance for total cloud A	SRADCLUP	W m^{-2} str^{-1}
Radiance for low cloud A	RADLOWUP	W m^{-2} str^{-1}
Mean time SIGMA of radiance for low cloud A	SRADLWUP	W m^{-2} str^{-1}
Radiance for mid cloud A	RADMIDUP	W m^{-2} str^{-1}
Mean time SIGMA of radiance for mid cloud A	SRADMDUP	W m^{-2} str^{-1}
Radiance for high cloud A	RADHIUP	W m^{-2} str^{-1}
Mean time SIGMA of radiance for high cloud A	SRADHIUP	W m^{-2} str^{-1}
Radiance for clear sky A	RADCLRUP	W m^{-2} str^{-1}
Mean time SIGMA of radiance for clear sky A	SRADCLRU	W m^{-2} str^{-1}
Percent high cirrus detected	HICIRRUS	%
Total percent cloudiness D	TOTCLDDN	%
Mean time SIGMA of total cloudiness D	STOTCLDN	%

Appendix 6 – Continued

Field	Processor Name	Units
Percent low cloudiness D	LOWCLDDN	%
Mean time SIGMA of low cloudiness D	SLOWCDN	%
Percent mid cloudiness D	MIDCLDDN	%
Mean time SIGMA of mid cloudiness D	SMIDCDN	%
Percent high cloudiness D	HICLDDN	%
Mean time SIGMA of high cloudiness D	SHICDN	%
Radiance for total cloud D	RADCLDDN	$W\ m^{-2}\ str^{-1}$
Mean time SIGMA of radiance for total cloud D	SRADCLDN	$W\ m^{-2}\ str^{-1}$
Radiance for low cloud D	RADLOWDN	$W\ m^{-2}\ str^{-1}$
Mean time SIGMA of radiance for low cloud D	SRADLWDN	$W\ m^{-2}\ str^{-1}$
Radiance for mid cloud D	RADMIDDN	$W\ m^{-2}\ str^{-1}$
Mean time SIGMA of radiance for mid cloud D	SRADMDDN	$W\ m^{-2}\ str^{-1}$
Radiance for high cloud D	RADHIDN	$W\ m^{-2}\ str^{-1}$
Mean time SIGMA of radiance for high cloud D	SRADHIDN	$W\ m^{-2}\ str^{-1}$
Radiance for clear sky D	RADCLRDN	$W\ m^{-2}\ str^{-1}$
Mean time SIGMA of radiance for clear sky D	SRADCLRD	$W\ m^{-2}\ str^{-1}$
Total percent cloudiness Avg of A and D	TOTCLD	%
Total percent cloudiness A-D	DIFTOTCL	%
Percent low cloudiness Avg of A and D	LOWCLD	%
Percent low cloudiness A-D	DIFLOWCL	%
Percent mid cloudiness Avg of A and D	MIDCLD	%
Percent mid cloudiness A-D	DIFMIDCL	%
Percent high cloudiness Avg of A and D	HICLD	%
Percent high cloudiness A-D	DIFHICLD	%
Radiance for total cloud Avg of A and D	RADCLD	$W\ m^{-2}\ str^{-1}$
Radiance for total cloud A-D	DIFRADCL	$W\ m^{-2}\ str^{-1}$
Radiance for low cloud Avg of A and D	RADLOW	$W\ m^{-2}\ str^{-1}$
Radiance for low cloud A-D	DIFRADLW	$W\ m^{-2}\ str^{-1}$
Radiance for mid cloud Avg of A and D	RADMID	$W\ m^{-2}\ str^{-1}$
Radiance for mid cloud A-D	DIFRADMD	$W\ m^{-2}\ str^{-1}$
Radiance for high cloud Avg of A and D	RADHI	$W\ m^{-2}\ str^{-1}$
Radiance for high cloud A-D	DIFRADHI	$W\ m^{-2}\ str^{-1}$
Radiance for clear sky Avg of A and D	RADCLR	$W\ m^{-2}\ str^{-1}$
Radiance for clear sky A-D	DIFRDCLR	$W\ m^{-2}\ str^{-1}$
Air Force surface temperature A	SURTEMPU	K
Air Force surface temperature D	SURTEMPD	K

Appendix 6 – Continued

4.5° Data	
MS PATHNAME	"DAY" (MONTH) SINCE JAN 74
/CTSAT/N7CMAT/4.5DG/CCM1H/7904	64
/CTSAT/N7CMAT/4.5DG/CCM1H/7905	65
/CTSAT/N7CMAT/4.5DG/CCM1H/7906	66
/CTSAT/N7CMAT/4.5DG/CCM1H/7907	67
/CTSAT/N7CMAT/4.5DG/CCM1H/7908	68
/CTSAT/N7CMAT/4.5DG/CCM1H/7909	69
/CTSAT/N7CMAT/4.5DG/CCM1H/7910	70
/CTSAT/N7CMAT/4.5DG/CCM1H/7911	71
/CTSAT/N7CMAT/4.5DG/CCM1H/7912	72
/CTSAT/N7CMAT/4.5DG/CCM1H/8001	73
/CTSAT/N7CMAT/4.5DG/CCM1H/8002	74
/CTSAT/N7CMAT/4.5DG/CCM1H/8003	75
/CTSAT/N7CMAT/4.5DG/CCM1H/8004	76
/CTSAT/N7CMAT/4.5DG/CCM1H/8005	77
/CTSAT/N7CMAT/4.5DG/CCM1H/8006	78
/CTSAT/N7CMAT/4.5DG/CCM1H/8007	79
/CTSAT/N7CMAT/4.5DG/CCM1H/8008	80
/CTSAT/N7CMAT/4.5DG/CCM1H/8009	81
/CTSAT/N7CMAT/4.5DG/CCM1H/8010	82
/CTSAT/N7CMAT/4.5DG/CCM1H/8011	83
/CTSAT/N7CMAT/4.5DG/CCM1H/8012	84
/CTSAT/N7CMAT/4.5DG/CCM1H/8101	85
/CTSAT/N7CMAT/4.5DG/CCM1H/8102	86
/CTSAT/N7CMAT/4.5DG/CCM1H/8103	87
/CTSAT/N7CMAT/4.5DG/CCM1H/8104	88
/CTSAT/N7CMAT/4.5DG/CCM1H/8105	89
/CTSAT/N7CMAT/4.5DG/CCM1H/8106	90
/CTSAT/N7CMAT/4.5DG/CCM1H/8107	91
/CTSAT/N7CMAT/4.5DG/CCM1H/8108	92
/CTSAT/N7CMAT/4.5DG/CCM1H/8109	93
/CTSAT/N7CMAT/4.5DG/CCM1H/8110	94
/CTSAT/N7CMAT/4.5DG/CCM1H/8111	95
/CTSAT/N7CMAT/4.5DG/CCM1H/8112	96

Appendix 6 – Continued

4.5° Data	
MS PATHNAME	"DAY" (MONTH) SINCE JAN 74
/CTSAT/N7CMAT/4.5DG/CCM1H/8201	97
/CTSAT/N7CMAT/4.5DG/CCM1H/8202	98
/CTSAT/N7CMAT/4.5DG/CCM1H/8203	99
/CTSAT/N7CMAT/4.5DG/CCM1H/8204	100
/CTSAT/N7CMAT/4.5DG/CCM1H/8205	101
/CTSAT/N7CMAT/4.5DG/CCM1H/8206	102
/CTSAT/N7CMAT/4.5DG/CCM1H/8207	103
/CTSAT/N7CMAT/4.5DG/CCM1H/8208	104
/CTSAT/N7CMAT/4.5DG/CCM1H/8209	105
/CTSAT/N7CMAT/4.5DG/CCM1H/8210	106
/CTSAT/N7CMAT/4.5DG/CCM1H/8211	107
/CTSAT/N7CMAT/4.5DG/CCM1H/8212	108
/CTSAT/N7CMAT/4.5DG/CCM1H/8301	109
/CTSAT/N7CMAT/4.5DG/CCM1H/8302	110
/CTSAT/N7CMAT/4.5DG/CCM1H/8303	111
/CTSAT/N7CMAT/4.5DG/CCM1H/8304	112
/CTSAT/N7CMAT/4.5DG/CCM1H/8305	113
/CTSAT/N7CMAT/4.5DG/CCM1H/8306	114
/CTSAT/N7CMAT/4.5DG/CCM1H/8307	115
/CTSAT/N7CMAT/4.5DG/CCM1H/8308	116
/CTSAT/N7CMAT/4.5DG/CCM1H/8309	117
/CTSAT/N7CMAT/4.5DG/CCM1H/8310	118
/CTSAT/N7CMAT/4.5DG/CCM1H/8311	119
/CTSAT/N7CMAT/4.5DG/CCM1H/8312	120
/CTSAT/N7CMAT/4.5DG/CCM1H/8401	121
/CTSAT/N7CMAT/4.5DG/CCM1H/8402	122
/CTSAT/N7CMAT/4.5DG/CCM1H/8403	123
/CTSAT/N7CMAT/4.5DG/CCM1H/8404	124
/CTSAT/N7CMAT/4.5DG/CCM1H/8405	125
/CTSAT/N7CMAT/4.5DG/CCM1H/8406	126
/CTSAT/N7CMAT/4.5DG/CCM1H/8407	127
/CTSAT/N7CMAT/4.5DG/CCM1H/8408	128
/CTSAT/N7CMAT/4.5DG/CCM1H/8409	129
/CTSAT/N7CMAT/4.5DG/CCM1H/8410	130
/CTSAT/N7CMAT/4.5DG/CCM1H/8411	131
/CTSAT/N7CMAT/4.5DG/CCM1H/8412	132
/CTSAT/N7CMAT/4.5DG/CCM1H/8501	133
/CTSAT/N7CMAT/4.5DG/CCM1H/8502	134
/CTSAT/N7CMAT/4.5DG/CCM1H/8503	135

Climatologies for each month have been produced from the six years of CMATRIX data, so January through March averages include the years 1980–1985, while the other nine months include 1979–1984. All of the fields have been averaged, except for the SIGMA fields. No attempt has been made to correct for possible biases introduced into the data, so the following fields should be used with caution. The mean fields have the same processor names and units as above, but they are in "TYPEc = SAVTAV" format at 4.5° resolution.

4.5° Data

MS PATHNAME
/CTSAT/N7CMAT/4.5DG/SAVTAV/JAN8085
/CTSAT/N7CMAT/4.5DG/SAVTAV/FEB8085
/CTSAT/N7CMAT/4.5DG/SAVTAV/MAR8085
/CTSAT/N7CMAT/4.5DG/SAVTAV/APR7984
/CTSAT/N7CMAT/4.5DG/SAVTAV/MAY7984
/CTSAT/N7CMAT/4.5DG/SAVTAV/JUN7984
/CTSAT/N7CMAT/4.5DG/SAVTAV/JUL7984
/CTSAT/N7CMAT/4.5DG/SAVTAV/AUG7984
/CTSAT/N7CMAT/4.5DG/SAVTAV/SEP7984
/CTSAT/N7CMAT/4.5DG/SAVTAV/OCT7984
/CTSAT/N7CMAT/4.5DG/SAVTAV/NOV7984
/CTSAT/N7CMAT/4.5DG/SAVTAV/DEC7984

Appendix 7. NOAA OLR data on the Mass Store.

This appendix describes access to the archived OLR field from NOAA satellites. Monthly data from June 1974 through December 1991 have been archived in "TYPEc = CCM1" history tape format at both 2.5° and T42 resolutions. Data are not available from March through December 1978, and these months have been coded as missing (1.E+36). Updates will continue in the future. Note that the "day" parameter (ICP "DAYSc") actually refers to monthly means.

FIELD LIST

Field	Processor Name	Units
Outgoing longwave radiation	OLR	$W\ m^{-2}$
	T42 Data	
MS PATHNAME /CTSAT/NOAA/T42/CCM1H/7491		"DAY" (MONTH) SINCE JAN 74 6 – 216
	2.5° Data	
MS PATHNAME /CTSAT/NOAA/2.5DG/CCM1H/7491		"DAY" (MONTH) SINCE JAN 74 6 – 216

Climatologies for each month have been made using the data after 1978 so that 13 years have been averaged. No attempt has been made to correct for biases introduced into the data by sampling problems or changes in the analysis method. The mean OLR fields have the same processor name and unit as above, but they are in "TYPEc = SAVTAV" format at 2.5° and T42 resolution. Only the T42 climatologies are listed, but the 2.5° data can be accessed by changing "T42" in the Mass Store pathnames to "2.5DG."

T42 Data

MS PATHNAME
/CTSAT/NOAA/T42/SAVTAV/JAN7991
/CTSAT/NOAA/T42/SAVTAV/FEB7991
/CTSAT/NOAA/T42/SAVTAV/MAR7991
/CTSAT/NOAA/T42/SAVTAV/APR7991
/CTSAT/NOAA/T42/SAVTAV/MAY7991
/CTSAT/NOAA/T42/SAVTAV/JUN7991
/CTSAT/NOAA/T42/SAVTAV/JUL7991
/CTSAT/NOAA/T42/SAVTAV/AUG7991
/CTSAT/NOAA/T42/SAVTAV/SEP7991
/CTSAT/NOAA/T42/SAVTAV/OCT7991
/CTSAT/NOAA/T42/SAVTAV/NOV7991
/CTSAT/NOAA/T42/SAVTAV/DEC7991

Appendix 8. Surface flags.

This appendix describes access to the archived surface flags for T42, 2.5° and 4.5° grid resolutions. Flags have been created to mark land and ocean surfaces only, which is useful for several algorithms in the CCM processor which require surface type masking. The surface flags can be accessed by the ICP "SFCTTAP." An example of surface type masking for horizontal averages is given in Appendix 9.

T42 Data

MS PATHNAME
/CTSAT/SFC/T42/ORO

2.5° Data

MS PATHNAME
/CTSAT/SFC/2.5DG/ORO

4.5° Data

MS PATHNAME
/CTSAT/SFC/4.5DG/ORO

Q-2

Appendix 9. Sample CCM Processor Jobs.

Several sample plots produced by the CCM processor are listed below. Also included are the Input Control Parameters (ICPs) used to produced the plots. For additional examples and a detailed description of the CCM processor, see Wolski (1987,1989.)

Example 1: Area averaging

The following processor job deck will produce a land-only area average for the ISCCP field ISCCP72 at T42 resolution (from July 1983 to June 1988). Please note the "DAYSc" parameter as well as the "SFCTTAP" parameter.

```
C
C ICPs to create land-only area average from monthly ISCCP data
C
  TITLEA  = 'AREA AVERAGE'
  MSPFXIA = '/CTSAT/ISCCP/T42/CCM1H/ALL/'
  TAPESA  = '8307,'8308,'8309',
  '8310','8311','8312',
  '8401','8402','8403','8404',
  '8405','8406','8407','8408',
  '8409','8410','8411','8412',
  '8501','8502','8503','8504',
  '8505','8506','8507','8508',
  '8509','8510','8511','8512',
  '8601','8602','8603','8604',
  '8605','8606','8607','8608',
  '8609','8610','8611','8612',
  '8701','8702','8703','8704',
  '8705','8706','8707','8708',
  '8709','8710','8711','8712',
  '8801','8802','8803',
  '8804','8805','8806'
  TYPEA   = 'CCM1'
  DAYSA   = 115.,174.,1.
  TIMAVGA = 'NO'
  FIELDA1 = 'ISCCP72'
  SFCTTAP = '/CTSAT/SFC/T42/ORO'
  TSPALA1 = 'ISCCP72','LAND' ,'LAND' ,1000.,0.,0.,0.,0.,0.,0.
  ENDOFDATA
```

The following plot is the resulting metacode file produced by the CCM processor.

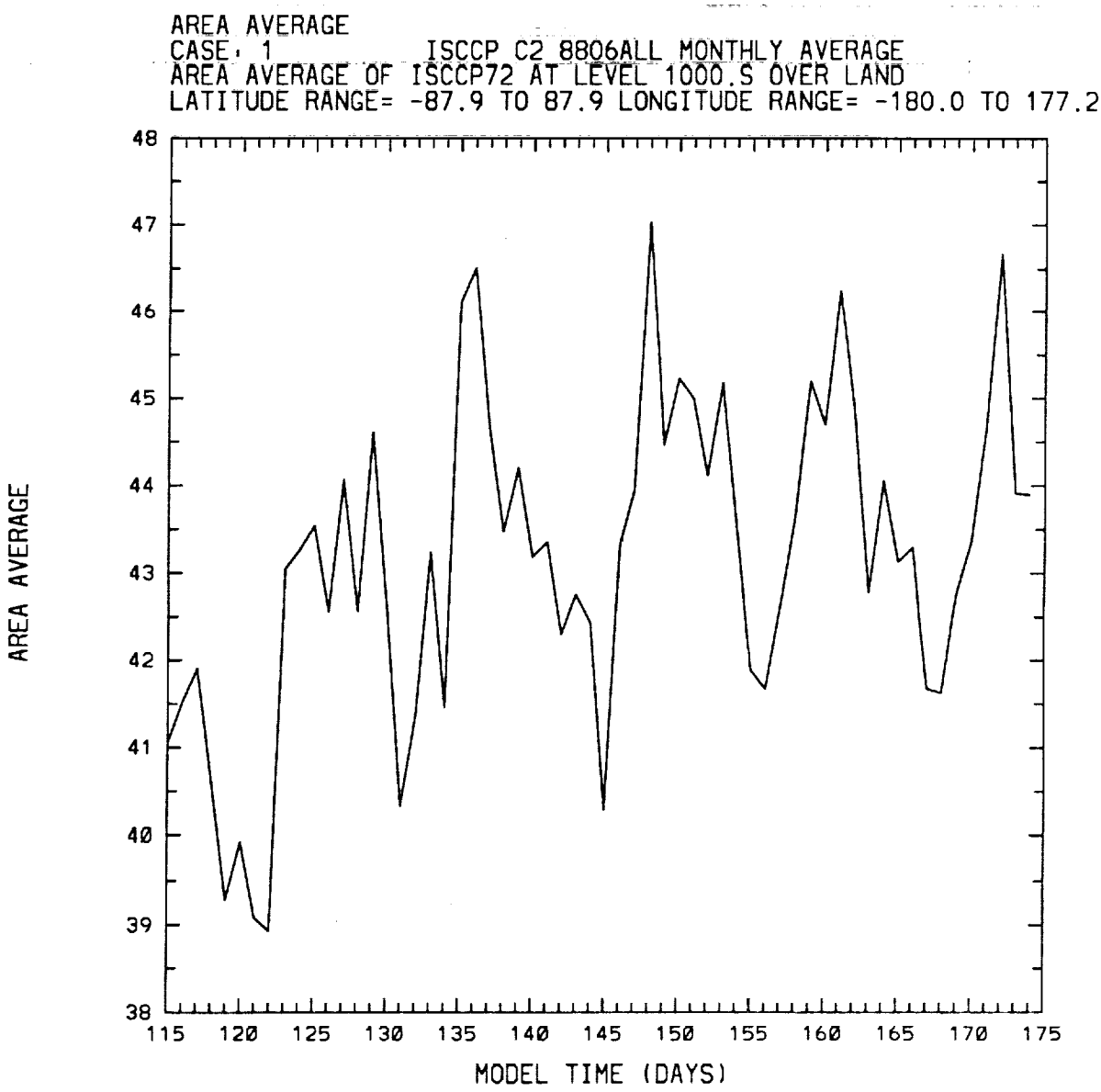

Example 2: Horizontal plot from a CCM history tape

The following processor job deck will generate a horizontal plot of OLR from ERBE T42 data for January 1987. Note that an equatorial cylindrical equidistant projection is requested through the ICP "HPROJ."

```
C
C ICPs to create a horizontal plot from ERBE data
C
  TITLEA  = 'JANUARY 1987'
  MSPFXIA = '/CTSAT/ERBE/T42/CCM1H/'
  TAPESA  = '8588'
  TIMAVGA = 'NO'
  TYPEA   = 'CCM1'
  DAYSA   = 157.,157.,1.
  FIELDA1 = 'MLWD'
  HPROJ   = 'RECT'
  HPRBNDS = 0.,360.,-90.,90.
  HPCINT  = 'MLWD',1000.,25.
  ENDOFDATA
```

The metacode file resulting from Example 2 is shown below.

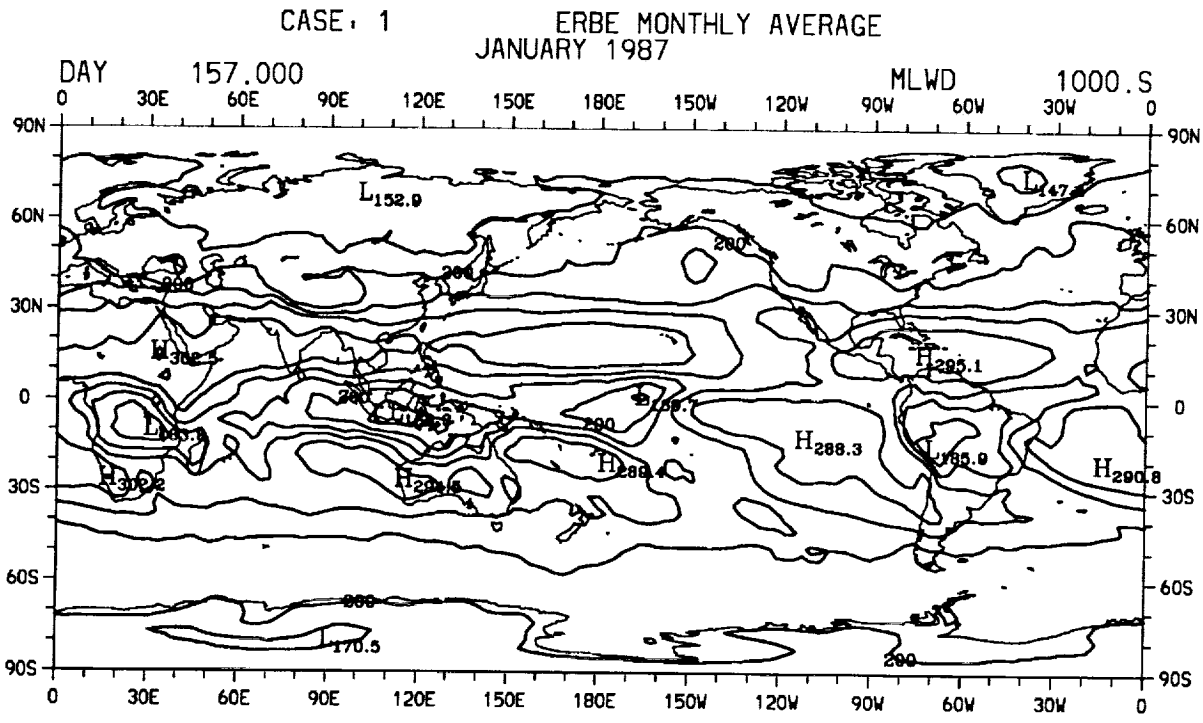

Contour from 150 to 300 by 25

Example 3: Horizontal plot from a time average save tape

The following processor job deck will generate a horizontal plot for the July climatology of the ERBE "NETD" field at T42 resolution.

```
C
C ICPs to create a horizontal plot of ERBE data
C
  TITLEA  = 'JULY 1985-1988'
  MSPFXIA = '/CTSAT/ERBE/T42/SAVTAV/'
  TAPESA  = 'JUL8588'
  TYPEA   = 'SAVTAV'
  FIELDA1 = 'NETD'
  HPROJ   = 'RECT'
  HPCINT  = 'NETD',1000.,25.
  ENDOFDATA
```

The following plot is the metacode file that results from Example 3.

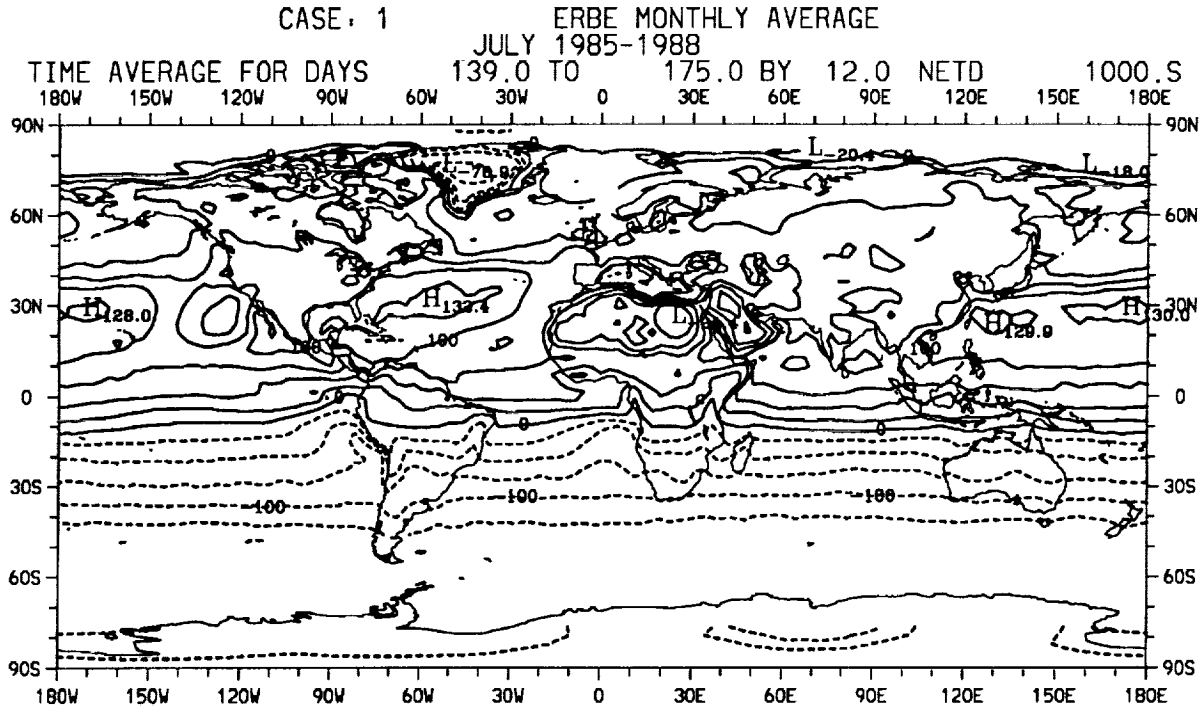

Contour from -150 to 125 by 25

Example 4: Zonal average plots

The following processor job deck will generate a zonally averaged plot of MSU channel 2 brightness temperature anomalies for the 156 months of January 1979 through December 1991.

```
C
C ICPs for zonal average of MSU data
C
  MSPFXIA = '/CTSAT/MSU/T42/CCM1H'
  TAPESA  = '7991A'
  TIMAVGA = 'NO'
  TYPEA   = 'CCM1'
  DAYSA   = 61.,216.,1.
  FIELDA1 = 'CH2TANOM'
  CONZERO = 'NO'
  TSPZCA1 = 'CH2TANOM',1000.,0.4,0.,0.
  ENDOFDATA
```

The metacode file below is produced by Example 4.